

Aus dem Bereich Systemische Neurowissenschaften und
Neurotechnologie, Theoretische Medizin und Biowissenschaften
der Medizinischen Fakultät der Universität des Saarlandes,
Homburg/Saar

**Neural Correlates of Binaural Interaction
Using Aggregate-System Stimulation
in Cochlear Implantees**

*Dissertation zur Erlangung des Grades eines
Doktors der Theoretischen Medizin
der Medizinischen Fakultät
der Universität des Saarlandes
2019*

vorgelegt von:
Erik Schebsdat, M.Sc.
geboren am 08. Mai 1988 in Worms

Tag der Promotion:	23.03.2020
Dekan:	Prof. Dr. med. Michael D. Menger
Berichterstatter:	Prof. Dr. rer. nat. Dr. rer. med. Daniel J. Strauss
	Prof. Dr. rer. nat. Tobias Hartmann

**Do not go where the path may lead,
go instead where there is no path and leave a trail.**

Ralph Waldo Emerson

Dedicated to all my companions in life.

Eidesstattliche Erklärung gemäß § 7 Abs. 1 Nr. 4

Ich erkläre hiermit an Eides statt, dass ich die vorliegende Arbeit ohne unzulässige Hilfe Dritter und ohne Benutzung anderer als der angegebenen Hilfsmittel angefertigt habe. Die aus anderen Quellen direkt oder indirekt übernommenen Daten und Konzepte sind unter Angabe der Quelle gekennzeichnet.

Bei der Auswahl und Auswertung folgenden Materials haben mir die nachstehend aufgeführten Personen in der jeweils beschriebenen Weise unentgeltlich/entgeltlich geholfen:

- Alle in der Danksagung des Dissertationsmanuskripts erwähnten Personen haben mir in der dort beschriebenen Weise unentgeltlich geholfen.

Weitere Personen waren an der inhaltlich-materiellen Erstellung der vorliegenden Arbeit nicht beteiligt. Insbesondere habe ich nicht die entgeltliche Hilfe von Vermittlungs- bzw. Beratungsdiensten (Promotionsberater/innen oder anderer Personen) in Anspruch genommen. Außer den Angegebenen hat niemand von mir unmittelbar oder mittelbar geldwerte Leistungen für Arbeiten erhalten, die im Zusammenhang mit dem Inhalt der vorgelegten Dissertation stehen.

Die Arbeit wurde bisher weder im Inland noch im Ausland in gleicher oder ähnlicher Form in einem anderen Verfahren zur Erlangung eines Doktorgrades einer anderen Prüfungsbehörde vorgelegt.

In versichere an Eides statt, dass ich nach bestem Wissen die Wahrheit gesagt und nichts verschwiegen habe.

Vor Aufnahme der vorstehenden Versicherung an Eides statt wurde ich über die Bedeutung einer eidesstattlichen Versicherung und die strafrechtlichen Folgen einer unrichtigen oder unvollständigen eidesstattlichen Versicherung belehrt.

Saarbrücken, den 05.06.2019

Unterschrift des Promovierenden
(Erik Schebsdat)

Unterschrift der die Versicherung an
Eides statt aufnehmenden Beamtin
bzw. des aufnehmenden Beamten

List of Abbreviations

ABR	auditory brainstem response
AC	auditory cortex
ACE	advanced combinational encoder
AEP	auditory evoked potential
ALR	auditory late response
AMLR	auditory middle-late response
AN	auditory nerve
BERA	brainstem evoked response audiometry
BIC	binaural interaction component
BM	basilar membrane
CI	cochlear implant
CIS	continuous-interleaved-sampling
CL(A)D	continuous-loop (averaging) deconvolution
C-level	most comfortable loudness level
CN	cochlear nucleus
DR	dynamic range
EABR	electrically evoked auditory brainstem response
EEG	electroencephalography
ERP	event-related potential
FFT	fast Fourier transformation
FIR	finite impulse response
HA	hearing aid
HL	hearing level
HLo	hearing loss
IC	inferior colliculus
IHC	inner hair cells
IIR	infinite impulse response
ILD	interaural loudness difference
ITD	interaural time difference
LL	lateral lemniscus
NH	normal hearing
OHC	outer hair cells
pe SPL	peak-equivalent sound pressure level
SNR	signal-to-noise ratio
SOC	superior olivary complex
SPL	sound pressure level
T-level	threshold level
WPSS	wavelet phase synchronization stability

Contents

List of Abbreviations	vi
List of Figures	x
List of Tables	xi
1 Abstract	1
1.1 Zusammenfassung	3
2 Introduction	5
2.1 Motivation	5
2.1.1 Thesis Organization	6
2.2 The Human Auditory System	7
2.2.1 The Ear	7
2.2.2 The Auditory Pathway	10
2.3 Human Hearing	13
2.3.1 Perception	13
2.3.2 Processing Cues	14
2.3.3 Hearing Loss and Deafness	16
2.4 The Cochlear Implant	18
2.4.1 General Requirements	18
2.4.2 Technical Inspection	20
2.4.3 Performance	24
2.4.4 Trends and Limitations	27
2.5 Auditory Evoked Potentials	29
2.5.1 Auditory Brainstem Responses	32
2.5.2 Electrically Evoked Auditory Brainstem Responses	33
2.5.3 Binaural Interaction Component	35
2.5.4 Comparability and Limitations	37
2.6 Contributions of this Work	40

3	Materials and Methods	43
3.1	Ethics Statement and Participant Recruitment	43
3.2	Study 1: Neural Correlates of Free-Field Evoked Auditory Brainstem Responses in Cochlear Implant Users	44
3.2.1	Experimental Procedure and Participants	44
3.2.2	Response Latency Estimations	46
3.2.3	Narrowband Filtering	46
3.2.4	Inter-Trial Phase Synchronization Measures	48
3.2.5	Data Acquisition and Preprocessing	49
3.3	Study 2: Quantification of Binaural Interaction Facilitated By Inter- aural Latency Compensation in Bimodal Cochlear Implant Users . .	51
3.3.1	Experimental Procedure and Participants	51
3.3.2	Interaural Latency Estimations	53
3.3.3	Stimulus Sequence Design	54
3.3.4	Data Acquisition and Preprocessing	55
3.3.5	Response Deconvolution	56
3.3.6	Binaural Computations	57
4	Results	59
4.1	Results of Study 1	59
4.1.1	Filter Settings and Scales	59
4.1.2	Free-Field Responses in Normal Hearing Listeners	63
4.1.3	Free-Field Responses in Cochlear Implantees	67
4.1.4	Confrontation and Statistics	71
4.2	Results of Study 2	75
4.2.1	Responses With and Without Delay Compensation	75
4.2.2	Binaural Interaction Components	79
4.2.3	Confrontation and Statistics	81
5	Discussion	83
5.1	Discussion of Study 1	83
5.1.1	Free-Field Apparatus	83
5.1.2	Response Alterations	87
5.1.3	Response Characteristics, Behavior, and Interpretation . . .	89
5.2	Discussion of Study 2	92
5.2.1	Sequencing and Deconvolution	92

5.2.2	Response Characteristics and Interpretation	94
5.2.3	Delay Compensations and Binaural Interaction	96
6	Conclusion	98
7	Appendix (Study 1)	101
	Bibliography	101
	List of Publications	116
	Acknowledgements	118
	Curriculum Vitae	121

List of Figures

2.1	Anatomic Representation of the Ear	8
2.2	Tonotopic Organization of the Cochlea	9
2.3	Schematic Representation of the Auditory Pathway	11
2.4	Jefress Model Describing the Encoding of ITDs	15
2.5	Schematic Representation of a Cochlear Implant System	21
2.6	Electrode Array inside of the Cochlea	23
2.7	Acoustic Evoked Potentials	30
2.8	Comparison of Click- and Chirp-Stimuli	31
2.9	Comparison of Electrically and Acoustically Evoked Brainstem Responses . . .	34
2.10	Representation of the Binaural Interaction Component	36
3.1	Schematic Representation of the Measurement Setup (Study 1)	45
3.2	Schematic Representation of the Measurement Setup (Study 2)	52
3.3	Optimized CL(A)D Stimulation Sequence (Study 2)	55
4.1	Grand Average NH Chirp Responses and Ringing Artifact (Study 1)	60
4.2	Grand Average NH Click Responses and Ringing Artifact (Study 1)	61
4.3	Grand Average NH Chirp Narrowband Responses (Study 1)	63
4.4	Grand Average NH Click Narrowband Responses (Study 1)	65
4.5	Grand Average CI Chirp Narrowband Responses (Study 1)	67
4.6	Grand Average CI Click Narrowband Responses (Study 1)	69
4.7	Confrontation of Response Variables (Study 1)	71
4.8	Determined Significance Values Using the Wilcoxon Rank-Sum Paired Difference Test (Study 1)	73
4.9	Grand Average ERPs With and Without Delay Compensation (Study 2)	76
4.10	Single User ERPs With and Without Delay Compensation (Study 2)	78
4.11	Binaural Interaction Component With and Without Delay Compensation (Study 2)	80
4.12	Detected Amplitudes of the Binaural Interaction Components (Study 2)	81

List of Tables

3.1	CI-Participants (Study 1)	45
3.2	CI-Participants (Study 2)	53
7.1	Significance Table (Study 1)	101

1 Abstract

The importance of binaural cues in auditory stream formation and sound source differentiation is widely accepted. When treating one ear with a cochlear implant (CI) the peripheral auditory system gets partially replaced and processing delays get added potentially, thus important interaural time encoding gets altered. This is a crucial problem because factors like the interaural time delay between the receiving ears are known to be responsible for facilitating such cues, e.g., sound source localization and separation. However, these effects are not fully understood, leaving a lack of systematic binaural fitting strategies with respect to an optimal binaural fusion.

To gain new insights into such alterations, we suggest a novel method of free-field evoked auditory brainstem response (ABR) analysis in CI users. As a result, this method does not bypass the technically induced intrinsic delays of the hearing device while leaving the complete electrode array active, thus the most natural way of stimulation is provided and the comparable testing of real world stimuli gets facilitated. Unfortunately, ABRs acquired in CI users are additionally affected by the prominent artifact caused by their electrical stimulation, which severely distorts the desired neural response, thus challenging their analysis. To circumvent this problem, we further introduce a novel narrowband filtering CI artifact removal technique capable of obtaining neural correlates of ABRs in CI users. Consequently, we were able to compare brainstem-level responses collected of 12 CI users and 12 normal hearing listeners using two different stimuli (i.e., chirp and click) at four different intensities each, what comprises an adaption of the prominent brainstem evoked response audiometry serving as an additional evaluation criterion. We analyzed the responses using the average of 2,000 trials in combination with synchronized regularizations across them and found consistent results in their deflections and latencies, as well as in single trial relationships

between both groups. This method provides a novel and unique perspective into the natural CI users' brainstem-level responses and can be practical in future research regarding binaural interaction and fusion. Furthermore, the binaural interaction component (BIC), i.e., the arithmetical difference between the sum of both monaurally evoked ABRs and the binaurally evoked ABR, has been previously shown to be an objective indicator for binaural interaction. This component is unfortunately known to be rather fragile and as a result, a reliable, objective measure of binaural interaction in CI users does not exist to the present date. It is most likely that implantees would benefit from a reliable analysis of brainstem-level and subsequent higher-level binaural interaction, since this could objectively support fitting strategies with respect to a maximization of interaural integration. Therefore, we introduce a novel method capable of obtaining neural correlates of binaural interaction in bimodal CI users by combining recent advances in the field of fast, deconvolution-based ABR acquisitions with the introduced narrowband filtering technique. The proposed method shows a significant improvement in the magnitude of resulting BICs in 10 bimodal CI users and a control-group of 10 normal hearing subjects when compensating the interaural latency difference caused by the technical devices.

In total, both proposed studies objectively demonstrate technical-driven interaural latency mismatches. Thus, they strongly emphasize potential benefits when balancing these interaural delays to improve binaural processing by significant increases in associated neural correlates of successful binaural interaction. These results and also the estimated latency differences should be investigated in larger group sizes to further consolidate the results, but confirm the demand for rather binaural solutions than treating hearing losses in an isolated monaural manner.

Keywords: Cochlear Implant & Auditory Brainstem Response & Binaural Interaction & Interaural Time Difference & Free-Field & Stimulus Sequencing & Deconvolution & Full-Range-Potential

1.1 Zusammenfassung

Die Notwendigkeit binauraler Verarbeitungsprozesse in der auditorischen Wahrnehmung ist weitestgehend akzeptiert. Bei der Therapie eines Ohres mit einem Cochlea-Implantat (engl. cochlear implant (CI)) wird das periphere auditorische System teilweise ersetzt und verändert, sodass natürliche, interaurale Zeitauflösungen beeinflusst werden. Dieses Problem ist entscheidend, denn Faktoren wie interaurale Laufzeitunterschiede zwischen den aufnehmenden Ohren sind verantwortlich für die Umsetzung der erwähnten binauralen Verarbeitungsprozesse, z.B. Schallquellenlokalisation und -separation. Allerdings sind diese Effekte nicht ausreichend verstanden, weshalb bis heute binaurale Anpassstrategien mit Rücksicht auf eine optimale Fusionierung fehlen.

Um neue Einsichten in solche zeitlichen Verzerrungen zu erhalten, schlagen wir ein neues Verfahren der Freifeld evozierten auditorischen Hirnstammpotential (engl. auditory brainstem response (ABR)) in CI-Nutzern vor. Diese Methode beinhaltet explizit technisch-induzierte Laufzeiten verwendeter Hörhilfen, sodass eine natürliche Stimulation unter Verwendung von realitätsnahen Stimuli ermöglicht wird. Unglücklicherweise sind ABRs von CI-Nutzern zusätzlich mit Stimulationsartefakten belastet, wodurch benötigte neurale Antworten weiter verzerrt werden und eine entsprechende Analyse der Signale deutlich erschwert wird. Um dieses Problem zu umgehen, schlagen wir eine neue Artefakt-Reduktionstechnik vor, welche auf spektraler Schmalbandfilterung basiert und somit den Erhalt entsprechender, neuraler ABR Korrelate ermöglicht. Diese Methoden erlaubten die Interpretation neuraler Korrelate auf Hirnstammebene unter Verwendung von zwei verschiedenen Stimuli (Chirps und Klicks) unter vier verschiedenen Lautstärken in 12 CI-Nutzern und 12 normalhörenden Probanden. Die beschriebene Prozedur adaptiert somit die weitläufig bekannte Hirnstammaudiometrie (engl. brainstem evoked response audiometry (BERA)), deren Ergebnisse zur zusätzlichen Evaluation des vorgestellten Verfahrens dienten. Die Untersuchung der aus 2000 Einzelantworten erhaltenen Mittelwerte in Kombination mit der Analyse synchronisierter Regularitäten über den Verlauf der Einzelantworten ergab dabei konsistente Beobachtungen in gefundenen Amplituden, Latenzen sowie in Abhängigkeiten zwischen Einzelantworten in beiden Gruppen. Das vorgestellte Verfahren erlaubt somit auf einzigartige Weise neue und ungesehene Einsichten

in natürliche, neurale Antworten auf Hirnstammebene von CI-Nutzern, welche in zukünftigen Studien verwendet werden können, um binaurale Interaktionen und Fusionen weiter untersuchen zu können. Interessanterweise hat sich, die auf ABRs basierende, binaurale Interaktionskomponente (engl. binaural interaction component (BIC)) als objektiver Indikator binauraler Integration etabliert. Diese Komponente (d.h. die arithmetische Differenz zwischen der Summe der monauralen Antworten und der binauralen Antwort) ist leider sehr fragil, wodurch ein sicherer und objektiver Nachweis in CI-Nutzern bis heute nicht existiert. Dabei ist es sehr wahrscheinlich, dass gerade Implantatsträger von einer entsprechenden Analyse auf Hirnstammebene und höherrangigen Ebenen deutlich profitieren würden, da dies objektiv Anpassstrategien mit Rücksicht auf eine bestmögliche binaurale Integration ermöglichen könnte. Deshalb stellen wir ein weiteres, neuartiges Verfahren zum Erhalt von neuronalen Korrelaten binauraler Interaktion in bimodal versorgten CI-Trägern vor, welches jüngste Erfolge im Bereich der schnellen, entfallungsbasierten ABR Akquisition und der bereits vorgestellten Schmalbandfilterung zur Reduktion von Stimulationsartefakten kombiniert. Basierend auf diesem Verfahren konnten signifikante Verbesserungen in der BIC-Amplitude in 10 bimodal versorgten Patienten sowie 10 normalhörenden Probanden, basierend auf umgesetzte, interaurale Laufzeitkompensationen technischer Hörhilfen, aufgezeigt werden.

Insgesamt demonstrieren beide vorgestellten Studien technisch-induzierte, interaurale Laufzeitunterschiede und betonen demnach sehr deutlich potenzielle Vorteile in assoziierten neuronalen Korrelaten binauraler Interaktionen, wenn solche Missverhältnisse zeitlich ausgeglichen werden. Die aufgezeigten Ergebnisse sowie die getätigte Abschätzungen technischer Laufzeiten sollte in größeren Gruppen weiter untersucht werden, um die Aussagekraft weiter zu steigern. Dennoch unterstreichen diese Einsichten das Verlangen nach binauralen Lösungsansätzen in der zukünftigen Hörrehabilitation, statt bisheriger isolierter und monauraler Therapien.

2 Introduction

2.1 Motivation

The World Health Organization estimates that currently around **466 million people worldwide** suffer from disabling hearing loss (HLo) (including 34 million children). Importantly, this results in an **annual global cost of US\$ 750 billion**, caused by unaddressed HLos. It is estimated that by now 1.1 billion young people (12-35 years) are at risk of developing a HLo based on noise exposure and recreational settings. It is further estimated that in 2050 over 900 million people will suffer from disabling HLo.

Today, the most successful neural prosthesis that can restore partial hearing to a totally deafened person via electric stimulation of the residual auditory nerve is the cochlear implant (CI). It offers the unique opportunity to bypass the cochlea and thus gives the possibility to partially regain the sense of hearing. After implantation, the CI user has to learn to interpret the electric stimulation as an auditory impression, therefore the brain has to undergo essential neural changes to adapt to the new input. Thus, for getting the most therapeutic benefit, it is essential to fit the implant perfectly to the implantee, fit the CI system to the demands of the user, and for the user himself to take part in auditory training. Without a doubt, this is a challenging and time consuming process. However, so far it is not clear which processes are influencing the potential hearing outcome of such an implantation. Possible influencing parameters that are discussed today are the usage of different hearing devices, different hearing-biographies, different periods of deafness, and more. Consequently, the outcome of a CI implantation varies a lot between subjects, thus the prognosis prior a CI implantation regarding the potential beneficial hearing outcome is limited to say the least. Furthermore challenging is the current CI rehabilitation phase - if any present at all. It is

characterized by learning processes and the hearing outcome is verified only by subjective measurements like thresholds and understanding of speech. Unnecessary to say, these subjective responses prone possible mistakes or are even not possible at all (e.g., infants, who can not give their subjective feedback and/or are not able to describe their hearing perception). Note that needed objective measurements are already missing when treating one ear isolated. Special implantation, fitting, and rehabilitation rules as well as objective measurements aiming for an optimal binaural hearing (i.e., Binaural Fusion) are not available. This still negatively affects patients who are treated unilateral, bimodal (i.e., a CI combined with a contralateral hearing aid (HA)), and bilateral (i.e., a CI contralaterally combined with a second CI) today. This seems to be a substantial lack of knowledge and techniques, especially when taking recent neurophysiological, neurobiological, and neuromodeling research into account, which emphasize the necessity of a high spatiotemporal precision of neural coincidence detection circuit activations to mediate binaural interaction and fusion. Thus, especially encouraged by the shattering trend in future hearing, there is a need for robust methods that provide objective insights into the neural processing of CI users, which are suitable for use in diagnostics and research. Such insights could be used to enhance the CI fitting with respect to the users' individual neural behavior and furthermore offer a general comparison between the neural reaction of CI users and that of normal hearing listeners - and perhaps an alignment of the neural responses in the future. This work addresses these demands and aims for advanced and objective measurements potentially supporting binaural integration in CI implantees.

2.1.1 Thesis Organization

In order to capture the full picture involving current solutions and their limitations, it is important to gain general knowledge about the topic. Therefore, Section 2 gives comprehensive background information regarding the anatomy and physiology of the human auditory system, the human hearing, the development of HLo, the state-of-the-art of current CI systems, and of current electroencephalographic measurements in audiology. This Section ends with a description of the facilitated contributions of this work. Section 3 introduces the implemented studies, in which the utilized methods and materials are explained, whereas their results are shown in Section 4. Finally, they are discussed in Section 5 and concluded in Section 6.

2.2 The Human Auditory System

The human auditory system can be separated into two major parts - the ear and the auditory pathway. While the ear consists of the outer ear, middle ear, and inner ear, including the cochlea, the auditory pathway names the passage from the auditory nerve (AN) to the auditory cortex (AC) [Buchner and Armbruster, 2005]. It consists of the auditory brainstem with numerous clusters of neurons (nuclei) [Purves et al., 2004], complexly connected with multiple crossing paths [Buchner and Armbruster, 2005].

2.2.1 The Ear

The **outer ears** purpose, involving the pinna and the ear canal (shown in Figure 2.1), is to gather, bundle and amplify incoming sound. Additionally, it acts as a directional selectivity filter, offering first sound source localization possibilities [Kandel et al., 2000]. The ear canal resonates frequencies at about 3 kHz, supportingly amplifying incoming sound pressure of approximately, 10 dB at the tympanic membrane [Moller, 2006]. The subsequent middle ear basically includes three ossicles (Malleus, Incus, and Stapes), which transform the impedance from so far air (low) to the fluid (high) filled inner ears cochlea. On the one hand, this mechanism exploits the area difference between the tympanic membrane and oval window, the site where the ossicles contact the inner ear. On the other hand, a second amplifier is based on the lever action of the ossicular chain [Buchner and Armbruster, 2005]. These two mechanical processes causing a frequency dependent sound pressure gain, especially around the audible mid-frequency range, of possibly 30 dB [Moller, 2006]. Note that without these necessary steps most of the collected sounds would get lost [Moller, 2006]. The medial **inner ear** persists of two major parts, the cochlea and the vestibular organ. While the vestibular organ contributes to sense, balance and the spatial orientation of the body, the cochlea is the part that is responsible for sound processing [Schmidt et al., 2013]. The snail shaped, bony structured cochlea has approximately 2.5 turns, an uncoiled length of 31-33 mm, and a height of 5 mm (see Figure 2.1 and Figure 2.2). It is embedded in the temporal bone consists of the scala tympani, scala media and scala vestibuli. These three fluid-filled compartments are separated by the basilar membrane (BM) (scala media from scala tympani) and Reissner's membrane (scala vestibuli from

2.2 The Human Auditory System

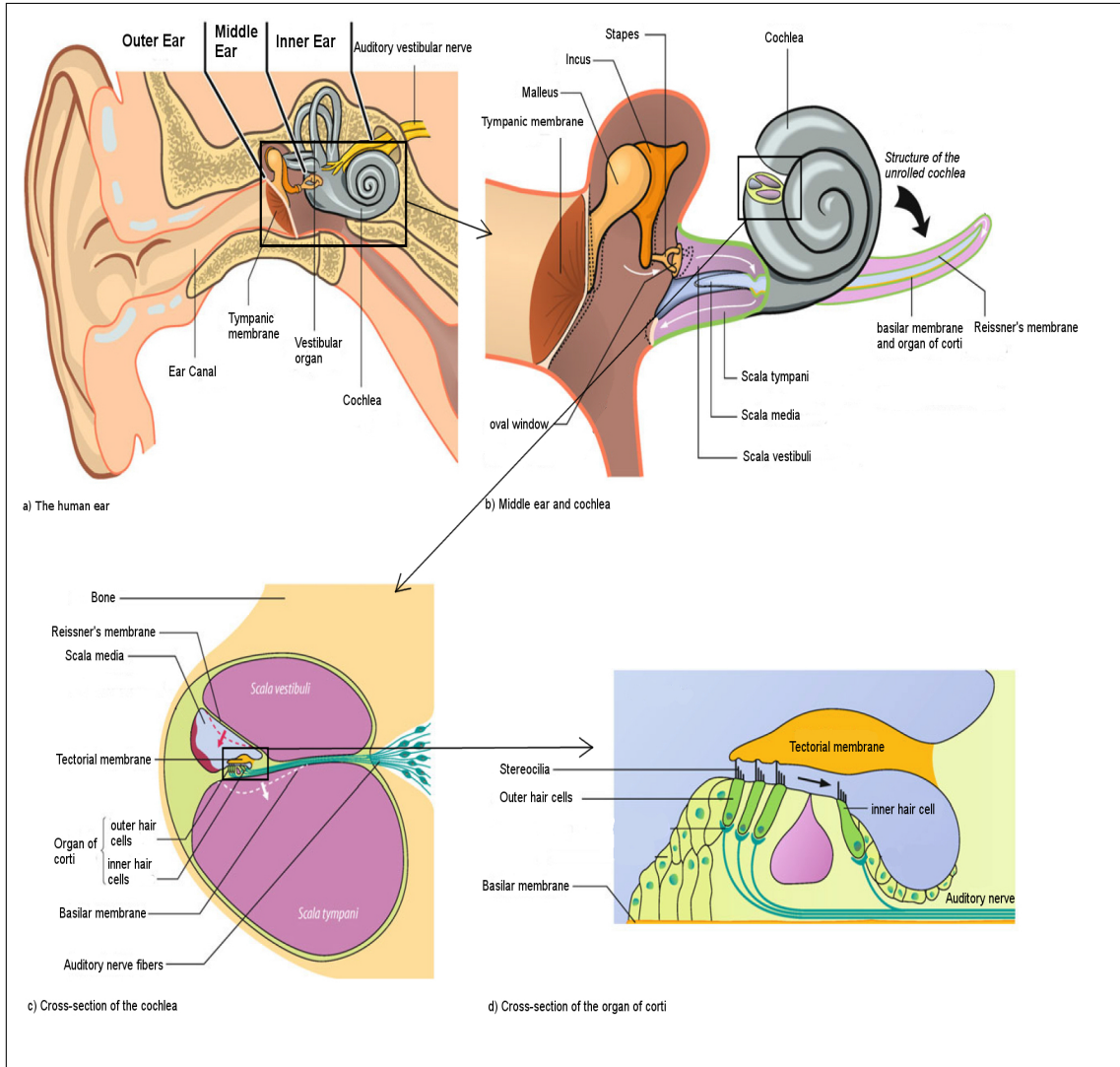


Figure 2.1: Anatomic representation of the ear in different magnifications (Images adapted from Schmidt et al. [2013]).

scala media) [Moller, 2006], where the tissue between scala media and scala tympani is called organ of Corti [Schmidt et al., 2013]. It embeds one row of approximately 3,500 inner hair cells (IHC) and three to five rows of approximately 12,000 outer hair cells (OHC) which are organized along the BM [Dallas, 1992; Moller, 2006] (see Figure 2.1). Based on resulting oscillating pressure differences at the oval window, caused by received and transmitted sound waves, a traveling wave is created on the BM [Kandel et al., 2000]. The longitudinal stiffness of the BM varies (the basal end is stiffer than the apex), facilitating an anatomical and natural spectrum analyzer [Moller, 2006]. High frequencies are processed on the basal end and low frequencies on the apical end, overall giving sensitivity for frequencies in the range of 20 Hz to 20 kHz in humans (see Figure 2.2A). The movement of the BM is passed to the

2.2 The Human Auditory System

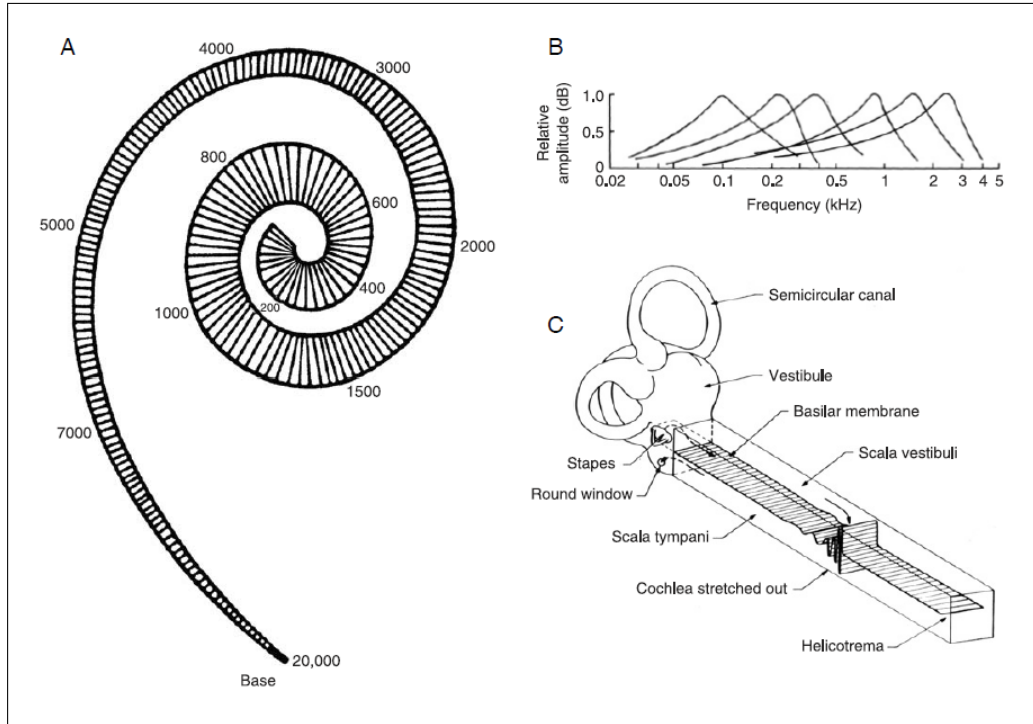


Figure 2.2: A) The tonotopic cochlea processing high frequencies at the base and low frequencies at the apex. B) Resulting vibration amplitudes at different locations along the BM in dependence of spectral information. C) The uncoiled cochlea enclosing the propagating traveling wave, which is heading to the apex of the BM. (Pictures adapted from Moller [2006])

organ of corti and the tectorial membrane, which is in touch with the stereocilia of the OHC [Kandel et al., 2000] (Figure 2.1). The OHC are responsible for modifying the vibration of the BM and increasing the frequency selectivity, especially in low intensities, serving as an inner cochlear amplifier. Contrarily, the IHC responsible for transforming the vibration of the BM into neural code [Moller, 2006]. The stereocilia of the IHC move from side to side with the movement of the BM, causing inner ion channels to pass positively charged potassium ions. A change in the bioelectric voltage occurs, further causing the release of neurotransmitters that produce an electrical impulse at the AN [Eysenck, 2004]. According to Kandel et al. [2000], each IHC is sensitive to a certain and characteristic frequency (tonotopic organization, depicted in Figure 2.2). Because each neuron of the AN is innervated by one IHC, the neurons share this characteristic excitement based on certain frequencies [Birbaumer et al., 2006]. As the hair cells release transmitter only when depolarized, the connected AN fibres fire only during positive phases of the sound, thus the firing pattern reflects the waveform of the received sound, therefore

providing the contained temporal information (phase-locking). However, this temporal principle of frequency discrimination through phase-locking is only available at low frequencies. Based on the tonotopic organization of the BM, a fine place coding of frequency discrimination is additionally achieved [Moller, 2006; Purves et al., 2004]. In other words, single nerve fibres are tuned to selective frequencies, each having a specific tuning curve. The intensity of a sound stimulus is assumed to be correlated with the number of activated neurons and their firing rates of the AN, thus greater firing rates and more activated IHC represent a larger received sound intensity [Bear et al., 2007].

2.2.2 The Auditory Pathway

The central auditory pathway names the passage from the AN at brainstem-level to the AC [Moller, 2006; Glackin et al., 2010]. It consists of numerous clusters of neurons (nuclei), depicted in Figure 2.3, that are connected via ascending and descending paths.

The **auditory nerve (AN)** connects the cochlea to the auditory brainstem and consists of approximately 30,000, mostly afferent fibres. Afferent fibres are linked to one IHC through one synapse, fewer efferent fibres terminate in multiple OHC [Birbaumer et al., 2006]. Based on the mentioned place coding, frequency information of the received sound is transmitted through a selective spot of excitation of the BM and the corresponding IHC. Through either an increase in the firing rate of the nerve fibres or a greater population of excited nerve fibres the intensity information is transmitted [Clark, 2006]. All afferent fibres terminate in the cochlear nucleus (CN) [Horch and Dhillon, 2004]. The tonotopically organized CN consists of the anteroventral, posteroventral cochlear nuclei and the dorsal CN. While the dorsal CN processes higher frequencies, the ventral CN processes lower frequencies [Celesia and Hickok, 2015]. Interestingly, the functionality of the CI is based on CN stimulation and its tonotopically organization [Horch and Dhillon, 2004]. The superior olivary complex (SOC) can be separated into its medial and lateral part as well as the trapezoid body. The largest and most important part is the medial olive with 10,000 to 12,000 neurons, responsible for frequencies below 8 kHz. The lateral superior olive has 2,400 neurons and a characteristic frequency above 5 kHz [Moore, 1987]. The trapezoid body is quite similar to the lateral

2.2 The Human Auditory System

part of the olive and they are probably connected with each other by a single neural circuit [Moore, 1987]. In the lateral olive, high frequencies are processed in the lateral area and low frequencies in the medial area [Biacabe et al., 2001]. Noteworthy, the **SOC** is the first nuclei along the auditory pathway, that **includes**

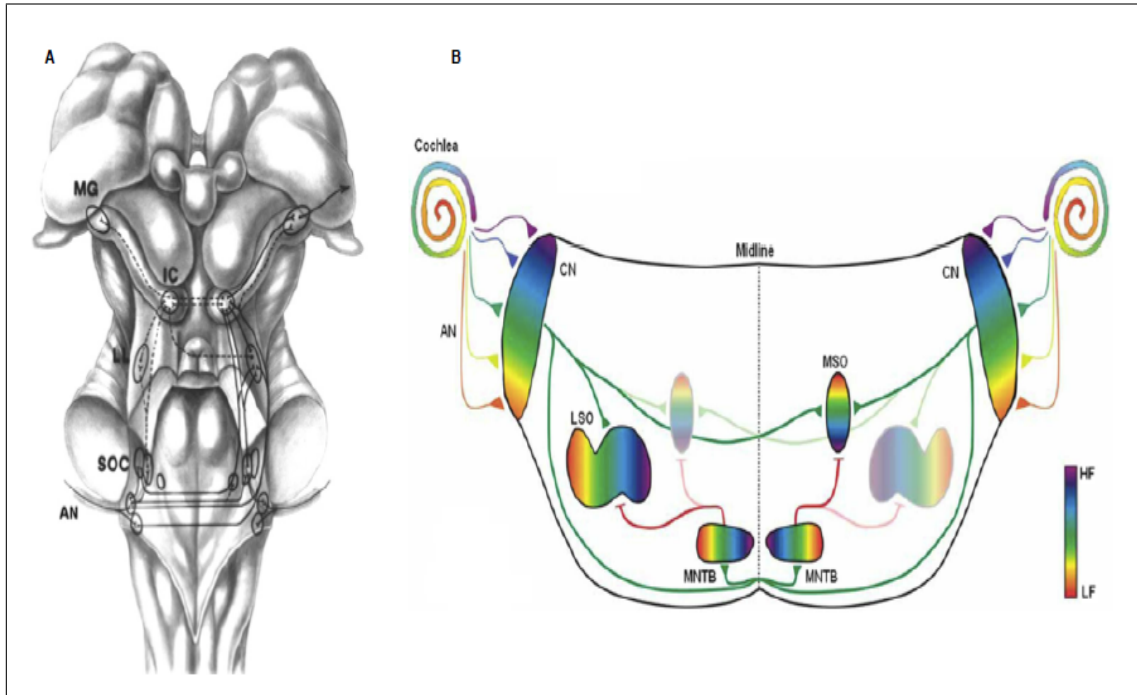


Figure 2.3: A) Schematic Representation of the ascending auditory pathways depicting the anatomical locations of the main nuclei (picture taken from [Moller, 2006]). B) Depiction of the underlying tonotopy, where the locations of spectral information processes are indicated by different colors. (Picture taken from Glackin et al. [2010])

information from both ears [Moller, 2006; McLaughlin et al., 2010] (see Figure 2.3). Therefore it is involved in the **directional hearing** with the medial olive comparing the arrival time of the neural activity, and the lateral olive comparing the intensity difference [Moller, 2006]. The difference in the arrival time is called the interaural time difference (ITD) and the difference in the loudness is called the interaural loudness difference (ILD) (see section 2.3). The fibres from the SOC join the ascending fibres from the CN to form the lateral lemniscus (LL) [Glendenning et al., 1981]. The LL can be divided into the ventral and the dorsal LL [Moore, 1987]. While the dorsal part receives input from both ears, the ventral part only processes information from the contralateral ear [Roeser et al., 2011]. This nuclei has about 200,000 fibers [Augustine, 2014] and is again tonotopically organized [Clark, 2006]. The inferior colliculus (IC) is the largest nuclei in the auditory

2.2 The Human Auditory System

brainstem and almost all ascending pathways synapse in it. It is divided into the central IC and the external IC. The central IC is connected to both sides of the brainstem, consequently being important for interaural processing [Moller, 2006]. The central IC is well organized with purely auditory fibres, while the external IC surrounds the central IC and is composed of auditory and somatosensory fibres [Moller, 2006]. The IC is important for frequency discrimination [Clark, 2006] and is tonotopically organized, where high frequencies are processed ventral and low frequencies dorsal [Moller, 2006]. However, the exact neural architecture of the auditory pathway as well as individual tasks and responsibilities of single nuclei are still discussed.

2.3 Human Hearing

2.3.1 Perception

In general, sound is a vibration that travels as an audible wave of pressure through a transmission medium and is described by waveform, amplitude, phase and frequency [Purves et al., 2004]. There are two major requirements for sound waves: vibratory disturbance and an elastic medium (i.e., air, liquids, and solids) [Hering et al., 2012]. The most rudimentary form of a sound wave is a pure tone consisting of a single vibratory frequency. However, sound waves from natural sound sources, like human speech, are very complex. They can be described as a summation of a multiplicity of pure tones varying in their describing parameters. In sound and speech perception, major information is carried by **spectral information**. The lowest frequency in the signal is related to the pitch of the received sound, whereas subsequent peaks in the spectrum are called formants [Newman, 2010]. Formant structure and their relative distance are different for varying speech sounds [Abrams, 2008]. The frequency range of normal hearing (NH) humans is about 20 Hz to 20 kHz, while human speech covers the spectral area from approximately 100 Hz to 8 kHz [Madell and Flexer, 2013]. The received **sounds intensity** and level is related to the amplitude of the received sound pressure [Purves et al., 2004]. Importantly, the sound level perceived by the listener is, however, referred to as **loudness** which differs from the actual sounds amplitude. The loudness of a perceived sound, therefore, depends on its intensity in combination with its frequency. which differs from the actual sounds amplitude. The loudness of a perceived sound, therefore, depends on its intensity in combination with its frequency. For example, a pure tone, having a level of 20 dB sound pressure level (SPL) at 1 kHz, is perceived louder than a pure tone at 250 Hz with the same intensity [Moore et al., 2010]. The psychophysical unit phon supportingly matches the perceived loudness to the physical intensity of a pure tone. Here, at a reference frequency of a pure tone at 1 kHz, both units always match in value. At all other audible frequencies, the phone describes the relative ratio between the perceived sounds loudness and the actual intensity [Hartmann, 2004; International Organization for Standardization, 2014], where the resulting linearization is measured in dB hearing level (HL). Another often used measure is the dB sensation level, which reflects the individual hearing threshold for each subject and for each type of stimulus [Hall, 2007].

2.3.2 Processing Cues

Since sound has no spatial dimension, the human auditory system has mainly to focus on frequency resolution [Eysenck, 2004]. Therefore, humans use the information provided by the interaction of the incoming sound with their body and ears to localize the source of sound signals. Utilizing such localization cues, which offer the human to locate the sound source to some extent, distinctions are made between monaural and binaural localization cues. More precisely, **monaural cues** are responsible for localization of sources in the vertical plane, while binaural cues provide information about the position of the sound source in the horizontal plane [Moore et al., 2010]. To determine a sound source location, both important cues are merged [Moore et al., 2010]. As shown in Section 2.2, received sounds interact with the human body and ears, whereas the ears act as a filter toward the sound signal, collecting frequency specific modifications in the amplitude and phase characteristics [Grothe et al., 2010]. The resulting changes in the collected spectrum can be described by an acoustic transfer function, called the head related transfer function. This function strongly depends on the origin of the sound, its spatial direction, and the individual anatomic dimensions of body and pinna. This results in subjective transfer functions for different sound source locations and for different individuals [Meddis et al., 2010]. Thus, in monaural cues, specific notches in the sounds spectrum, which change as the location of the source shifts in elevation, are exploited [Grothe et al., 2010]. Furthermore, sources in front and/or back can be discriminated [Meddis et al., 2010]. **Binaural localization cues** are based on the comparison of the sound signals received by both ears, interpreting the **interaural time difference (ITD)** and the interaural loudness difference (ILD). The time difference between the arrivals of sound wavefronts at the ears is called the ITDs, described by the received onset (onset ITD) and during the receiving of a sound (ongoing ITD). One can imagine, that a sound collected from an angle of $\pm 90^\circ$ to the head needs longer to reach the contralateral ear, causing a received delay of the same sound. On the other hand, a sound originated in the front creates no ITD. In other words, ITDs vary with the azimuthal position of the sound source, thus different angles are reflected by corresponding ITDs, respectively. The physiological range of ITDs depends on the maximum perceivable time difference, that appears when the sound source is directly to left or right of the receiving person. The maximal perceivable ITD in adults is about $\pm 600 \mu\text{s}$,

2.3 Human Hearing

whereas the smallest discriminable stepsize is about $10\text{-}20\ \mu\text{s}$ [Campbell and King, 2004]. This is remarkable, because the duration of an action potential is about 50 times longer in comparison, necessitating high precision phase-lock encoding between the ears [Joris and Yin, 2007].

A basic model regarding the process of detecting and interpreting ITDs was given by Jeffress [1948], where coincidence detectors are triggered depending on the neuronal latency to decode the source position in space (see Figure 2.4). When

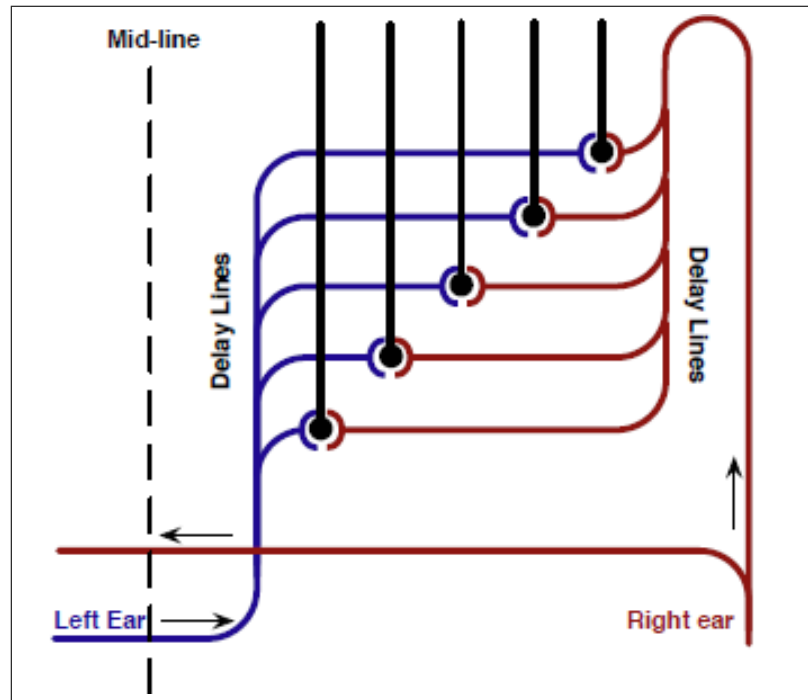


Figure 2.4: Jeffress model for the right brain hemisphere, where red axons coming from the right and blue axons coming from the left ear collide in coincidence detectors (denoted by black dots). (Picture modified and taken from Joris et al. [1998])

analyzing the fine structure of incoming sound, the ongoing ITD seems even more important for the localization than the onset ITD, since it stores interaural phase information [Buell et al., 1991]. Besides the ITD itself, the frequency of sound is critical. If the wavelength of the signal is shorter than twice the distance between both ears, ongoing phase differences between signals received at both ears cannot be discriminated clearly, thus a source determination is not possible. Only sounds below 1.4 kHz provide useful ITD information for sound source localization, due to interaural phase differences [Buser and Imbert, 1992]. Additionally, phase-lock encoding is only available for frequencies below 3-5 kHz [Purves et al., 2004]. By contrast, at higher frequencies analyzing the ILDs is necessary [Jeffress, 1948;

Baars and Gage, 2010], because when sounds arrive from an angle, an acoustic shadow constituted by the human head cause the sounds reaching the near ear to be louder than at the contralateral ear. This effect depends on the frequency, especially the associated wavelength, of a sound. Sounds are most likely to be reflected by the head, when their wavelength is small compared to the width of the head. Frequencies with a larger wavelength can therefore bend around the head causing no significant ILD. Today's literature offers a critical frequency-range of approximately 1.5-2.0 kHz [Roeser et al., 2011; Purves et al., 2004]. Thus, the maximum ILD is achieved when the sound arrives from an azimuth angle of $\pm 90^\circ$, but it equals zero when the sound source is located directly in front, above or behind the receiving person. As a result, high frequency sounds can be localized in the horizontal plane utilizing the perceived ILD.

2.3.3 Hearing Loss and Deafness

People with hearing loss (HLo) have a particular loss in the ability to hear a certain range of frequencies (i.e., elevated hearing thresholds in these frequencies), in which deafness is the most extreme version, where the loss does not allow anymore sound perception even when amplified [Elzouki et al., 2012]. A loss can be ranked as slight (16-25 dB HL), mild (26-40 dB HL), moderate (41-54 dB HL), moderately severe (55-70 dB HL), severe (71-90 dB HL), profound (≥ 91 dB HL), and totally deaf (no sound perception) [Elzouki et al., 2012]. A generally disabling HLo is defined as a loss greater than 40 dB HL in the better hearing ear in adults and a HLo greater than 30 dB HL in children. It can develop at any age and may be caused by many different factors, like genetics, ageing, exposure to noise, infections, and more [Elzouki et al., 2012], where the origin can be categorized as sensorineural, conductive, mixed, and central [Elzouki et al., 2012]. While a sensorineural HLo results from damage of the sensory hair cells of the inner ear or the supplying nerves, a conductive loss is caused by diseases or obstructions in the outer or middle ear, and a mixed loss refers to a combination of conductive and sensorineural loss caused by all anatomical parts of the ear. A central HLo results from damage or impairment of the nerves or nuclei of the central nervous system, either in the pathways to the brain or in the brain itself [Elzouki et al., 2012]. However, most HLos propagate from higher frequencies in the audible spectrum as from lower frequencies [Dillon, 2012; Simpson et al., 2005], detectable by a

2.3 Human Hearing

sloping audiogram. Thus, people with high-frequency HLo have limited access to contents of sounds as well as difficulties in understanding speech in background noise [Simpson, 2009]. This is based on the resulting loss of formant information which is essential for vowel, as well as for consonant recognition. Furthermore, as mentioned in Section 2.3, high frequencies hold important information for sound source localization, thus causing a disability in such cues when missing. Noteworthy are medical disease patterns, which involve HLos in other areas of the audible spectrum [Elzouki et al., 2012].

Of possible help can be the usage of a hearing aid (HA), having the main purpose to amplify inaudible auditory signals [Bernarding, 2015]. However, not all people with high-frequency HLo can benefit from conventional amplification, based on potential acoustic feedback resulting in discomfort prior a sufficient audible amplification on the one hand [Bohnert et al., 2010; Serman et al., 2012]. On the other hand, possible dead regions in the cochlea, causing the actual HLo, cannot be stimulated sufficiently, even when confronted with high amplified sounds [Huss and Moore, 2005]. For more details regarding HAs please see, Hall [2007]; Bernarding [2015]; Klauke et al. [2015]. Fortunately, there are further advanced hearing devices -*like the cochlear implant (CI)*- which take over in such HLo treatments (see Section 2.4).

2.4 The Cochlear Implant

The cochlear implant (CI) brings together a huge branch of professions and combines a multiplicity of research in engineering, medicine and neuroscience as well as signal processing worldwide. It is the only intervention that can restore partial hearing to a totally deafened person via electric stimulation of the residual AN by partially replacing the peripheral auditory system [Zeng, 2004]. Thus, it is **the first man-made device, that restores perception in such a beneficial and incomparable way**. Its initial purpose was to enhance lip-reading and provide sound awareness to deaf people, however, it evolved to a complex multielectrode device that supports even communication via telephone to most of its estimated [The Ear Foundation, 2019]. At present, the three major CI manufacturers are the Advanced Bionics Corp. (a division of Sonova, Swiss), MED-EL (Austria), and Cochlear Ltd. (Australia). However, this achieved artificial perception is based on three fundamental mechanisms [Stevens, 1937; Stevens and Jones, 1939; Jones et al., 1940]. The first relates to the electromechanical effect, where electric stimulation causes the IHC to vibrate, which results in a perceived tonal pitch at the frequency of the corresponding area within the cochlea. The second mechanism relates to the tympanic membranes conversion of the electric signal into an acoustic signal, that causes a tonal pitch perception at the doubled signal frequency. The third one describes the direct electric activation of the AN.

2.4.1 General Requirements

On the one hand, there is the **anatomical and physiological perspective**, where one major issue is to determine which structures need to be intact to guarantee some kind of positive effect in general. Since the outer ear and the middle ear get bypassed by the CI, these can be limited to the integrity of the subsequent AN, auditory pathway, and AC [Zeng, 2004; Mühler and Ziese, 2010]. Thus, without these major structures being intact, there is no potential benefit of using a CI. Note that a well-established technique in audiology, which offers insights into the integrity of the residual AN, is the measurement of auditory event-related potentials (ERPs) at brainstem-level (e.g., brainstem evoked response audiometry (BERA)) [Hall, 2007; Corona-Strauss, 2009]. This method consists of multiple acquisitions of ABRs at different intensity levels and is supportingly

2.4 The Cochlear Implant

used as a preliminary investigation prior a CI implantation [Zeng, 2004]. For more details see Section 2.5.1. However, in a deafened ear, residual AN fibres exhibit unhealthy shrinkage, loss of dendrites and demyelination, whereas electric stimulation has been shown to be a potent instrument of promoting nerve survival [Zeng, 2004]. In contrast to acoustic stimulation, the AN is directly activated by membrane potential changes during electric stimulation. The AN excitation pattern is purely determined by the electric field distribution, the cochlear electrical impedance and the excitability of the nerve tissues rather than passive or active mechanical tuning [Frijns et al., 1996]. Besides, there are two additional differences between acoustic and electric stimulation, producing significant consequences in nerve responses. First, the loss of cochlea compression produces much steeper rate-intensity functions in electric stimulation as in acoustic stimulation [Javel and Sheperd, 2000]. Second, the lack of stochastic synaptic transmission produces highly synchronized firing in electrically stimulated nerves [Litvak et al., 2001]. While the highly synchronized response is potentially contributing to the fine temporal-modulation detection in CI users, contrarily, the steep rate-intensity function is likely to contribute to their demonstrated narrow dynamic range (DR) [Zeng, 2004]. However, the central auditory system shows a great degree of plasticity in response to deprivation of sensory input and its re-introduction via electric stimulation [Kral et al., 2002; Giraud et al., 2001]. For example, in response to such deprivation CN cells shrink, but come back to normal size as a result of electric stimulation [Kral et al., 2002].

On the other hand there is the **audiological and clinical perspective**. The audiologic criteria for CI implantation has continuously relaxed in the last decades. It moved from bilateral total deafness (>100 dB HL) in the 1980s, to severe HLo (≥ 71 dB HL) in the 1990s. By now, it is in the range of suprathreshold speech-based criteria in combination with the individuals' audiometric threshold [Zeng, 2004]. Please note that there are still no strict and unambiguous definitions, which regulate the selection process today, often leaving the decision to personal experiences. Unfortunately supportive is today's lack of reliable and accurate presurgical predictors, which approximate the postsurgical outcome in sound and speech perception. It is known, that different factors like duration and aetiology of deafness as well as presurgical auditory and speech performance correlate with the postsurgical performance [van Dijk et al., 1999; Gomaa et al., 2003],

2.4 The Cochlear Implant

however, there are no significant factors that would allow reliably estimated possible outcomes of the use of a CI. It still remains a problem and needs to be solved. Unsurprisingly, there are no formal or generalized structured rehabilitation protocols, too. Most CI users receive only basic follow-up visits, if any, to adjust the provided electric stimulations. Interestingly, a currently outstanding and unique rehabilitation concept shows the MediClin Bosenberg Kliniken, St. Wendel, Germany. It consists, beside the technical tuning of the processor, of advanced hearing-training, technical education lessons around the implant and devices, as well as training in sound source localization during a stationary residence of the patient for several weeks. However, comparable concepts are rare or not present at all, potentially leaving a beneficial CI, hearing worse or ineffectively. Note that the necessity of such expanded postsurgical rehabilitation schemes not only get supported by educational and linguistic findings. Interestingly, it is shown that early implantation promotes the maturation process in the ACs and furthermore normal language development [Zeng, 2004] and that electric stimulation can restart this maturation process in young children ($\lesssim 7$ years) [Sharma et al., 2002]. Supportingly, language development measures have shown that children implanted with CIs performed significantly better in comparison to not implanted deaf children. They further reached a comparable rate compared to NH children [Svirsky et al., 2000]. However, individual variability is large in terms of both the speed of adaptation and the final average performance [Zeng, 2004].

2.4.2 Technical Inspection

As described in Section 2.2, in NH listeners, sound travels from the outer ear to the cochlea, where it is converted into natural electric pulses. By contrast, a CI bypasses this natural conversion process by directly stimulating the AN with artificial electric pulses, potentially imitating the natural way of hearing [Hall, 2007; Zeng, 2004]. Hence, the CI will have to mimic and replace auditory functions of the external as well as the internal ear. Noteworthy, all CI systems share features like a microphone that picks up the sound, a sound processor that converts the sound into electrical stimulation patterns and transfers them to the implant, and an electrode array that is inserted into the cochlea [Loizon, 1998]. The electrodes stimulate the AN connected to the central nervous system, where the electrical pulses can be interpreted as sounds. Although the specific components and designs

2.4 The Cochlear Implant

may be different among the implant manufacturers, the general working principles are the same [Mühler and Ziese, 2010]. Figure 2.5 depicts a modern CI with the sound processor worn behind the ear.

The **sound processor** (or speech processor), is the fundamental operating core that extracts acoustic features specifically, codes them and sends the resulting electrical stimulation patterns alongside the required power wireless to the implant (see Figure 2.5). According to Zeng [2004]; Mühler and Ziese [2010]; Loizon [1998];

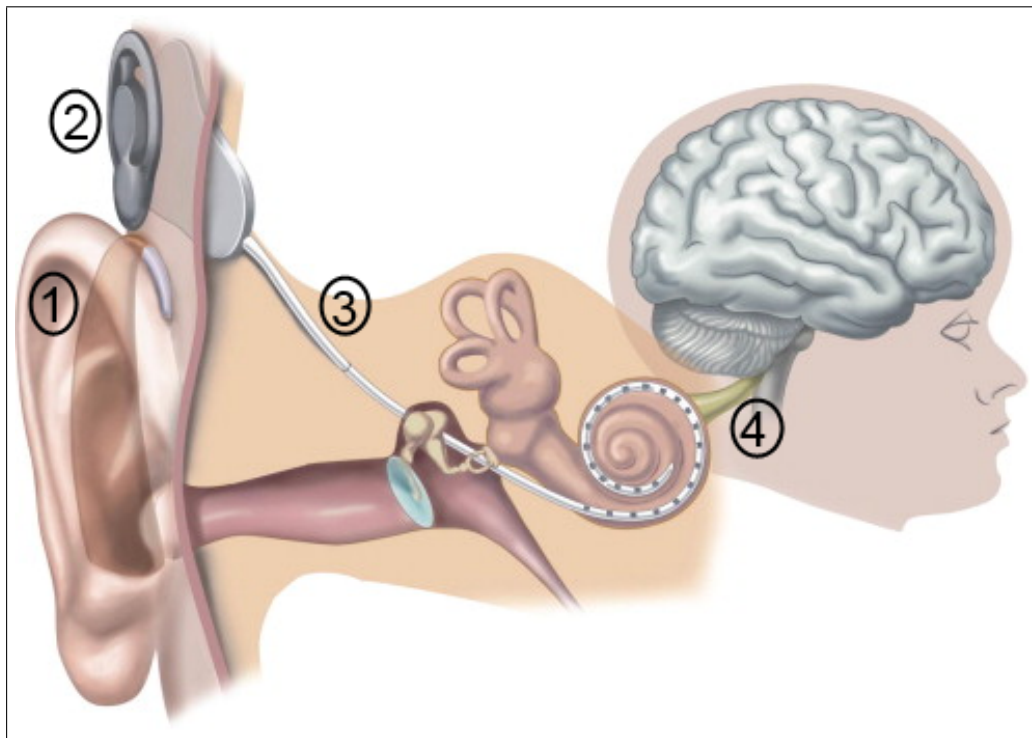


Figure 2.5: Schematic representation of a cochlear implant system with the sound processor (1), the transmission coil (2), the implant with the electrode array (3), and the AN (4). (Picture adopted and modified from Kral [2013])

Clark et al. [1984], implemented filter-banks divide received sounds or speech into different frequency bands partially mimicking the tonotopic organization of the cochlea (see Section 2.2). However, systems distinguish in processing strategies to extract, encode, and deliver the appropriate features. Here, the **stimulation strategy**, responsible for converting the received sounds into electric stimulation patterns, plays an extremely important role by arranging the activations of electrodes during each processing cycle [Wilson et al., 1991; Kiefer et al., 2001; Koch et al., 2004; Wilson and Dorman, 2008]. Consequently, it needs to consider the number of channels selected to mimic the spectrum of the received sound,

2.4 The Cochlear Implant

the number of activated electrodes to establish each channel, the number of necessary processing cycles, and the sequence scheduling. Beyond a doubt, the best stimulation strategy is the one that represents the received sound most closely. Today's most used strategies are the advanced combinational encoder (ACE), the continuous-interleaved-sampling (CIS), and the HiRes120. The ACE strategy is used in the Nucleus implant consisting of 22 individual electrodes. Those generate 22 fixed channels, each representing an individual frequency-band. Based on the extracted envelope of the received sound per cycle, 8-10 frequency bands are activated and the corresponding electrodes resume the stimulation. Thus, each channel is generated by one single electrode, while the original spectrum of the received sound is spanned by 8-10 fixed channels [Kiefer et al., 2001]. The CIS strategy is covered by all major CI manufacturers. Each electrode represents a band-pass filter, while the envelopes of these bands are extracted by rectifiers and low-pass filters. However, in the CIS strategy all frequency bands are then stimulated within one processing cycle using biphasic pulses modulated with extracted sound envelopes. Thus, each channel is generated by one single electrode, while the original spectrum of the received sound is spanned by all active electrodes [Wilson et al., 1991]. However, due to limitations in electrode design, these electrodes can only excite a small portion of auditory nerve fibers, thus only a limited stimulation selectivity can be achieved. One possibility is to introduce virtual channels [Donaldson et al., 2005]. This technique is obtained by current steering provoked by two adjacent electrodes to control the intermediate electrical interaction, therefore it allows for a more precise stimulation space [Donaldson et al., 2005]. Today, this technique is implemented in the HiRes120 strategy (Advanced Bionics Corp.), which allows for 120 virtual channels based on independent power sourcing [Koch et al., 2004]. The up to date implant of the Advanced Bionics Corp. consists of 16 electrodes represented by 15 band-pass filters (15 possible pairs) [Koch et al., 2004].

Furthermore, there is the **implant holding the electrode array**. The implants from all manufacturers share the general design consisting of hermetically closed electronics (due to biocompatibility and -stability), a transmitting coil, a magnet and an electrode array [Mühler and Ziese, 2010]. There is no electrically conductive connection between the sound processor and the implant nor does it contain a power source, thus it remains passive. The information as well as the

2.4 The Cochlear Implant

energy gets transferred wirelessly and transcutaneously, where the small magnet is used to hold the transmitting coil on the counter side of the skin [Mühler and Ziese, 2010]. However, the major part of the implant is the electrode array and the reference electrode(s). Implant and manufacturer specific, there are 12-22 platinum or platinum-iridium alloy electrodes along an effective length of up to 26 mm on a high flexible silicone carrier with a diameter of less than 1 mm [Mühler and Ziese, 2010; Zeng, 2004]. Figure 2.6 depicts an implanted electrode array inserted into the scala tympani (bottom compartment) of the cochlea. Importantly, the

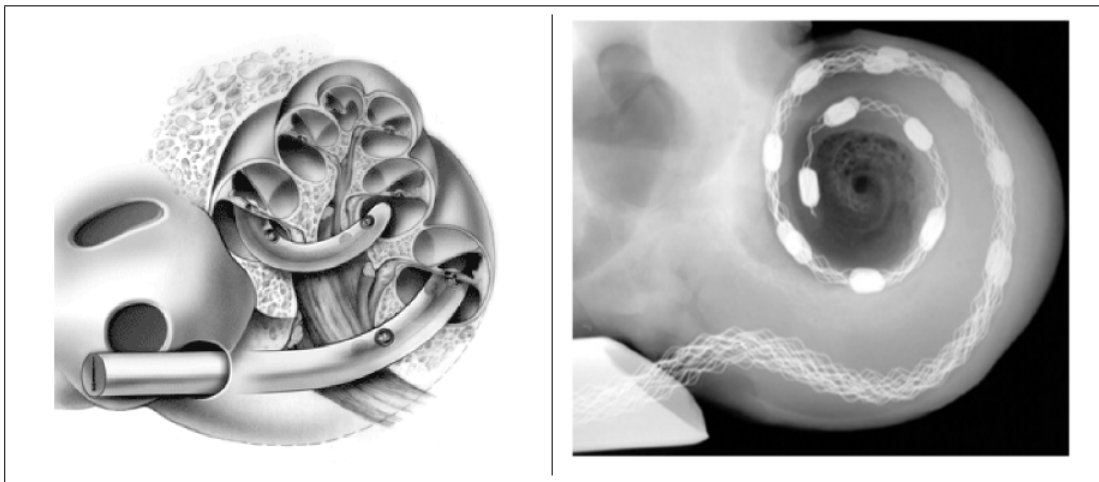


Figure 2.6: Implanted electrode array inside the cochlea. Schematic representation is on the left, whereas a xray depiction is on the right. (Pictures adopted from Mühler and Ziese [2010])

electrode configurations can vary in the mode of monopolar, bipolar, and tripolar stimulation, based on the position of the reference electrode [Zeng, 2004]. In monopolar mode, the return electrode is located outside of the cochlea (usually in the temporalis muscle), whereas in bipolar mode, the return electrode is a neighboring intra-cochlea electrode within the array. In tripolar mode, the return electrodes are two neighboring electrodes, each receiving half of stimulation power. Furthermore, indispensable CI telemetry functions allow accurate monitoring of electrode impedances and measurements of electrical field distributions and nerve activities [Mühler and Ziese, 2010]. Hence, it can detect open and shorted electrodes, what is essential in CI fitting. Note that each implantee has to be individually fitted (or mapped) to ensure a safe and effective electric stimulation [Mühler and Ziese, 2010; Zeng, 2004; Loizon, 1998]. Consequently, the audiologists spend the most time in calibrating current values on each individual electrode to replicate hearing sensations. Typical parameters are the threshold level (T-level)

and most comfortable loudness level (C-level), which span the electric DR, defined by the individuals' subjective sensations '*just audible*' and '*maximum comfortable*'. Thus, the resulting area compresses and maps the input acoustic DR to accommodate the amplitude variations in speech and sounds [Zeng et al., 2002]. Clearly, a compression that causes realistic loudness sensations tends to provide better speech intelligibility and quality [Fu and Shannon, 1998]. However, individual mapping procedures are time consuming and tiring.

2.4.3 Performance

Human communication, summarized as **speech**, consists of three temporal cues processed by NH listeners. The envelope ($\approx 2\text{-}50\text{ Hz}$) is supposedly perceived by temporal mechanisms, the fine structure ($\approx 500\text{-}10,000\text{ Hz}$) is likely perceived by spectral mechanisms, whereas the periodicity ($\approx 50\text{-}500\text{ Hz}$) is supposed to be perceived by a combination of both [Hall, 2007]. In a CI, on the other hand, this mechanisms of extracting and encoding temporal cues need to be artificially implemented. The temporal envelope information, for instance, is obtained by rectifying and low-pass filtering the received sound [Zeng, 2004]. Although theoretically possible, periodicity and fine-structure information cannot be extracted similarly based on perceptual limitations of amplitude modulations [Zeng, 2004]. However, speech recognition has been systematically measured by comparing the number of spectral bands in NH listeners against the number of electrodes in CIs [Shannon et al., 1995; Friesen et al., 1999]. Surprisingly, even using high-context speech materials, temporal envelope cues based on only three spectral bands are sufficient to support speech intelligibility. This indicates a potential gain in CI speech recognition when utilizing three or more channels, however, it flattens in slope when utilizing 16 or more bands [Zeng, 2004].

The wide individual variability in CIs outcome performance can not only be described by anatomical, technical, or psychophysical factors. Additionally, individuals' **cognitive factors** like learning, memory, and information processing contribute to the large spread shown by CIs. Today, in quiet situations CI users can potentially catch listening scores demonstrated by NH listeners, but this behavior is not automatically shown by every individual user [Zeng, 2004]. Unsurprisingly, several other cognitive measures such as attention, categorization, learning, and

2.4 The Cochlear Implant

memory have been suggested for assessing the central cognitive processing efficiency in CIs [Zeng, 2004]. For instance, Pisoni and Cleary [2003] account the short-term working memory for the large variability in CIs performance. Besides, learning abilities have shown to additionally impact the outcome, since NH listeners are able to adapt to CI perception [Rosen et al., 1999]. Furthermore, single CI users are able to remember numerous frequency-to-electrode allocations, suggesting that these subjects had learned two or even more sets of maps [Fu et al., 2002]. However, how to account for this large individual performance and variability is still a major problem in ongoing diagnostics and research.

Intensive, spectral, and temporal processing provide critical information regarding stimulation coding in electric hearing, whereas cochlea processing is responsible for auditory perception. Therefore, it is important to compare the **psychophysical performance** between acoustic and electric hearing. For instance, NH listeners feature a 120 dB DR spanned by 200 discriminable steps, whereas a CI user is limited to a narrow DR spanning only a fraction of discriminable steps [Zeng, 2004; Zeng and Shannon, 1999]. While in acoustic hearing, loudness grows as a power function of intensity, in electric hearing loudness grows like an exponential function, likely due to the loss of cochlea processing [Zeng, 2004]. In NH, time coding is based on the phase-lock mechanism caused by an acoustic event. Frequency is encoded spatio-temporal by the cochlea, which is comparable to a filter-bank dividing received sounds into separate bands [Hall, 2007]. Thus, certain frequencies correspond to different areas of the BM (see Section 2.3). In CIs, time coding is mimicked by varying the stimulation rate, which is limited to a narrow range. Importantly, place coding is approximated by electrode positions, affected by differences in electrode insertion depth, electrode dimensions, used device, nerve survival patterns, and more [Zeng, 2004]. NH listeners temporal integration function slopes ≈ 3 dB per doubling duration in the range of 100-200 ms, whereas CI implantees show a much shallower slope, most likely due to the loss of cochlea compression [Donaldson et al., 1997]. A beneficial consequence in temporal processing allows CI users to detect smaller amplitude modulations and eventually outperform NH listeners [Shannon, 1992]. Furthermore, traditional measures in temporal processing including temporal integrations, gap detections, and temporal modulation transfer functions suggest that CI users can reach a performance state in quiet listening situations comparable to NH listeners [Donaldson et al., 1997].

2.4 The Cochlear Implant

However, today's most important unsolved task is to quantify the binaural processing capability in CIs, since a proper coordinated binaural sensation (i.e., matching in time, place, and excitation level) is essential in hearing processing cues (see Section 2.3.2). Long et al. [2003] suggests, that people with bilateral CIs rather use ILDs, but less effectively than the ITDs by NH listeners, since binaural pitch sensations are required to match. So far, individuals' benefit when asymmetrically treated (e.g., bimodal listeners) shows high variability [Ching et al., 2007; Guerit et al., 2014]. Factors describing this variability might be the used devices, their fitting, and differences in the amount of residual hearing, whereas variability in implant insertion depth, electrode placement, and cochlear duct length among patients seems rather feasible since it is all but impossible to binaurally activate nerve fibers with a similar frequency-to-place allocation [Guerit et al., 2014]. Today's clinical standard across CI implantees, however, is a device based frequency-to-electrode allocation, assuming that the brain can adapt and balance small mismatches in perceived pitch sensations [Skinner et al., 2002]. However, in case of large mismatches the possibility of a complete adaptation gets challenged [Rosen et al., 1999; Siciliano et al., 2010; Kan et al., 2013]. Noteworthy, behavioral pitch-matching experiments showed that they are irritating, time consuming, and that they most likely do not offer reliable insights [Carlyon et al., 2010; James et al., 2001; Lin et al., 2013; Francart et al., 2011]. Therefore, objective electroencephalographic measures, like the binaural interaction component (BIC) (see Section 2.5.3), were used to enhance insights into pitch perception in CIs recently [He et al., 2010], but reliable correlations seem far [He et al., 2012]. Summarizing, these findings suggest that the relative electrode positions within the cochlea are important for the binaural hearing in CIs as well as that there is an intense necessity in establishing objective measurements which estimate this individual assessment [Guerit et al., 2014]. **Nevertheless, reliable measurements accounting individuals' time- and place-coding are missing, thus objective CI fitting procedures with respect to binaural interaction and fusion, incorporating precise assessments in perceived ITDs and ILDs, are still unavailable today.**

2.4.4 Trends and Limitations

The CI has ever evolved in the fields of diagnostics and research, which is evidenced by the exponential growth in the patient population and the quantity and quality of scientific research. Future advances in engineering aim to provide significant changes in the next-generation systems, which potentially improve CIs outcome performance. New advances in signal processing strategies eventually allow to extract, encode, and deliver important acoustic features, like spectral and temporal fine structure, in symmetrical and asymmetrical treatment. This will support speech recognition in noise, music appreciation, sound source localization, and sound source segregation, eventually supporting to narrow the wide variety in today's outcome performance across CI implantees [Zeng, 2004]. Of course, **this poses several demands addressed to the CI diagnostics and research, therefore facing an overwhelming variability in inter-implantees' as well as within individuals' performance influencing factors, like presurgical state, surgical efficiency, device type, insertion depth of the array, electrode dimensions, pitch mismatch, device fitting, contralateral hearing condition, etc..** One associated clinical issue is based on the lack of possible post surgical rehabilitation procedures, potentially contributing to the large inter-implantee variability. General fitting protocols alongside monitored rehabilitation schemes are rare. Today, if at all, clinics develop individual procedures causing incomparability across individuals' perceptual learning, cross-modality training, language development, music appreciation, and other cognitive rehabilitations [Zeng, 2004]. Thus, there is a need for a globally unified rehabilitation protocol [Beutner et al., 2018]. A hybrid clinical-technical issue of today is the presurgical evaluation and prediction of the postsurgical outcome performance, like speech recognition performance. Although, a lot of ongoing research using electroencephalographic measures, brain imaging, and cognitive measures address this issue, there is still no accurate and reliable presurgical prediction method and based on the overwhelming amount of influencing factors, a reliable implementation seems far.

Consequently, there is a major need in making these influencing factors reliably accessible. Since subjective and behavioral measurements [Carlyon et al., 2010; James et al., 2001; Lin et al., 2013; Francart et al., 2011]

2.4 The Cochlear Implant

showed to be tedious, time consuming, and imprecise, there is the demand for an objective technical based solution. A promising opportunity to gain such objective insights into inter-implantees variability as well as into the individuals' bilateral imbalance in time and place-coding, could be the electroencephalographic analysis of the individuals' state, but based on employing a more advanced procedure, accompanied problems impair such a solution at least in CIs yet (see Section 2.5) [He et al., 2012]. Thus, this work aims for a suitable and reliable way to access such factors [Schebsdat et al., 2015, 2016, 2017, 2018, 2019; Kohl et al., 2019a,b]. Potentially on the long road, such insights could objectively support CI fitting procedures with respect to binaural interaction and fusion, incorporating precise assessments in the perceived ITDs and ILDs. such fittings strongly depend on the subjective responses, feedback, and the cooperation of the individual CI users, thus special implantees who cannot give reliable feedback (e.g., infants), are automatically handicapped when configuring their electrical hearing. Nevertheless, this negatively affects all unilateral, bimodal, and bilateral CI implantees of all ages today.

2.5 Auditory Evoked Potentials

The term "event-related potential (ERP)" is defined to designate the general class of potentials, that display stable time relationships to a definable reference event [Vaughan, 1969], whereas the auditory evoked potential (AEP), a special form of electroencephalographic ERPs, shows the macroscopic **neural activity of the auditory system in response to an acoustic stimulation**. The evoked reaction of the underlying neural system results in typical waveforms representing changes in voltage distributions [Hall, 2007]. During the last decades, the clinical use of AEPs has increased due to user-friendly recording methods and affordable measurement setups, offering a wide variety of applications, like the estimation of the auditory sensitivity in newborns, diagnosis of inner ear diseases or tumors, pathology in the central auditory system, monitoring during brain surgery, and diagnosis of brain death [Burkard et al., 2007]. The categorizations and the typical waveforms, according to their temporal and spatial appearance along the auditory pathway, are depicted in Figure 2.7. It depicts responses of the stages at brainstem-level (**auditory brainstem response (ABR)**), the auditory pathway (auditory middle-late response (AMLR)), and the AC (auditory late response (ALR)) [Tharpe and Seewald, 2016]. The total duration is between 1 ms and 500 ms, time-locked to the acoustic stimulation, where the temporal gap between presentation of the stimulus and appearance of the wave peaks is called peak latency [Burkard et al., 2007]. Note that deterministic features like the peak latency, the wave morphology, and the small amplitudes ($\approx 1\text{-}10\,\mu\text{V}$) are consequently important parameters to evaluate such responses [Hall, 2007; York, 1990; Karpoff and Labus, 2007]. However, they are additionally superimposed by stochastic signal contaminations like muscle movements and/or electrical noise as well as ongoing electroencephalographic signals. Usually, the multiple obtained transient responses (coined trials) get amplified, bandpass filtered, and averaged. Thereby, averaging exploits in the deterministic behavior of the true responses, where underlying features should occur in a comparable fashion, whereas stochastic noise gets diminished in the resulting mean response [Hall, 2007]. Interestingly, new signal processing methods in AEP analysis showed the benefit of examining time- and frequency-specific correlations among single trials [Haab, 2015; Strauss et al., 2004, 2013]. For instance, such methods allow a fast detection of ABRs even when using low stimulation intensities [Strauss et al., 2004]. Introducing mathematical

2.5 Auditory Evoked Potentials

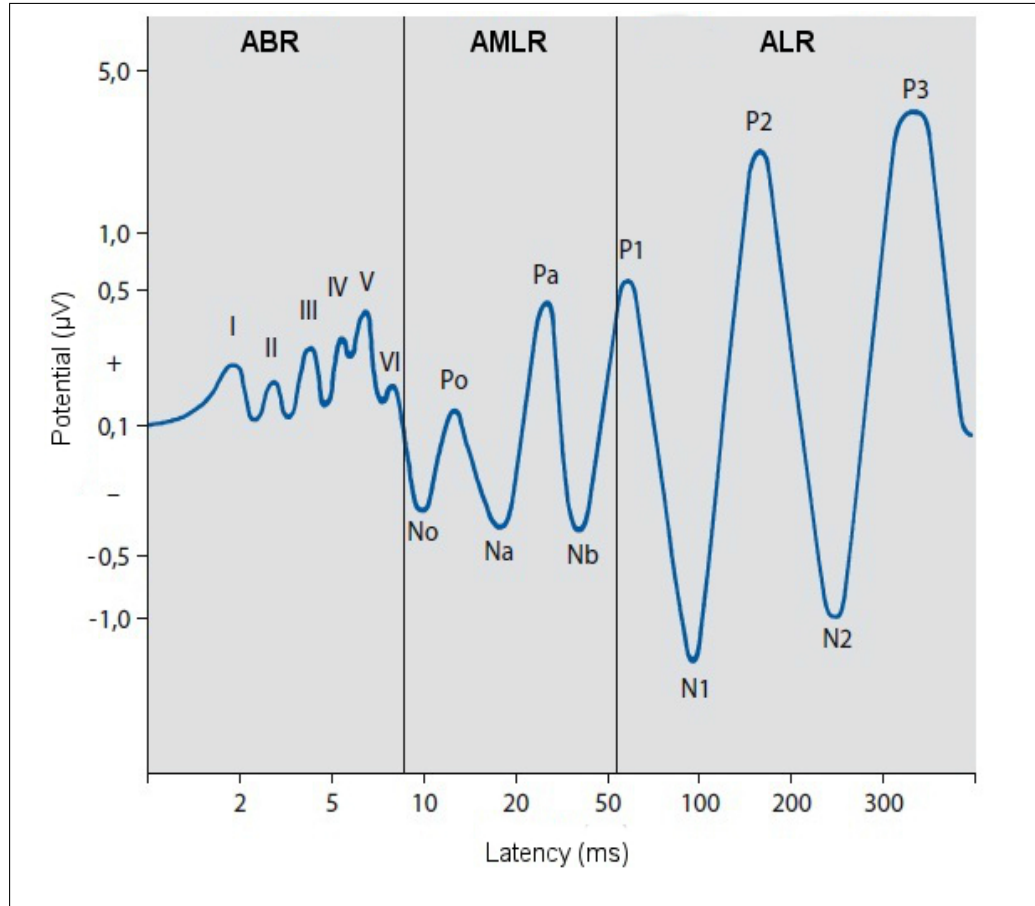


Figure 2.7: Depiction of the early AEP (ABR), middle AEP (AMLR) and late AEP (auditory late response (ALR)). The waves of the ABR are chronologically labeled by roman numerals, whereas the waves of the AMLR as well as of the ALR are labeled by their deflection (positive (P) or negative (N)) in combination with their chronological appearance. (Image modified and taken from Maurer et al. [2005])

transformations (e.g., the gabor transform) the ERP detection can additionally be enhanced [Corona-Strauss et al., 2010, 2009]. Even the extraction of correlates describing individuals' listening effort seems possible [Bernarding et al., 2010, 2011].

However, typical stimulation sounds are clicks and chirps [Hall, 2007; Riedel and Kollmeier, 2002; Dau et al., 2000; Fobel and Dau, 2004]. Since the click has a very short duration of less than a 1 ms and because of its sharp edges and morphology, it includes frequencies up to 10,000 Hz to evoke the most synchronous neural activity [Riedel and Kollmeier, 2002]. The chirp, on the other hand, attempts to compensate the temporal dispersion along the BM [Dau et al., 2000]. Its main stimulation frequency rises from low (≈ 100 Hz) to high ($\approx 10,000$ Hz), probably causing a uniform activation of neurons along the BM [Fobel and Dau,

2.5 Auditory Evoked Potentials

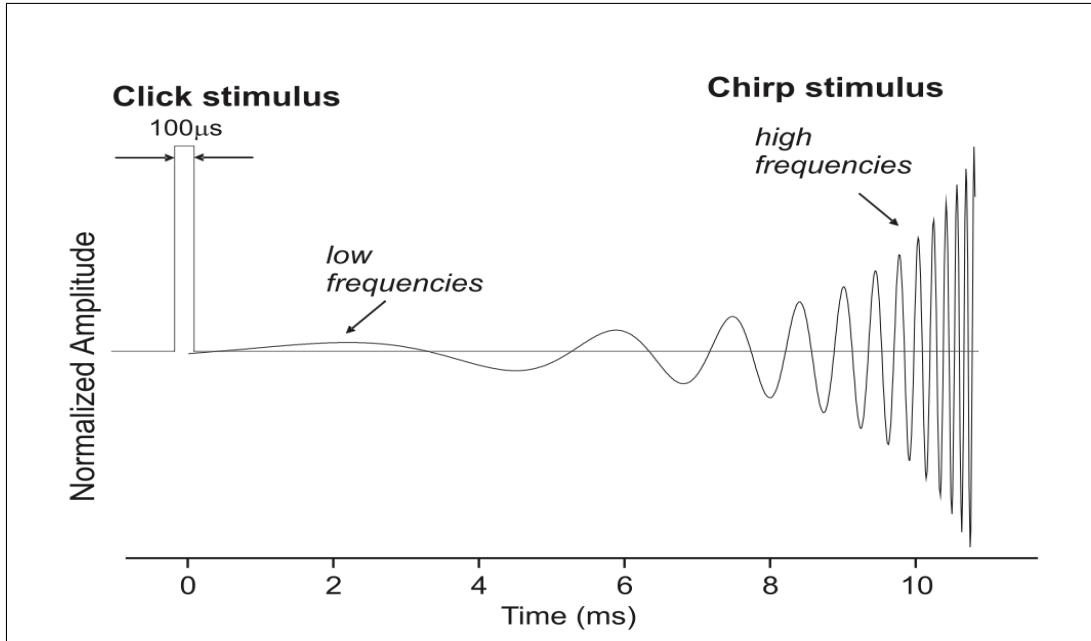


Figure 2.8: Comparison of the click- and chirp-stimuli. The short duration (≤ 1 ms) of the click and its sharp edges and morphology causing a spectral bandwidth of up to 10,000 Hz, therefore causing the most synchronous neural activity along the BM. In the chirp, spectral information shifts from low (100 Hz) to high (10,000 Hz) according to its run-time to compensate for its travelling time along the BM, therefore causing the most uniform neural activity along the BM. (Picture adopted from Corona-Strauss [2009])

2004] (see Figure 2.8). To calibrate the intensity of such real world stimuli, the peak-equivalent method is often used [International Electronic Commission, 2014]. Since real world stimuli are frequency non-stationary signals, one cannot simply control and calibrate their intensity by the use of a sound level meter. Therefore, the SPL of a reference sine (e.g., 1,000 Hz) gets controlled using a sound level meter and adjusted to the wanted intensity. With a digital oscilloscope the resulting peak-to-peak voltage gets measured, thus in the following the amplitude of a real world stimulus can get adjusted to the same voltage level to represent a matched intensity [Corona-Strauss, 2009]. It is then labeled as dB peak-equivalent sound pressure level (pe SPL).

2.5.1 Auditory Brainstem Responses

ABRs are not influenced by most subject states or by most drugs, hence offering the possibility to investigate while the subject is asleep or during operations using anesthesia [Roeser et al., 2011]. Consequently, it is represented in a variety of clinical applications including auditory screening and auditory sensitivity estimations in newborns and difficult-to-test patients as well as to monitor the AN and the auditory brainstem intraoperatively [Burkard et al., 2007]. Interestingly, the BERA, consisting of multiple acquisitions of ABRs at different stimulus intensity levels, is also used as a **preliminary investigation prior to a CI implantation** (see anatomical and physiological demands in Section 2.4) [Hall, 2007; Zeng, 2004]. However, ABRs only allow **insights into the integrity of the ear and the auditory pathway** until brainstem-level [Hall, 2007]. In general, the 10 ms lasting responses are measured utilizing at least three electrodes placed on the vertex (reference), measurement electrode near the ear (mastoid or earlobe), and a ground electrode at the forehead [Atcherson and Stoody, 2012]. As depicted in Figure 2.7, the ABR consists of up to seven characteristic waves labeled chronologically by roman numerals. At a high stimulation intensity, the very first maximum (labeled W_I) usually appears at ≈ 1.5 ms, subsequently followed by other maxima separated about ≈ 1 ms [Atcherson and Stoody, 2012]. However, even today a precise model describing the generation of the prominent responses based on underlying neural generators is not existent [Dau, 2003; David et al., 2006]. So far, it is assumed, that single ABR waves are generated by multiple neural generators, and furthermore, that single generators can contribute to multiple ABR waves [Hall, 2007]. While the W_I is probably contributed by the whole AN, the W_{II} is more associated with its proximal part [Hashimoto et al., 1981]. This was concluded by revisions of the interwave latency, the spatial dimension of the AN, and its slow conduction time [Hashimoto et al., 1981; Hall, 2007]. Interestingly, the W_{III} was found to be generated by the SOC and the CN [Melcher and Kiang, 1996; Moller and Jannetta, 1983], which establish the first binaural information transfer along the auditory pathway (see Section 2.2.2) [Moller, 2006; McLaughlin et al., 2010]. While W_{IV} is assumed to be generated by the SOC [Burkard et al., 2007], findings in intracranial recordings showed that the W_V is likely generated by LL fibers, which lead into the contralateral IC [Hall, 2007]. To sum up, neural generators causing the W_{III} , W_{IV} , and W_V are still not entirely clear, related to the complexity of the underlying

temporal and spatial summation of brainstem activity [Hall, 2007]. Importantly, the stimulus intensity is influencing the resulting ABR waves, where a higher stimulus intensity causes an increase in amplitude and a decrease in latency [Hall, 2007; Corona-Strauss, 2009]. However, based on its robustness, the most prominent peak is the W_V . Often, it is the only observable wave near ABR thresholds [Norrix et al., 2012].

2.5.2 Electrically Evoked Auditory Brainstem Responses

A **more advanced and special form of the ABR** is the electrically evoked auditory brainstem response (EABR) in which the auditory system is **stimulated by electrical pulses** (e.g., by an isolated electrode of the CI implant) [Bahmer et al., 2010; Miller et al., 2008]. Before CI implantation the electrical stimulus is delivered through a needle-electrode placed on the promontory of the ear with transtympanic technique [Hall, 2007], whereas after implantation the stimulus is directly delivered by the electrode of the CI inserted into the scala tympani [Shallop, 1993]. The obtained responses are quite comparable to those obtained by conventional ABR measurements [Hall, 2007; Bahmer et al., 2010; Shallop, 1993], since electrical activations of the auditory system generate neural activity in similar anatomical regions as an acoustical stimulation [van den Honert and Stypulkowski, 1986]. In general, the **responses look similar** but with a more rounded morphology [Abbas and Brown, 1991] and shorter latencies [Gordon, 2007; Thai-Van et al., 2007]. On the one hand, this is caused by the direct stimulation of the neural pathway and on the other hand, by excluding the processing chain from an earphone to the inner ear [Thai-Van et al., 2007]. With increased stimulus intensity, amplitudes increase while latencies decrease as in ABRs [Hall, 2007]. But altered stimulus intensities affect the response latency only little or sometimes not at all [van den Honert and Stypulkowski, 1986], probably due to a more synchronized activation of nerve fibres [Gordon et al., 2003]. The latencies of the single waves also depend on the site of the stimulating electrode, where apical electrodes elicit responses with shorter latencies and larger amplitudes than basal electrodes [Gordon et al., 2007; Firszt et al., 2002]. Besides, the morphology of the EABR depends also on the stimulus rate and type of lead [Clark, 2006]. In Figure 2.9 the differences between an ABR and an EABR are shown. However, exact neural generators are not known so far (see Section 2.5.1). W_I in EABRs

2.5 Auditory Evoked Potentials

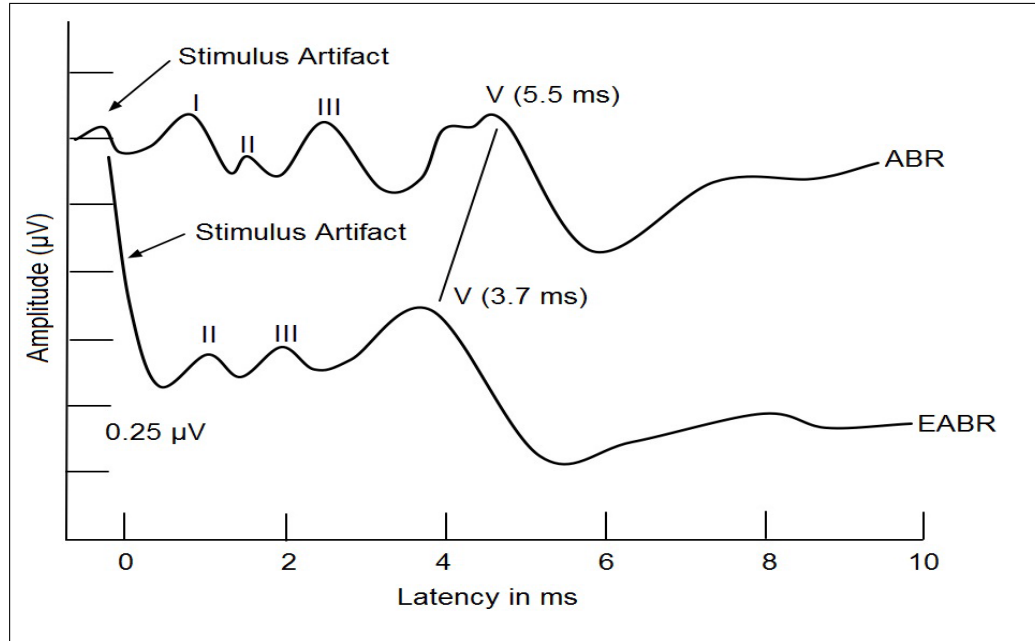


Figure 2.9: Comparison of the electrically (EABRs) and the acoustically evoked brainstem responses (ABRs), both illustrating differences in amplitudes and latencies, where the EABR is shorter in duration and looks more rounded. Note that the superimposing stimulus artifact, which partially overlaps the neural response, consequently challenging their interpretation. (Picture taken and modified from Hall [2007])

is most often superimposed by the latter discussed stimulus artifact, whereas the W_V is also the most robust response component, therefore most of the times being analyzed [Thai-Van et al., 2007; Firszt et al., 2002]. In comparison to ABRs, it is assumed that W_{II} is generated by the AN, W_{III} arises by population of nerves near the CN, and W_V is generated perhaps by neurons of the LL or IC. This is still being discussed, since electrical stimulations lead to specific effects on axonal conduction and synaptic delays [Gordon et al., 2006].

Unfortunately, stimulation parameters and CI configurations, like the electrode array (e.g., longitudinal, radial), stimulation mode (e.g., bipolar, monopolar), time and location of recordings (e.g., pre-, intra- or postoperative), stimulation (e.g., morphology, duration, rate), and recording parameters (e.g., filter settings, amplifier gain, sampling rate), vary a lot across different EABR studies [Firszt et al., 2002; Chatterjee et al., 2006; Bahmer et al., 2010]. So far, **no standardized method and parameters for EABR recordings have been generally established.**

Stimulus Artifact

One major issue when investigating evoked potentials in CI users is the prominent CI artifact, which can **overlap the desired response** pattern, making the interpretation difficult or even impossible especially when considering conventional artifact filtering [Gordon, 2007; Shalloo, 1993]. Thus, a lot of effort is made to establish artifact removal techniques [Sinkiewicz et al., 2017; McLaughlin et al., 2013; Friesen and Picton, 2010; Gilley et al., 2006; Atcherson et al., 2011], where some studies applied short duration stimuli aiming for a mismatch in the overlap time window [Martin, 2007; Gilley et al., 2006], while others applied subtraction techniques to varying evoked responses, whereas the artifact remains constant [Friesen and Picton, 2010; Atcherson et al., 2011]. Besides, designing special recording electrode configurations shows large variability between findings in individuals [Martin, 2007]. While some methods concentrate on single-channel approaches [McLaughlin et al., 2013; Friesen and Picton, 2010], others concentrate on multi-channel approaches (e.g., independent component analysis), therefore holding the threat of falsely characterizing artifacts due to the manual selection processes [Martin, 2007; Gilley et al., 2006; Wong and Gordon, 2009]. Besides artifact removal methods in cortical potentials, there are subtraction techniques for EABRs based on alternating stimulus polarities [Hu et al., 2015]. **However, all methods are missing the actual neural responses (artifact free) for evaluation.**

2.5.3 Binaural Interaction Component

As binaural hearing involves the interaction of both monaural streams of auditory information into an unified auditory percept [Gelfand, 2009], a reliable, **objective quantification** of neurophysiological correlates associated with binaural fusion has a lot of potential applications in both neuroscience research and clinical diagnostics [Mussiek and Chermak, 2007; Moore, 2006]. Therefore, a classic objective measure of binaural interaction at brainstem-level is the resulting BIC in ABRs. It is defined as the arithmetical difference between the sum of both monaurally evoked responses and the binaural response [Jewett, 1970; Stollman et al., 1996; McPherson and Starr, 1993; Hosford et al., 1979]:

$$\text{BIC} = \text{MONO}_{\text{Right}} + \text{MONO}_{\text{Left}} - \text{BIN} \quad (2.5.1)$$

2.5 Auditory Evoked Potentials

The BIC is said to **prove the presence of binaural interaction at brainstem-level** due to the fact that the binaurally evoked response is smaller in amplitude relatively compared to the resulting amplitude of the sum of monaural responses [Jewett, 1970]. Thus, the difference in the amplitudes indicates interaction of ipsi- and contralateral information processing chains at brainstem-level [Ainslie and Boston, 1980; Dobie and Norton, 1980; Shuman, 2008], where the residual peak at the downslope of W_V [Strauss et al., 2004] in the resulting average waveform is often called β -wave. It occurs in the temporal region of W_V due to latency differences between monaural and binaural stimulation responses [Brantberg et al., 1999] with a resulting residual amplitude, that is only a fraction of the original W_V (see Figure 2.10). But for all that, exact underlying processes which cause the latency

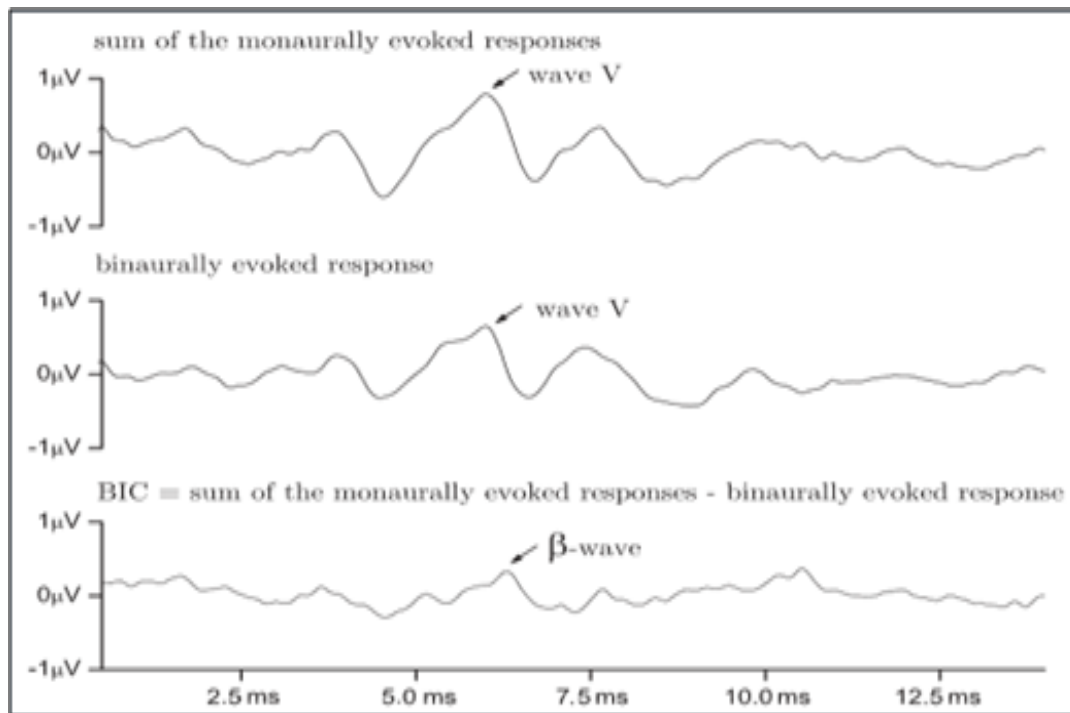


Figure 2.10: Representation of the binaural interaction component (BIC) with the sum of the monaurally evoked brainstem responses (top), the binaurally evoked brainstem response (middle), and the calculated BIC showcasing a small positive deflection in the temporal range of W_V (bottom). The presence of this deflection, often coined β -wave, indicates binaural interaction. (Picture adopted from Strauss et al. [2004])

and amplitude differences are so far not known [Riedel and Kollmeier, 2002; Hall, 2007]. Interestingly, there are suggestions which aim for an adaption of this procedure at higher anatomical regions [McPherson and Starr, 1993]. However, the correlate is **often very difficult (or even impossible) to detect** due to its small amplitude, which is difficult to separate from superimposed background noise

[Hall, 2007], but it is accepted that **interaural lags exceeding 0.6-1 ms will arguably prohibit meaningful integration of binaurally presented information at the brainstem-level altogether** [Bures, 2012; Agmon-Snir et al., 1998; Jeffress, 1948; Strauss et al., 2004].

2.5.4 Comparability and Limitations

The fundamental idea behind developing reliable EABR measurement methods is to achieve objective insights into underlying neurophysiologies, which can then be compared to those of NH listeners [Bahmer et al., 2010; Miller et al., 2008] - and to eventually align them in the future. However, facing such an overwhelming variety of inter-groups' and intra-groups' influencing factors in their respective response acquisition one can call this into question.

Methods aim to limit the spatial excitement of AN fibers in NH listeners by special stimulus-designs [Corona-Strauss et al., 2012], but based on the frequent, deterministic frequency-to-electrode allocation in clinical standards as well as due to limitations in postsurgical pitch-matching procedures (see Section 2.4.3), **a temporal and spatial matching stimulation in NH listeners and CI users seems far**. Especially, since most EABR studies are based on single electrode stimulations and, therefore, being limited to dictated, unknown areas along the BM. **This also prevents from applying stimuli, which are comparable in temporal resolution and morphology, like real world stimuli (e.g., click, chirp)**. Additionally, there is no reference in the individuals' perceived loudness other than their subjective feedback and their respective T- and C-level [Schebsdat et al., 2017], where the latter also strongly depend on previous subjective callbacks (see Section 2.4.2). Furthermore, EABR measurements are **distorted by CI stimulation artifacts**, which can overlap the desired response pattern, strongly challenging their interpretation [Sinkiewicz et al., 2017; Gordon, 2007; Shallop, 1993]. In general, artifact removal techniques are limited in their evaluation value and they lack the artifact free response for evaluation [Sinkiewicz, 2015], thus an adaptation of such methods to eliminate artifacts of whole-array stimulations caused by real world stimuli is not available yet.

Thus, **one can argue that we currently compare responses, which strongly differ in their root stimulus design, their caused stimulation, and their collected responses as well as their signal-to-noise ratio (SNR).** Furthermore, there might be additional limitations, which are not investigated much yet, but become obvious when considering the fundamental working principle of a CI. It is able to restore partial hearing via electric stimulation of the residual AN by partially replacing the peripheral auditory system (see Section 2.4.2) [Zeng, 2004]. Consequently, it might add unknown, technical driven processing delays, which eventually alter the temporal processing chain, consequently affecting binaural ITDs negatively to some extent. These effects are far from being understood, but based on today's method of EABR acquisitions, which obviously do not incorporate the full processing chain of a CI, reliable insights that include such information are restricted. **Note that while in current EABR measurements the stimulation is provided directly, therefore potentially bypassing intrinsic technical processes (e.g., filter-banks), this does not represent an individual CI users' daily-life perception, where the microphone collects incoming sounds, the sound processor translates them into stimulation patterns, and the implant involving all active electrodes stimulate the AN (see Section 2.4.2).** This seems to be a substantial lack of knowledge and techniques, especially when taking recent neurobiological and neuromodeling research into account. Those emphasize the necessity of a high spatiotemporal precision of neural coincidence detection circuit activations to mediate binaural interaction (see Section 2.3.2) [Bures, 2012; Agmon-Snir et al., 1998; Jeffress, 1948]. Supportingly, Zirn et al. [2015] recently demonstrated that both hearing devices negatively affect the natural auditory processing chain by **adding processing delays ranging well into the milliseconds** and confirmed a beneficial enhancement in binaural localization cues using subjective behavioral tests when device-specifically compensating asynchronous technical delays [Zirn et al., 2019]. These insights are crucial, because the ITD is a fundamental cue necessary for the previously mentioned binaural fusion [Jeffress, 1948], where interaural lags exceeding 0.6-1 ms will arguably prohibit meaningful integration of binaurally presented information at the brainstem-level altogether [Bures, 2012; Agmon-Snir et al., 1998; Jeffress, 1948] (see Section 2.5.3). **Thus, rendering ITD-based auditory cues useless in asymmetric treatment conditions without careful interaural delay compensation,** which is technically realizable by appropriately delaying the leading hearing device [Zirn

2.5 Auditory Evoked Potentials

et al., 2015, 2019; Wess et al., 2017]. Consequently, to accomplish more comparable insights including the real processing chains in both groups, one needs to equalize stimulation conditions as far as possible, where it is mandatory to encompass device-specific technical latencies [Zirn et al., 2015, 2019]. However, respective values are limited in literature or data sheets [Zirn et al., 2015, 2019; Wess et al., 2017].

2.6 Contributions of this Work

In the previous Sections, we covered the anatomy and physiology of the NH human auditory system, which collects incoming physical sound waves using the outer ear in combination with the tympanic membrane and preprocesses the absorbed information characteristics to be able to get translated into neural activity using the hair cells embedded in the BM of the cochlea [Dallas, 1992; Buchner and Armbruster, 2005]. Based on its underlying fine place coding mechanism, first frequency discrimination is achieved, contents are further transferred, employing the AN connected to the auditory brainstem [Moller, 2006]. Although the complex architecture and underlying neurophysiological details of this tonotopically organized stage of the auditory pathway are still being discussed [Birbaumer et al., 2006; Horch and Dhillon, 2004; Moore, 1987; Clark, 2006], it is known that it establishes first processing in auditory perception and localization cues [Moore et al., 2010; Meddis et al., 2010; Campbell and King, 2004], besides serving as a neurological information transfer interface connected to upper brainstem-level stages and the AC. The interaction [Jeffress, 1948] of binaural information streams in the temporal range of microseconds [Campbell and King, 2004], consequently forming an unified binaural percept (Binaural Fusion), seems to play an initial and crucial role in NH auditory perception when processing such cues [Buell et al., 1991]. However, we also introduced the consequences when people suffer from HLos, the associated annual global costs of several hundred billions of US\$, and the proposed negative trend based on recreational settings. The CI, the only intervention that can restore partial hearing via electric stimulation of the residual AN, demonstrated promising benefits in the last years, even when suffering from severe-disabling HLos. Therefore, it partially replaces the peripheral auditory system, what suggests to alter the auditory processing chain to some extent [Zirn et al., 2015, 2019], but shares the component of a sound collecting membrane embedded in the microphone.

Since the analysis of ABRs, a special form of electroencephalographic ERPs, demonstrated a reliable method to gain insights into the neurophysiology and integrity of the auditory brainstem and pathway, a lot of efforts were made to accomplish similar insights in CI implantees. These cover the basic stimulation principle (compare [Fobel and Dau, 2004] and [Bahmer et al., 2010]), the actual stimulation method of the AN (compare [Corona-Strauss, 2009] and [Firszt et al.,

2002; Chatterjee et al., 2006; Bahmer et al., 2010]) as well as the response processing influenced by stimulation artifacts [Hu et al., 2015], unfortunately facing an overwhelming degree of freedom based on inter- and intra-groups' influencing factors, therefore limiting their comparability. One can imagine that, to accomplish such comparable insights including the real processing chains in both groups, the amount of influencers needs to be reduced eventually by trying to equalize stimulation conditions as far as possible in the first place. Interestingly, promising and comparable details both processing chains share are the sound collecting membranes, like the tympanic membrane in NH listeners (see Section 2.2) and the microphone of the sound processor in CIs (see Section 2.4.2). Adjusting perspectives in problem analysis, one can hypothesize that **free-field (i.e., acoustic stimulus is transmitted via air) evoked ABRs could potentially offer such insights**, since the collected responses represent the real world listening conditions in both groups rather than customized EABRs. Even if the acoustic stimulus gets distorted during its travel period, both membranes would receive an equal resulting stimulus version as long as the system is sufficiently calibrated and benchmarked, supporting the robustness of such an approach. Consequently, this will result in altered ERP morphologies which need to be analyzed, however, both groups responses will consequently share the same underlying cause while incorporating their total processing chain, making these responses, in fact comparable. Note that this approach also faces distortion of stimulation artifacts in CIs, but since altered response morphologies are additionally expected based on the unique way of stimulation, this invites unique approaches in signal processing. **Therefore, it is the first major contribution of this work to analyze and interpret free-field auditory evoked brainstem responses of CI implantees while applying new filtering and signal processing techniques (Study 1 in Section 3.2).**

Besides CI implantation comes the demand of evaluating the implementation as well as the potential benefit. Especially, when considering potentially implemented device based latency alterations of the auditory processing chain ranging well into the milliseconds eventually affecting binaural cues altogether [Zirn et al., 2015, 2019; Wess et al., 2017]. Behavioral tests showed that they are irritating, time consuming, and that they most likely do not offer reliable insights [Carlyon et al., 2010; James et al., 2001; Lin et al., 2013; Francart et al., 2011], therefore

raising the demand for objective insights. As a potential solution, there is **the objective measure and detection of binaural interaction at brainstem-level**, therefore analyzing the BIC derived from objective, electroencephalographic ABR measurements [Jeffress, 1948]. Unsupportive, expected differential amplitudes are less than a microvolt [McPherson and Starr, 1993] consequently demanding good SNRs of the analyzed responses, thus such investigations in CI users get challenged. This occurs especially when considering differences in response morphologies, the superimposing stimulation artifact, and unknown technical driven processing delays. When conventionally averaging ABRs, this will cause an uncomfortable amount of trials and measurement length to encompass sufficient SNRs [Delgado and Özdamar, 2004], furthermore, when aiming for synchronous investigations of upper brainstem-level stages [McPherson and Starr, 1993; Hall, 2007; Tharpe and Seewald, 2016]. Unfortunately, a necessary solution to investigate neural correlates exceeding isolated stages in CI implantees is unavailable yet. Various methods to reduce the acquisition time by disentangling overlapping ERPs obtained at higher stimulation rates have been proposed [Bardy et al., 2014; Delgado and Özdamar, 2004; Wang et al., 2006; Woldorff, 1993], where most of them focus on deconvolution approaches. The continuous-loop (averaging) deconvolution (CL(A)D) method showed to be promising when obtaining high-quality ABRs alongside AMLRs simultaneously to high stimulation rates [Holt and Özdamar, 2014, 2016]. **Therefore, it is the second major contribution of this work to investigate binaural interaction at brainstem-level and upper level stages while applying new stimulation, filtering, and deconvolution based signal processing techniques as well as changes in interaction when carefully compensating device based ITDs in bimodal users (Study 2 in Section 3.3).**

Please note that results of both studies are partially published in Schebsdat et al. [2015, 2016, 2018, 2019]; Kohl et al. [2019a,b].

3 Materials and Methods

3.1 Ethics Statement and Participant Recruitment

All studies of this thesis involving measurements in human adults were performed in accordance to the Declaration of Helsinki and were approved as scientific studies by the local ethics committee (Ärztchamber des Saarlandes; Medical Council of the Saarland, Germany). All participants were informed about the content of the individual study in a one-to-one appointment prior actual measurements. The procedures were explained aurally and all questions of the participants related to the procedure and the consent form were answered in detail. After this, all participants provided written informed consent for the investigations and the subsequent data analysis. All measurements were conducted at the MediClin Bosenberg Kliniken, St.Wendel, Germany, as well as at the University of Applied Sciences (htw saar), Saarbrücken, Germany, and were performed on control-groups represented by NH listeners and on patient-groups represented by CI implantees. All with no further neurological disorders.

3.2 Study 1: Neural Correlates of Free-Field Evoked Auditory Brainstem Responses in Cochlear Implant Users

It is the aim of this study to introduce a novel method that offers the interpretation of narrowband filtered neural correlates of free-field evoked ABRs in CI users, using two different stimuli with four different intensities, respectively. This accomplished free-field BERA additionally supports evaluating the responses and analysis of respective relative changes related to the span of used stimulus intensities. All intrinsic delays of the auditory processing chains and activated implant electrodes are included, thereby potentially offering insights into the true-to-life temporal appearance of the CI implantees' responses. We additionally validate the approach using a NH control-group. With this method, we found consistent differences in both groups acquired response morphologies as well as in their inter-trial regularity.

3.2.1 Experimental Procedure and Participants

The measurements were conducted in an acoustically shielded room using an audiometric free-field configuration. Each participant sat on a comfortable chair in front of a loudspeaker (Control 1G Universe JBL, 1.0 m distance; Renkforce audio amplifier SAP- 702) and was asked to relax and keep eyes closed during the procedure. For the CI group all additional filters of the sound processor like noise blocks, wind blocks and gain controls were turned off and an omnidirectional microphone characteristic was used. In bilateral and bimodal users the contralateral device (CI or HA) was turned off. Two stimuli, the alternating-polarity A-chirp by Fobel and Dau [2004] (edge frequencies 10-10,000 Hz, total length of 10.17 ms, inter stimulus interval of 60 ms) and an alternating-polarity click shown by Corona-Strauss [2009] (total length of 100 μ s, interstimulus interval of 66.0 ms), were used. Both stimuli are depicted in Figure 2.8. Each stimulus was presented at four intensities of 40, 50, 60, and 70 dB peSPL, where each intensity was calibrated by employing the peak-equivalent method (see Section 2.5) using a sound level meter (Voltcraft SL-100) at the position of the participants head and a digital oscilloscope (TPS 2014, Tektronix, USA). The different intensity levels were randomized for each participant individually. Thus, a total of eight measurements were recorded with 3,000 trials

3.2 Study 1: Neural Correlates of Free-Field Evoked Auditory Brainstem Responses in Cochlear Implant Users

each (total procedure length of approximately 30 minutes) for each subject. We used a laptop with the digital audio workstation PreSonus Studio One 2 (2.5.0) and the Scarlett 2i4 USB audio interface to present the calibration sine (1,000 Hz) and the stimuli. The audio interface additionally offered the trigger signal, which bypassed the full measurement chain. A schematic depiction of the measurement setup can be seen in Figure 3.1. We conducted these measurements in 12 NH listeners (hear-

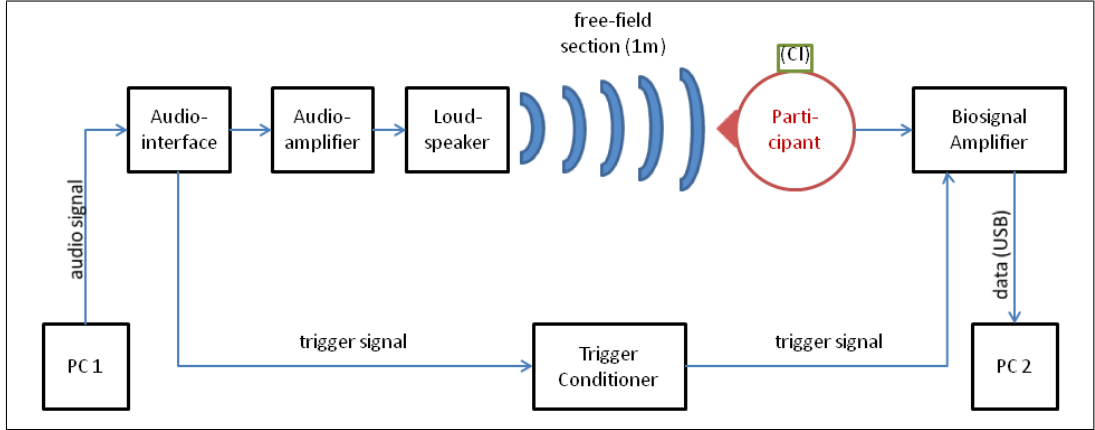


Figure 3.1: Schematic representation of the measurement setup to investigate free-field evoked ABRs in CI implantees. Here, PC 1 offers the stimuli as well as the trigger signal to the audio interface, where the stimulations get amplified and free-field transmitted to the participant (CI or NH). In both groups, ABRs are collected using a biosignal amplifier and are saved in PC 2. The full measurement chain is bypassed by a corresponding trigger signal.

ing thresholds of ≤ 15 dB HL across frequencies of 250-6,000 Hz; 7 female/ 5 male; ages 27.92 ± 8.7 yrs) and in 12 CIs (see Table 3.1, hearing thresholds ≤ 60 dB HL; 9 female/ 3 male; ages 49.83 ± 13.9 yrs) with no further neurological disorders.

Table 3.1: Overview of the 12 participated CI implantees with the equipped sound processor, implant, CI-configuration (monaural (ma); bilateral (ba)), and their individual CI-experience in months. In ma configurations the use of a contralateral HA was permitted.

Participant	Sound Processor	Implant	CI-Configuration/ Used Side	CI-Experience [months]
1	CP910	CI422	ba (right)	11
2	Naida Q70	HR90K Advantage (HiFOCUS ms)	ba (right)	26
3	Sonnet	Synchrony (Medium)	ma (right)	12
4	CP910	CI422	ma (right)	6
5	CP910	CI422	ba (right)	50
6	Sonnet	Synchrony (Flex28)	ma (right)	7
7	CP910	CI512	ba (right)	26
8	Naida Q70	HR90K Advantage (HiFOCUS ms)	ba (left)	15
9	CP910	CI24RE	ba (left)	78
10	Sonnet	SonatarTi100 (FlexSoft)	ba (left)	63
11	CP910	CI512	ba (left)	14
12	CP910	CI522	ba (right)	20

3.2.2 Response Latency Estimations

Since we present a novel method of measuring and analyzing free-field evoked ABR correlates, we need to estimate the temporal occurrence of the responses, more precisely, those of the prominent W_V . We calculated this temporal occurrence according to the used stimuli as:

$$\begin{aligned} t_{WV} = & \text{Stimulus Traveling Time} \\ & + \text{Latency of } W_V \\ & + \text{Stimulus Length.} \end{aligned} \tag{3.2.1}$$

The stimulus traveling time was calculated using the sound velocity ($343 \frac{m}{s}$) and the distance between the loudspeaker and the participant (1 m), and determined to be approximately 3 ms. For the neural delay of the W_V we used the constant of 5 ms from the literature [Neely et al., 1988; Corona-Strauss, 2009; Fobel and Dau, 2004]. According to Equation 3.2.1, these results in the following estimations:

$$\begin{aligned} t_{WV_{chirp}} & \approx 18 \text{ ms}, \\ t_{WV_{click}} & \approx 8 \text{ ms}. \end{aligned}$$

Note that this Equation does not encompass the technical driven latencies potentially caused by incorporated CIs as shown by Zirn et al. [2015, 2019]; Wess et al. [2017], thus found differences in their responses eventually offer an assessment of the desired, but unknown, technical delays.

3.2.3 Narrowband Filtering

One major issue when investigating evoked potentials in CI implantees is the prominent CI artifact [Sinkiewicz, 2015; Gordon, 2007; Shalloo, 1993], that can overlap the desired response pattern, making their interpretation difficult or even impossible especially when considering conventional artifact filtering (see Section 2.5.2). Conveniently, Luu and Tucker [2001] suggested that bandpass filtering around the peak frequency of the component of interest (in our case the W_V) can be used to remove the contribution of other superimposed components (in our case the CI artifact), thus uncovering the true underlying neural oscillations. According to Yeung et al. [2004], the exogenously driven synchronization of these oscillations

3.2 Study 1: Neural Correlates of Free-Field Evoked Auditory Brainstem Responses in Cochlear Implant Users

should produce a series of peaks of diminishing amplitude and result in the well-known ERP pattern in the average response. However, both Luu and Tucker [2001] and Yeung et al. [2004] demonstrated the downside of narrowband filtering ERPs, because this technique smears out parts of the signal in time due to the narrow filter bandwidth, causing a distortion, the so called ringing artifact. This artifact may create the appearance of oscillating activity where none is present. Although the magnitude of the ringing artifact will depend on the size of the original peak in the average waveform, the appearance of oscillations in narrowband filtered data is not definitely evidence of synchronized oscillations (the desired neural responses). In other words, applying this technique eventually helps to exclude unwanted superimposed components like the CI artifact, but in turn induces unwanted oscillations, which pose the threat of misinterpreting them as actual neural activity.

Please note that when employing the method of narrowband filtering ERPs, this causes a postponed argumentative mindset for the subsequent data analysis, based on the following reasoning:

1. Narrowband filtering of ABRs will cause ringing oscillations due to the time-frequency uncertainty principle, therefore altering commonly and classically visualized response morphologies (see Figure 2.7 and Figure 2.9) to some extent.
2. Narrowband filtering of ABRs in CI users seems to reduce the influence of the broadband stimulation artifact (see Section 2.5.2), however, a complete extinction is not expected, since even the smallest frequency window potentially admits residual, artificial signal components.

We strongly urge the reader to step back from expecting the familiar waveform morphology of ABRs in both groups and to assume a more abstract approach in interpreting the information content of ABRs, where, in a nutshell, the sense of hearing gets stimulated and the responses get measured and analyzed (see the definition of ERPs in Section 2.5). When strictly using identical (but uncommon) filter settings in both groups' free-field evoked responses to adapt and balance the method of their stimulations, this does not violate the fundamental principle of ERPs since responses related to auditory stimulations get collected, but suggests to change their shapes. Consequently, commonly expected phenomena, terms, and labels, like the prominent W_V , will lose their meaning to some extent,

3.2 Study 1: Neural Correlates of Free-Field Evoked Auditory Brainstem Responses in Cochlear Implant Users

based on the mentioned alteration, which unfortunately causes room for the misinterpretation of signal components (i.e., noise) as neural activity. To verify such potentially collected neural regularity, an investigation of relative changes across a subjects' responses respective to changes during stimulations becomes crucial [Corona-Strauss, 2009]. To accomplish such insights, we implemented the procedure of the prominent BERA (see Section 2.5.1) within this study, where we tested both used stimuli at four different intensities in a comparable manner to further investigate signal components, which eventually correlate with the expected neural behavior. Consequently, we stick with the term '*neural correlate*' rather than ABR throughout the subsequent analysis and argumentation.

However, since we expect changes in the response morphology due to the altered stimulation procedure, one can argue that the information loss resulting from narrowband filtering and the associated ringing oscillations can be considered neglectable as long as the underlying neural activity is reliably identifiable (e.g., via the pertinent wave latencies). To counter misinterpretations of false signal components, we introduce the wavelet phase synchronization stability (WPSS) as an additional objective measure (see Section 3.2.4 and Section 4.1.1), which is less affected by amplitude fluctuations [Corona-Strauss et al., 2007, 2009; Strauss et al., 2004], to further evaluate the narrowband filtered correlates.

3.2.4 Inter-Trial Phase Synchronization Measures

The wavelet phase synchronization stability (WPSS) reflects the phase stability between the single evoked trials in a specific frequency range and allows us to exclude noisy frequencies [Corona-Strauss et al., 2007, 2009]. By applying the continuous wavelet transform with a complex mother wavelet, the sixth derivative of the complex Gaussian function in this case, to the ABR signals, the instantaneous phase can be extracted. This wavelet function $\psi \in L^2(\mathbb{R})$ (L^2 denoting the Hilbert space of square integrable functions, i.e., all functions x that satisfy $\|x(t)\|_{L^2}^2 < \infty$) and satisfies admissibility criterion:

$$0 < C_\psi = \int_{\mathbb{R}} \frac{|\Psi(\omega)|^2}{|\omega|} d\omega < \infty \quad (3.2.2)$$

3.2 Study 1: Neural Correlates of Free-Field Evoked Auditory Brainstem Responses in Cochlear Implant Users

C_ψ is the admissibility constant and $\Psi(\omega)$ is the Fourier transform of the wavelet ψ . By stretching or compressing the mother wavelet $\psi \in L^2(\mathbb{R})$ corresponding to the scale parameter a and shifting in time according to the parameter b , a set of wavelets $\psi_{a,b}$ is obtained [Carmona et al., 1998]

$$\psi_{a,b}(\cdot) = |a|^{-1/2} \psi((\cdot - b)/a), \quad a, b \in \mathbb{R}, a \neq 0 \quad (3.2.3)$$

Using these, we are able to analyze signals simultaneously in time and scale.

The wavelet transform $\mathcal{W}_\psi : L^2 \rightarrow L^2(\mathbb{R}, \frac{da db}{a^2})$ of a signal $x \in L^2(\mathbb{R})$ is then given by the inner L^2 -product [Strauss et al., 2010]:

$$(\mathcal{W}_\psi x)(a, b) = \langle x, \psi_{a,b} \rangle_{L^2} = \int_{\mathbb{R}} x(t) \psi_{a,b}^*(t) dt \quad (3.2.4)$$

Note that the scale parameter a can always be associated with a so-called pseudofrequency f_a by

$$f_a = \frac{f_\psi}{a}, \quad (3.2.5)$$

where f_ψ is the center frequency of the wavelet in Hz. When using a complex wavelet, the instantaneous phase ϕ of a signal x can be extracted by

$$\phi_{a,b}(x) = \arg((\mathcal{W}_\psi x)(a, b)) \quad (3.2.6)$$

Now, the WPSS $\Gamma_{a,b}$ of an ABR sequence $X = \{x_m \in L^2(\mathbb{R}) : m = 1, \dots, M\}$ of M sweeps is defined by

$$\Gamma_{a,b}(X) := \frac{1}{M} \left| \sum_{m=1}^M e^{i\phi_{a,b}(x_m)} \right| \quad (3.2.7)$$

and assumes values between 0 and 1. Equal phase dispersion across single trials is represented by 0, whereas a perfect synchronization is represented by 1.

3.2.5 Data Acquisition and Preprocessing

Four passive silver/ silver-chloride electrodes were placed in total at the left and right mastoid, the reference at the vertex (CZ), and ground at the forehead. Impedances were kept below 5 k Ω . ABRs were recorded using a commercially available biosignal amplifier (g.USBamp, Guger Technologies, Austria) with a sampling rate of 19,200 Hz. To format the trigger signal of the auditory stimulation, a trig-

3.2 Study 1: Neural Correlates of Free-Field Evoked Auditory Brainstem Responses in Cochlear Implant Users

ger conditioner (g.TRIGbox, Guger Technologies, Austria) was used. First offline analysis was performed using MATLAB R2016a (Mathworks, USA) by applying a zero-phase finite impulse response (FIR)1 bandpass-filter of 150-1,500 Hz (conventional ABR frequency band as in [Corona-Strauss, 2009]) as well as a 50 Hz zero-phase infinite impulse response (IIR) notch (notches at all integer multiples of 50 Hz). To potentially attenuate the CI artifact [Gordon, 2007; Shallop, 1993] while still holding essential neural information, we separately applied five successive zero-phase FIR1 narrow bandpass-filters of 150-300 Hz, 301-450 Hz, 451-600 Hz, 601-750 Hz, and 751-1,000 Hz to the raw data, where we investigated the resulting response morphologies to evaluate the most suitable filter settings for the following analysis in CIs (see Section 3.2.3 and Section 4.1.1). In all cases, the artifact filter was set to $25.0\ \mu\text{V}$ yielding a total of 2,000 used artifact-free trials in each participant, respectively.

3.3 Study 2: Quantification of Binaural Interaction Faciliated By Interaural Latency Compensation in Bimodal Cochlear Implant Users

In this study, we apply a fast, deconvolution-based ABR acquisition technique based on the CL(A)D method, with SNR optimization according to Kohl et al. [2019a], using the narrowband frequency window suggested by Schebsdat et al. [2018] (further described in Section 3.2), to potentially detect ABRs and analyze their potential BIC in CI users. The aim of this study is to demonstrate the feasibility of the proposed ABR acquisition technique in obtaining a brainstem-level BIC and to compare the results with and without compensation of the device based interaural delay in bimodal CI users. We additionally validate the approach using a NH control-group. We assume that delay compensation will lead to a more synchronized stimulation and therefore result in an increase in brainstem-level auditory interaction (quantified by the brainstem BIC) in bimodal CI implantees as well as in the NH control-group, where the interaural delay is simulated by presentation using the corresponding ITDs.

3.3.1 Experimental Procedure and Participants

The measurements were conducted in an acoustically shielded room. Each participant sat on a comfortable chair and was asked to relax during the procedure. All participants of the patient-group were aided with a clinical HA (Naida[™] Q90-UP, Phonak) and a CI sound processor (Harmony[™], Advanced Bionics Corp.), both provided by the Advanced Bionics Corp.. The devices were configured based on the individuals' up-to-date hearing thresholds and CI-map, both provided by the clinic. The reason for using the Harmony[™] sound processor is the presence of a line-level direct audio input, which is not available in more recent sound processors (those include undesired wireless connections). The sound processor was configured with an input DR of 75 dB, all additional filters like noise and wind blocks were turned off, and the automatic gain control was disabled. During actual testing, both devices solely used the direct audio input without any T-coil or microphone ratio. Directly after exchanging the devices, CI participants were asked if there are any major changes in hearing, whereas merely changes in the perceived loud-

3.3 Study 2: Quantification of Binaural Interaction Facilitated By Interaural Latency Compensation in Bimodal Cochlear Implant Users

ness were reported. Since ABRs depend on the intensity/loudness (see Section 2.5.1) of the perceived stimuli [Corona-Strauss, 2009], both devices had to be adjusted individually. Therefore, we offered a rudimentary graphical user interface,

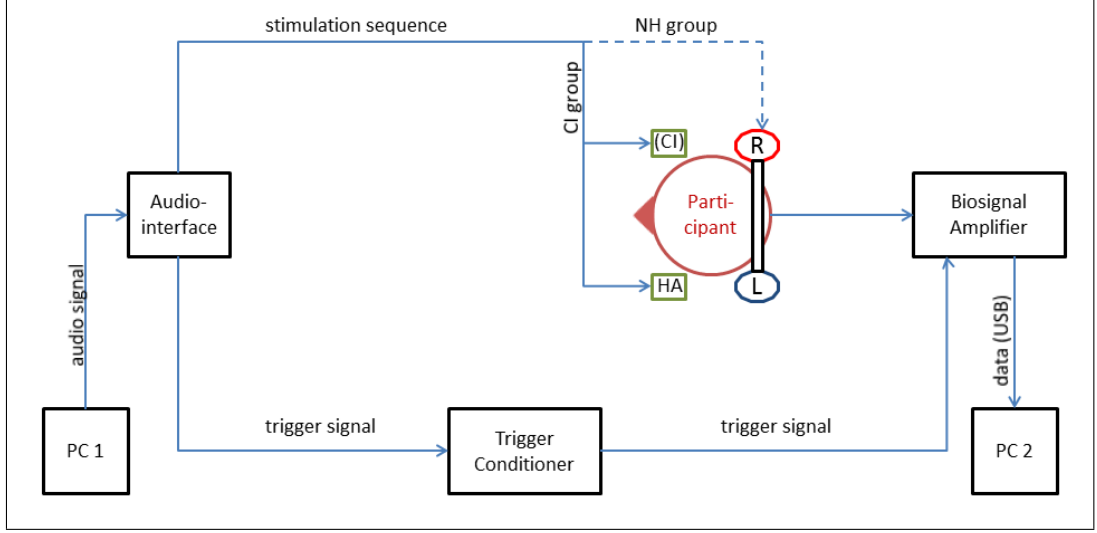


Figure 3.2: Schematic representation of the measurement setup to investigate binaural interaction in bimodal CI users and NH listeners. Here, PC 1 offers the stimulation sequence as well as the trigger signal to the audio interface. When testing the patient-group, the CI as well as the HA are connected directly to the audio interface, whereas when testing the control-group headphones are used. In both groups, ABRs are collected using a biosignal amplifier and saved in PC 2. The full measurement chain is bypassed by a corresponding trigger signal.

allowing individual participants of the patient-group to adjust their device based perceived loudness to '*loud-but-comfortable*' manually using iterative approximations with adaptive step size refinement in the following order, separately: CI, HA, and interaural balancing. Participants were always able to abort the procedure and start from the beginning when wrong inputs were made or the user was not satisfied with the adjustments, thus a balanced loudness configuration was achieved potentially. For the patient-group, both hearing devices were connected directly to the audio interface, whereas for the control-group Sennheiser HDA 400 headphones were used to present the stimuli at 70 dB pe SPL. A schematic representation of the measurement setup is depicted in Figure 3.2. To calibrate the headphones, the peak-equivalent method described in Section 2.5 was employed, using a sound level meter (type 2250, Brüel & Kjær, Denmark) with a prepolarized free-field 1/2" microphone (type 4189, Brüel & Kjær, Denmark) embedded in an artificial ear (type 4153, Brüel & Kjær, Denmark) alongside a commercially available oscilloscope (MSO-X 2024A, InfiniiVision, Germany). In both groups, the stimulation

3.3 Study 2: Quantification of Binaural Interaction Facilitated By Interaural Latency Compensation in Bimodal Cochlear Implant Users

sequence explained in Section 3.3.3 was presented in one piece, thus the individual measurement time amounted to approximately 25 minutes. We conducted the measurements in a control-group of 10 NH listeners (hearing thresholds of ≤ 15 dB HL across frequencies of 250-6,000 Hz, 6 female/ 4 male, ages 23.1 ± 1.97 yrs) and in a patient-group of 10 bimodal CI implantees (see Table 3.2, hearing thresholds of ≤ 60 dB HL (both sides), CI hearing experience of 2.1 ± 1.29 yrs, HA hearing experience of 19.8 ± 18.4 yrs, 6 female/ 4 male, ages 57.5 ± 14.44 yrs) with no further neurological disorders.

Table 3.2: Overview of the 10 participated CI implantees with the equipped implant, CI-side, and their individual CI-experience as well as their HA-experience in months.

Participant	Implant	CI-Side	CI-Experience [months]	HA-Experience [months]
1	HR90K Advantage	r	14	71
2	HiRes Ultra	r	13	579
3	HR90K Advantage	l	32	527
4	HiRes Ultra	r	12	324
5	HR90K Advantage	r	24	24
6	HR90K Advantage	r	42	70
7	HiRes Ultra	l	15	119
8	HR90K Advantage	l	40	167
9	HR90K Advantage	l	60	59
10	HR90K Advantage	l	25	515

3.3.2 Interaural Latency Estimations

Zirn et al. [2015] demonstrated that the actual interaural stimulation timing depends on the incorporated processing delays of both HAs and CIs (τ_{HA} and τ_{CI} in [Zirn et al., 2015, 2019]). However, respective device-specific values are not available in literature or data sheets, thus references are limited [Zirn et al., 2015, 2019; Wess et al., 2017]. Consequently, the technical latencies of both hearing devices had to be measured prior the actual study to investigate the potential effect in the resulting BIC with and without the estimated binaural latency compensation. To determine the latency of the CI, a $100 \mu\text{s}$ click was presented via the mentioned audio interface connected to the digital audio input of the HarmonyTM sound processor. This click was bypassed and used as latency offset, thus the differential duration (i.e. the technical delay) between the bypassed input and the caused first pulse detected at the implant electrode responsible for the lowest frequencies (i.e. #1) using the HR90K implant reference unit and a commercially available oscilloscope

3.3 Study 2: Quantification of Binaural Interaction Facilitated By Interaural Latency Compensation in Bimodal Cochlear Implant Users

was measured. The total latency amounts to $\tau_{CI} \approx 14.125$ ms. For the HA, the same click was presented via the previously mentioned audio interface using the direct audio input of the NaidaTM Q90-UP, where the input was also bypassed to serve as latency offset. The provoked response from the HA speaker was detected using the SonarworksTM XREF 20 measurement microphone connected to the mentioned oscilloscope. A differential latency of $\tau_{HA} \approx 7.59$ ms between offset and response was determined. Note that similar values for τ_{HA} are obtained by Zirn et al. [2015]; Wess et al. [2017]. By incorporating the additional traveling time along the BM of 4 ms at 500 Hz (value taken from Neely et al. [1988]), the spectral center of the employed stimulus, the total latency of the HA amounts to 11.59 ms. Overall, this results in a device-induced relative delay, where the HA leads by approximately 2.535 ms. This delay estimation, subsequently called 2.5 ms, was thereupon used to time-shift monaural stimulations and to manipulate binaural stimulation conditions in both groups (see Equation 3.3.9 and Equation 3.3.11).

3.3.3 Stimulus Sequence Design

An alternating-polarity narrowband 3-wave chirp stimulus following the A-chirp model of Fobel and Dau [2004] was designed based on the reasoning shown by Corona-Strauss et al. [2012], spanning the frequency range from 100-500 Hz to encompass the mutual spectral overlap of CI and HA. By employing the optimization method established by Kohl et al. [2019a], a sequence of 10 successive interstimulus intervals from the range 25-50 ms was optimized for ERP deconvolution using the CL(A)D method [Delgado and Özdamar, 2004] to subsequently attenuate additive noise in the recorded ERPs from 5-500 Hz (this frequency range was chosen to capture all relevant details of the early [Schebsdat et al., 2018] and subsequent auditory ERPs), resulting in a mean presentation rate of 30.25 Hz (additionally evoking large amplitude middle-latency components [Özdamar et al., 2007]) and deconvolution gain factors c_{dec} and g_{dec} of 6.5 dB and 2.2 dB over conventional averaging, respectively (see Figure 3.3). Here, c_{dec} assumes uniform distribution of additive noise across frequencies [Delgado and Özdamar, 2004], whereas g_{dec} assumes a $1/f^\alpha$ noise model [Peng et al., 2017]. Stimuli were presented at the determined individual intensities using a laptop with the digital audio workstation PreSonus Studio One 2 (2.5.0) and a Scarlett 2i4 USB audio interface. Stimulus waveforms consisted of four randomly interleaved conditions with 1,000 sequences each, i.e., monaural left

3.3 Study 2: Quantification of Binaural Interaction Facilitated By Interaural Latency Compensation in Bimodal Cochlear Implant Users

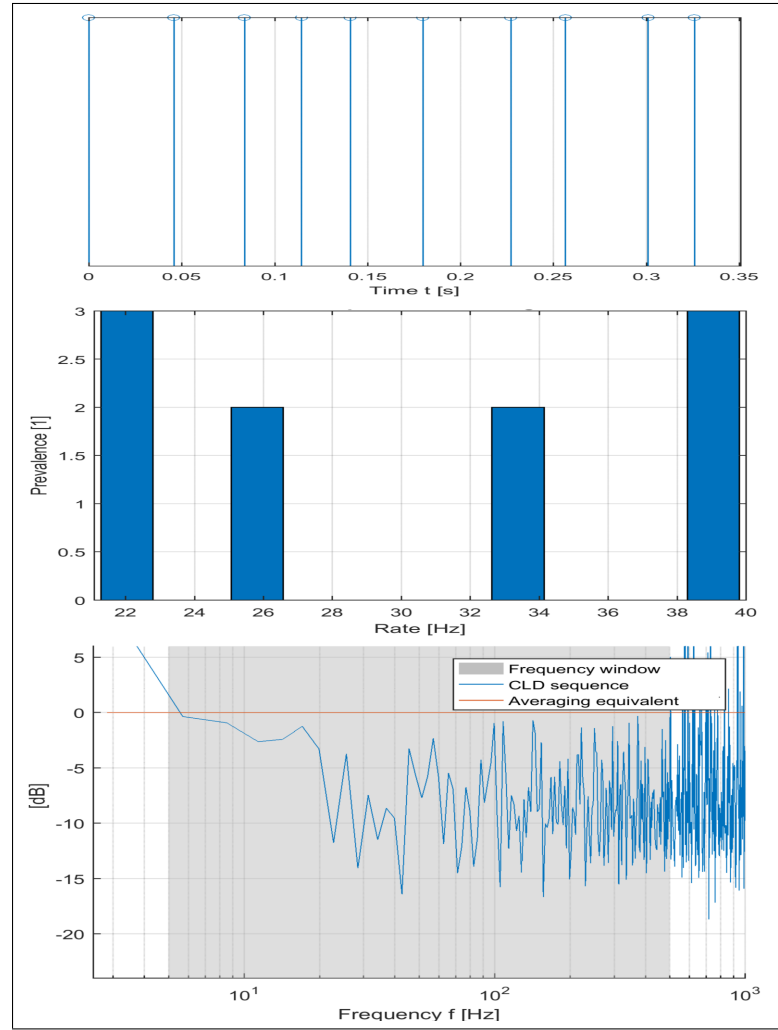


Figure 3.3: Properties of the optimized CL(A)D stimulus sequence depicting the stimulus onset train (top), the presentation rate histogram (middle), and the reciprocal transfer function (bottom; i.e., spectral noise amplification).

(MONO_{Le}), monaural right (MONO_{Ri}), binaural (BIN), and asynchronous binaural (BIN_{Asynch}) for the control-group as well as monaural HA (MONO_{HA}), monaural CI (MONO_{CI}), binaural (BIN), and binaural latency compensated (BIN_{COMP}) for the patient-group.

3.3.4 Data Acquisition and Preprocessing

Three passive silver/ silver-chloride-electrodes were placed in total with the measurement electrode at the nape (IZ), reference at the vertex (CZ) and ground at the forehead (FpZ). Impedances were kept below 5 k Ω . ABRs were recorded us-

3.3 Study 2: Quantification of Binaural Interaction Facilitated By Interaural Latency Compensation in Bimodal Cochlear Implant Users

ing a commercially available biosignal amplifier (g.USBamp, Guger Technologies, Austria) with a sampling rate of 19,200 Hz. To format the trigger signal from the audio interface, a trigger conditioner (g.TRIGbox, Guger Technologies, Austria) was used. Data analysis was performed offline using MATLAB R2016a (Mathworks, USA). First, the raw ERP recordings were conditioned by applying a 2nd order zero-phase Butterworth bandpass of 5-500 Hz and notch filters at all integer multiples of 50 Hz within this range. Sequence responses were epoched according to the recorded trigger signals.

3.3.5 Response Deconvolution

The most well-known ERP filtering method is the conventional averaging of the transient responses, which are acquired by using an interstimulus interval with little or no jitter (see Section 2.5). The acquisition time is always shorter than this interval, thus the actual neural response is completely framed within. Consequently, one response does not influence (i.e., overlap) the response of the successive stimulation [Delgado and Özdamar, 2004], hence the total measurement time depends on the anatomical region of interest, the interstimulus interval, and the number of trials necessary for SNR optimization [Hall, 2007]. Although, the acquisition of steady-state responses uses the same averaging technique as well as constant stimulation rates, it is incorporating shorter interstimulus intervals causing an overlapping of neighboring responses. Unfortunately, those responses can never be decomposed into their original, individual components due to the isochronous stimulation intervals [Bohórquez and Özdamar, 2008; Delgado and Özdamar, 2004]. However, various methods to reduce the acquisition time by disentangling such overlapping ERPs obtained at higher stimulation rates have been proposed [Bardy et al., 2014; Delgado and Özdamar, 2004; Wang et al., 2006; Woldorff, 1993], where most of them concentrate on deconvolution approaches. Especially the CL(A)D method has shown to be practical when obtaining high-quality ABRs alongside AMLRs simultaneously to high stimulation rates, although the obtained ALR waves suffer from substantial rate-induced detriment [Holt and Özdamar, 2014, 2016]. In this work we applied the CL(A)D method, where the transient auditory ERP to each successive presentation of the stimulus sequence were recovered using fast Fourier transformation (FFT)-based circular deconvolution with the presented stimulus sequence (see Section 3.3.3) and averaged separately for each condition.

3.3.6 Binaural Computations

The BIC is defined as the arithmetical difference between the sum of both monaurally evoked responses and the binaural response [Jewett, 1970; Stollman et al., 1996; McPherson and Starr, 1993; Hosford et al., 1979], as described in Section 2.5.3. According to Equation 2.5.1, the resulting difference [Stollman et al., 1996; McPherson and Starr, 1993] for the normal listening condition (ITD 0 ms) in the NH control-group was computed as:

$$\begin{aligned} \text{BIC} &= (\text{MONO}_{\text{Le}} + \text{MONO}_{\text{Ri}}) - \text{BIN} \\ &= \text{SUM}_{\text{MONO}} - \text{BIN} \end{aligned} \tag{3.3.8}$$

Whereas, in the artificially established asynchronous listening condition (ITD 2.5 ms) their difference was calculated as:

$$\begin{aligned} \text{BIC}_{\text{Asynch}} &= (\text{MONO}_{\text{Le-Asynch}} + \text{MONO}_{\text{Ri}}) - \text{BIN}_{\text{Asynch}} \\ &= \text{SUM}_{\text{MONO-Asynch}} - \text{BIN}_{\text{Asynch}} \end{aligned} \tag{3.3.9}$$

Here, $\text{MONO}_{\text{Le-Asynch}}$ represents the time-shifted MONO_{Le} signal and $\text{BIN}_{\text{Asynch}}$ represents the asynchronous binaural stimulation. In both cases the left stimulation was delayed. On the other hand, the BIC for the CI patient-group in the normal listening condition (ITD 2.5 ms) was computed as:

$$\begin{aligned} \text{BIC} &= (\text{MONO}_{\text{HA}} + \text{MONO}_{\text{CI}}) - \text{BIN} \\ &= \text{SUM}_{\text{MONO}} - \text{BIN} \end{aligned} \tag{3.3.10}$$

Whereas, in the artificially established compensated listening condition (ITD 0 ms) their difference was calculated as:

$$\begin{aligned} \text{BIC}_{\text{Comp}} &= (\text{MONO}_{\text{HA-Comp}} + \text{MONO}_{\text{CI}}) - \text{BIN}_{\text{Comp}} \\ &= \text{SUM}_{\text{MONO-Comp}} - \text{BIN}_{\text{Comp}} \end{aligned} \tag{3.3.11}$$

3.3 Study 2: Quantification of Binaural Interaction Facilitated By Interaural Latency Compensation in Bimodal Cochlear Implant Users

Note that $\text{MONO}_{\text{HA-Comp}}$ represents the time-shifted MONO_{HA} signal and BIN_{Comp} represents the compensated binaural stimulation. In both cases the HA was delayed (see Section 3.3.2). Waves were detected manually using the resulting maximum in the brainstem-level period.

4 Results

4.1 Results of Study 1

4.1.1 Filter Settings and Scales

Figure 4.1 and Figure 4.2 show our adaption of the work of Yeung et al. [2004] by presenting our grand average free-field evoked chirp and click responses at 60 dB pe SPL in NH listeners using the conventional ABR frequency band of 150-1,500 Hz (black) as well as the applied five subsequent narrow frequency bands (150-300 Hz (blue), 301-450 Hz (orange), 451-600 Hz (yellow), 601-750 Hz (purple), and 751-1,000 Hz (green)), where the induced ringing artifact is visible. Below the corresponding WPSS are depicted, respectively. Note that the prior estimated ABR latencies in NH listeners closely follow our findings using both stimuli (Equation 3.2.1), where the resulting W_V is marked by red arrows, respectively. The maximum phase synchronizations occur in the downslope area of the corresponding W_V s in the respective averaged potentials. Especially the pseudofrequency range of approximately 150-300 Hz (scales $\approx 40-75$) seems to embed a noteworthy regularity of oscillations when using both stimuli. Although the narrowband filtered, averaged responses appear more rounded and are further superimposed by oscillations, however, they represent correlating components of the conventionally filtered ABR, like the desired W_V [Hall, 2007]. Therefore, compare black and blue lines in Figure 4.1 and Figure 4.2. By contrast, the other tested narrowband filtered signals do, if at all, only minorly represent those components, consequently supporting the assumption that the band limitation to the suggested frequencies of 150-300 Hz (subsequently coined narrowband) might reduce the influence of the broadband CI artifact while still holding essential neural information of CI free-field responses. Thus, we subsequently used scales ranging from 40-75 (step size of 5) reflecting a

4.1 Results of Study 1

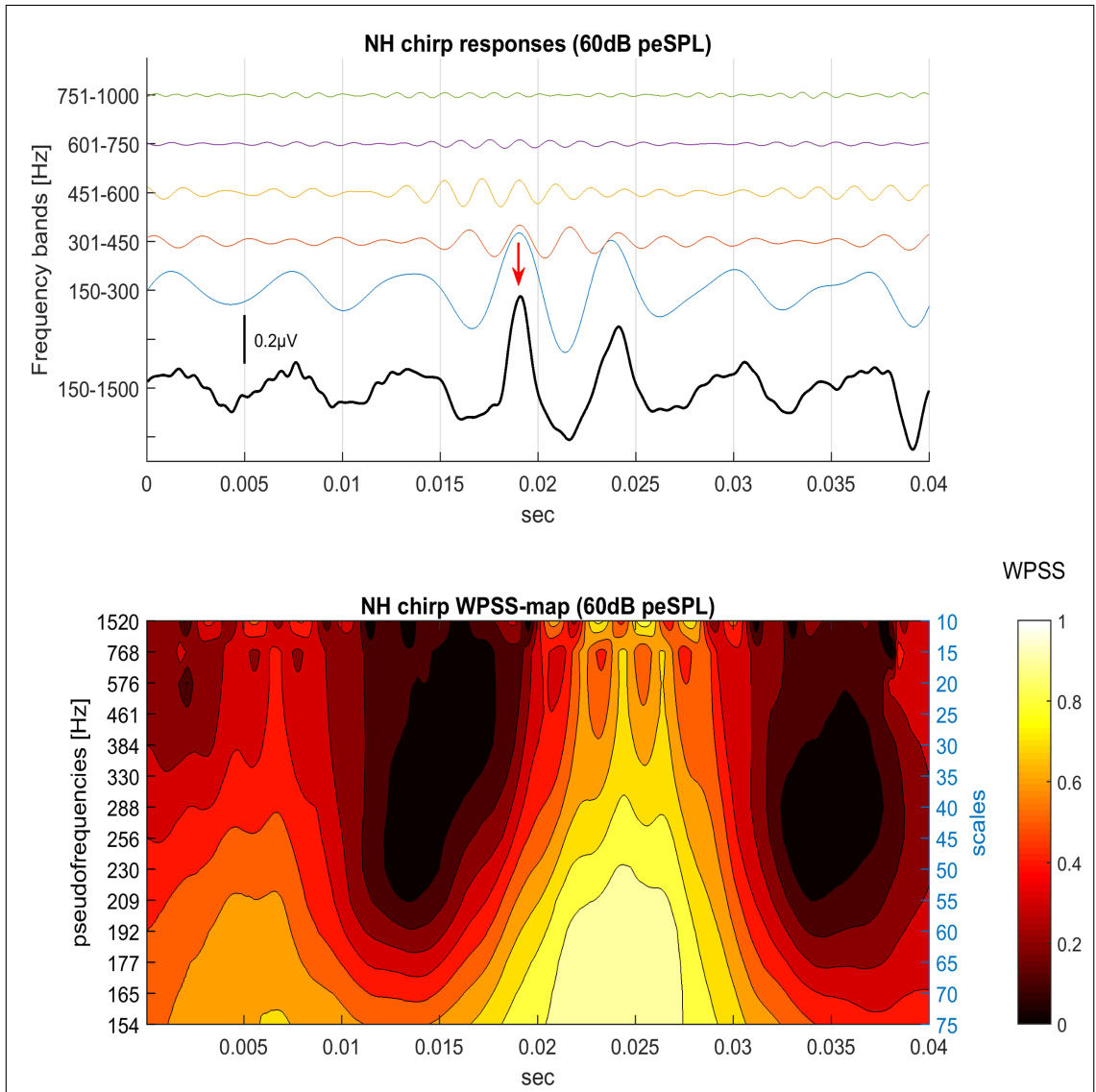


Figure 4.1: Grand average NH group chirp responses (60 dB peSPL) affected by different frequency bands and below the corresponding WPSS. The conventional ABR frequency band (150-1,500 Hz) is denoted by the black line, where the red arrow indicates the W_V . Additionally, the five narrowband filtered responses (150-300 Hz (blue), 301-450 Hz (orange), 451-600 Hz (yellow), 601-750 Hz (purple), and 751-1,000 Hz (green)) are shown. All tested frequency bands demonstrate superimposed oscillations (coined ringing artifact) due to narrowband filtering. Note that the corresponding phase synchronization has its maximum in the temporal downslope area of the corresponding W_V in the averaged potential, especially in the pseudofrequency range of approximately 150-300 Hz (scales 40-75), which is one of the drawn frequency bands (blue). This narrowband filtered response appears more rounded, but still reflects the desired features of the ABR (compare the black and blue average responses, especially around the temporal appearance of the individual W_V at ≈ 18 -19 ms).

4.1 Results of Study 1

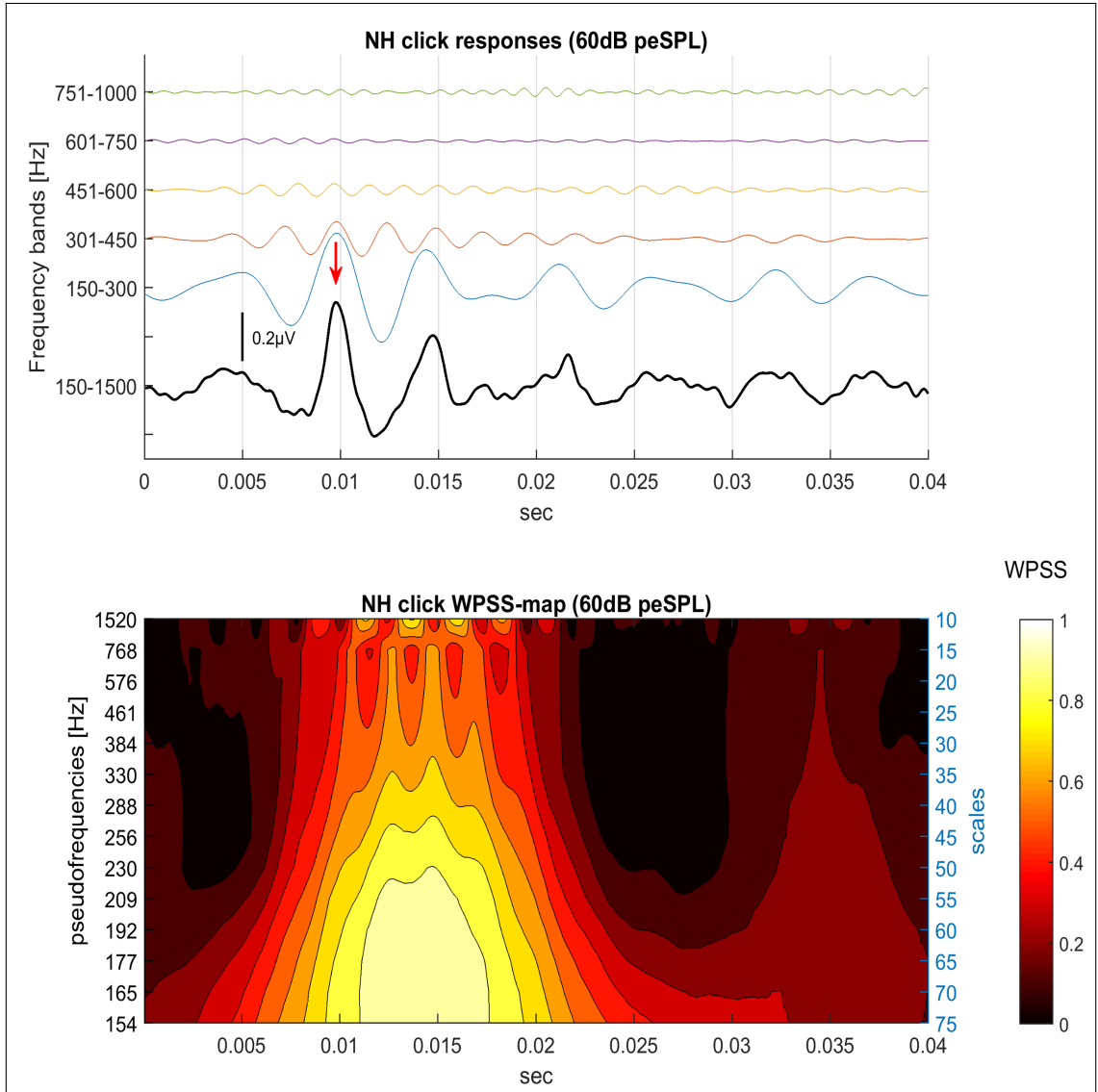


Figure 4.2: Grand average NH group click responses (60 dB peSPL) affected by different frequency bands and below the corresponding WPSS. Note that the Figure structure is being analogous to that of Figure 4.1. The WPSS-map shows a large patch of synchronous activity spanning the pseudofrequency range of approximately 150-300 Hz. This temporal period overlaps in time with the downslope of the W_V in the conventionally filtered response. The corresponding narrowband filtered response appears rounded, but still reflects the desired features of the ABR (compare the black and blue average response, especially around the temporal appearance of the individual W_V at ≈ 10 ms).

pseudofrequency range of 154-288 Hz (coined fullscale WPSS). However, since the temporal occurrences of the neural correlates in CIs are still unknown, we further used the individual WPSS maxima as temporal appearance indicators (as demonstrated within the NH group). Furthermore, the narrowband filtered responses still

4.1 Results of Study 1

exhibit considerable ringing, consequently challenging the true detection of the desired neural correlates at brainstem-level. To prevent misinterpretation of signal components, we tested both used stimuli at four different intensities to further investigate potential neural behaviors in a comparable manner as the commonly used BERA (see Section 2.5.1). We consequently expect a relative growth in amplitudes and in WPSS magnitudes as well as latency reductions of the collected responses according to increasing stimulus intensities based on the reasoning in Hall [2007]; Corona-Strauss [2009].

4.1.2 Free-Field Responses in Normal Hearing Listeners

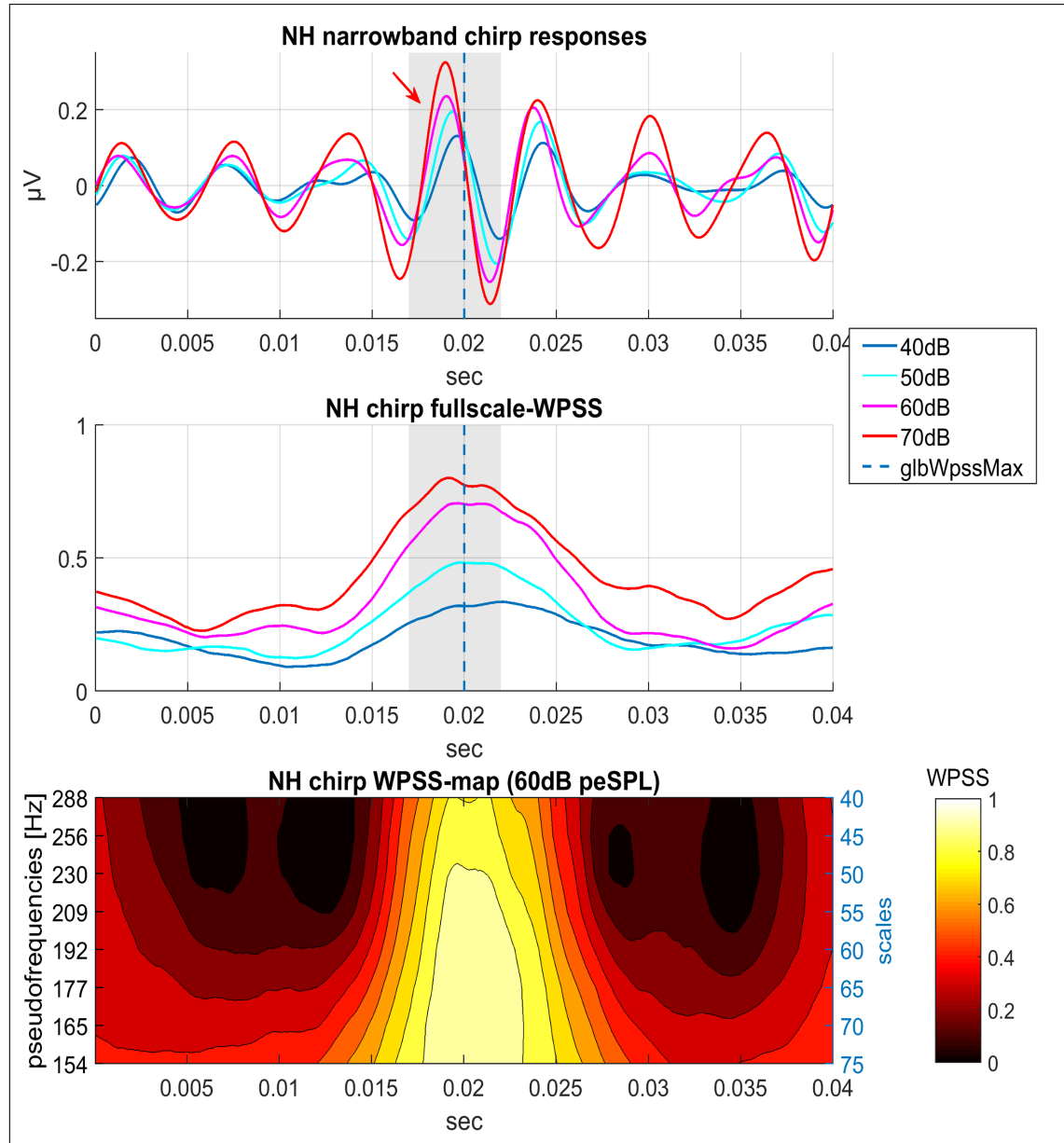


Figure 4.3: Grand average chirp free-field narrowband responses of the NH group, where the temporal position of the global WPSS maximum is denoted by the vertical dotted line at approximately 20ms. This point in time is subsequently used as temporal indicator to potentially detect the desired neural responses (prior these positions). The chirp responses show an intensity specific growth function in the time domain prior the WPSS based indicator (marked by a red arrow) as well as a latency shift (top). A comparable behavior is shown by the intensity specific fullscale WPSS (middle). To improve comparability, areas of interest are highlighted by grey boxes. The intensity specific WPSS-map (i.e., 60 dB peSPL) demonstrates a noteworthy synchronization of oscillations in the pseudofrequency range of 150-300 Hz (bottom).

4.1 Results of Study 1

Figure 4.3 depicts the grand average narrowband responses of the NH group using the chirp stimulus according to the different used stimulus intensities (top), their respective, narrowed fullscale WPSS for the range of pseudofrequencies of 150-300 Hz (middle), as well as the WPSS-map corresponding to the 60 dB peSPL stimulation (bottom). The map demonstrates a distinct inter-trial phase regularity across the narrowed range of pseudofrequencies (scales 40-75) from approximately 17.5-23 ms. The individual, intensity specific WPSS maxima confirm this time period, where the superpositioned global maximum, denoted by the dotted vertical lines, results in approximately 20 ms. The maximum phase synchronization occurs during the strongest stimulation intensity and values to about 0.75. When utilizing this regularity as temporal indicator of the desired W_{VS} as demonstrated in Section 4.1.1, the very first maxima in the averaged potentials prior this synchronization are chosen for further analysis. Noteworthy, this point in time is within the downslope period of the respective leading maxima in the averaged potentials, more precisely, in the zero-crossing. These maxima, denoted by a red arrow, occur approximately 18-20 ms after releasing the stimulus from the loudspeaker and demonstrate averaged amplitudes in the range of 0.15-0.25 μV . Overall, the grand average responses look more rounded and oscillatory, therefore distinguishing from the common ABR morphology (see Figure 2.9). However, the detected maxima increase in amplitude and decrease in latency according to increasing stimulus intensities, consequently offering distinguishable morphology patterns across the intensity specific grand averaged responses as well as in their WPSS, respectively.

Furthermore, Figure 4.4 depicts our findings in the the grand average narrowband responses of the NH group using the click stimulus according to different stimulus intensities. Note that the Figure structure is being analogous to that of Figure 4.3, where the grand average responses, their respective fullscale WPSS, and the intensity specific WPSS-map is shown. Here, the map shows a similar and distinct area of phase synchronization across the narrowed range of pseudofrequencies. Therefore, spanning from a temporal period of approximately 9-14 ms. The individual, intensity specific WPSS maxima also settle within this time period, where the global maximum results in approximately 11 ms. Here, the fullscale maxima respective to the used stimulus intensities of 60 and 70 dB peSPL are similar in their magnitude of about 0.75, whereas the deflection according to the strongest stimulation lags the other. As demonstrated when using the chirp,

4.1 Results of Study 1

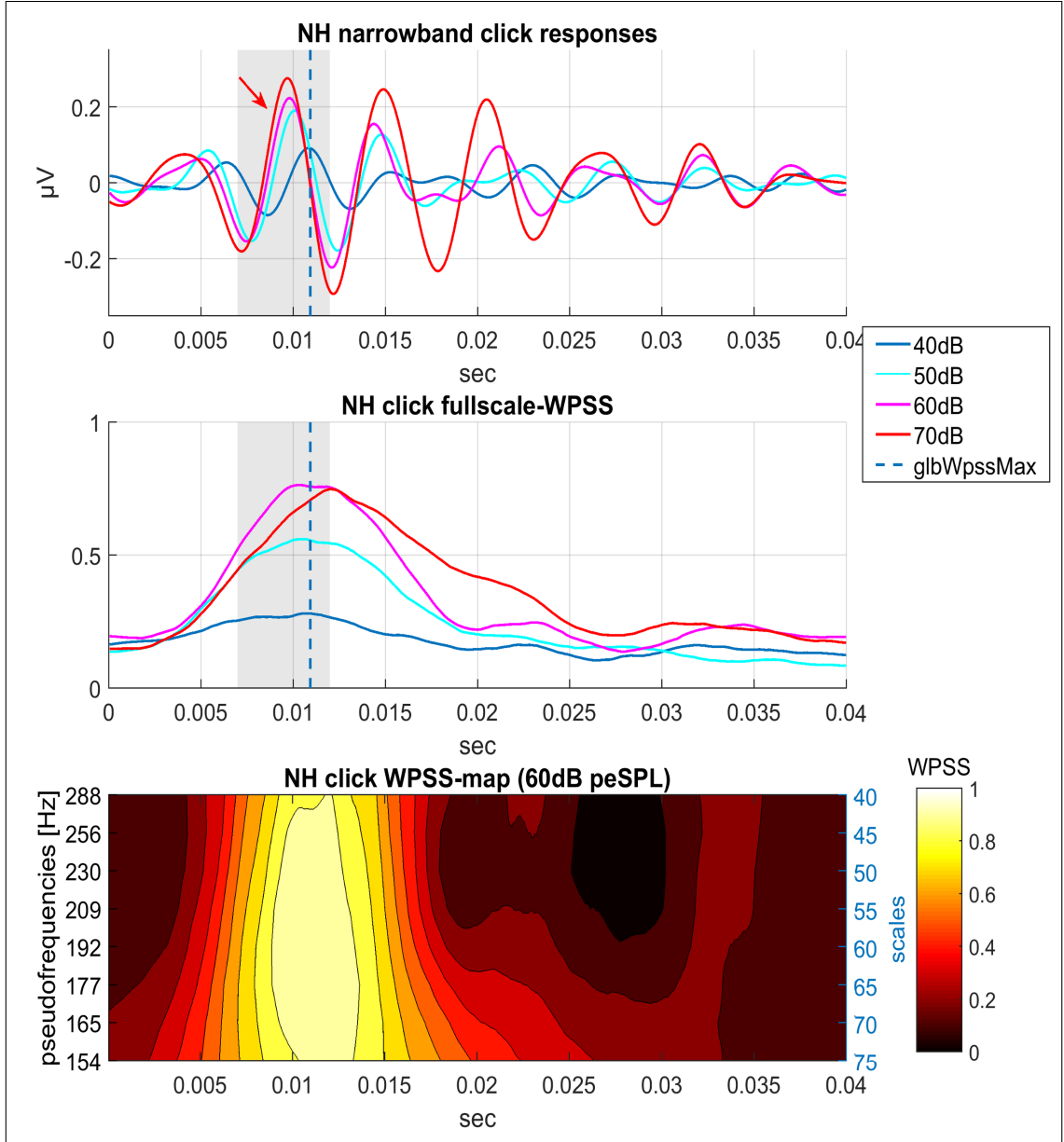


Figure 4.4: Grand average click free-field narrowband responses of the NH group, where the general Figure structure is being analogous to Figure 4.3. The temporal position of the global WPSS maximum is again denoted by the vertical dotted line at approximately 11 ms. This point in time is subsequently used as temporal indicator to potentially detect the desired neural responses (prior these positions). The click responses show an intensity specific growth function in the time domain prior the WPSS based indicator (marked by a red arrow) as well as a latency shift (top). A comparable behavior is shown by the intensity specific fullscale WPSS (middle). To improve comparability, areas of interest are highlighted by grey boxes. The intensity specific WPSS-map (i.e., 60 dB peSPL) demonstrates a noteworthy synchronization of oscillations in the pseudofrequency range of 150-300 Hz (bottom).

4.1 Results of Study 1

this point in time reflects zero-crossings of oscillations in the respective, intensity specific grand average waveforms when using all intensities, but 50 dB peSPL. This specific maxima seems to lag all other respective maxima, denoted by a red arrow, in the averaged potentials. However, the maxima occur in a time frame of approximately 9-10 ms, whereas the amplitudes are in the range comparable to those shown by the chirp stimulus. According to different stimulus intensities, an increase in amplitudes and a decrease in latencies is observable, again offering distinguishable response morphologies in the averaged potentials as well as within their WPSS, respectively.

4.1.3 Free-Field Responses in Cochlear Implantees

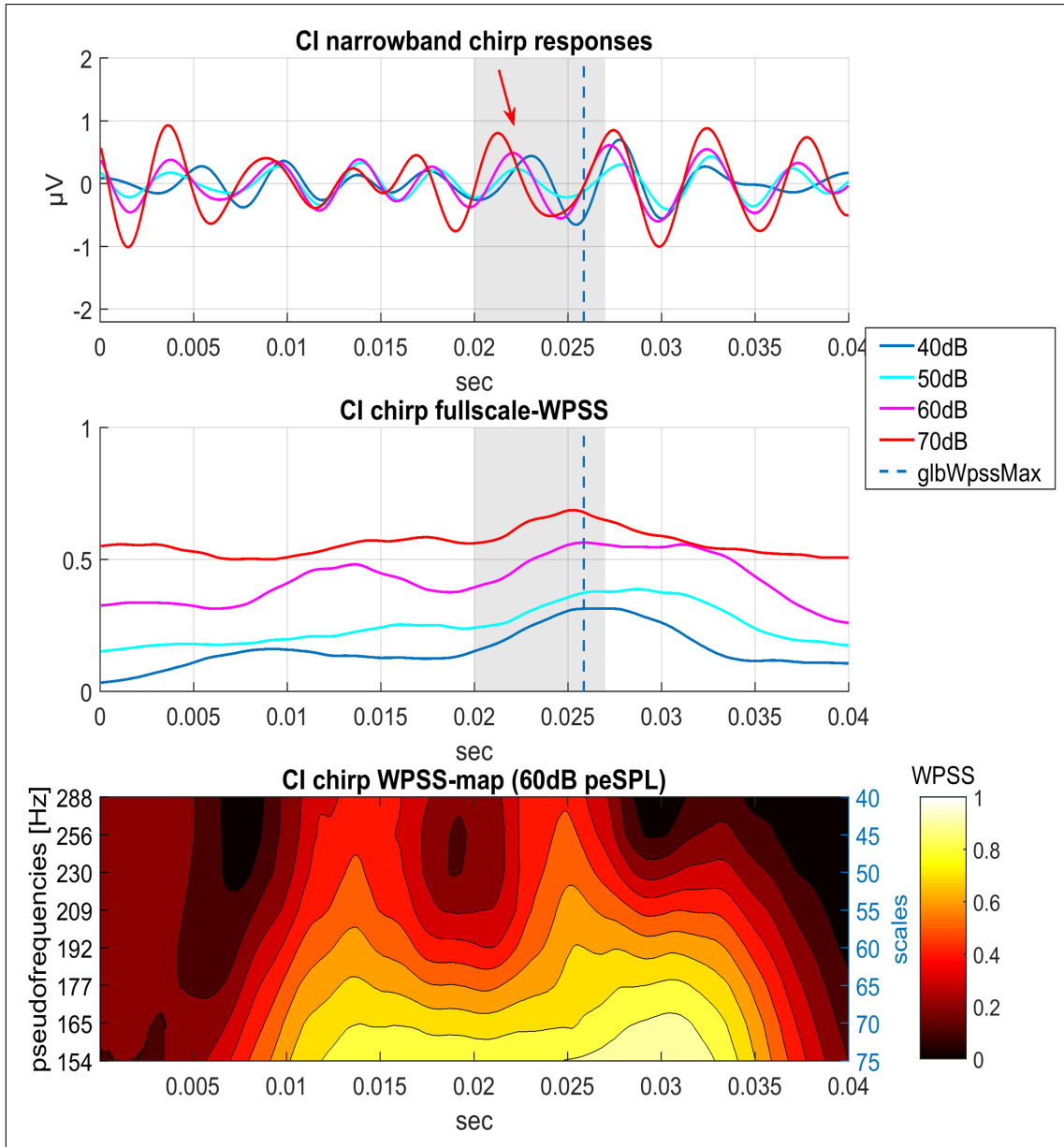


Figure 4.5: Grand average chirp free-field narrowband responses of the CI group, where the general Figure structure is being analogous to Figure 4.3. The temporal position of the global WPSS maximum is again denoted by the vertical dotted line at approximately 26 ms. This point in time is subsequently used as temporal indicator to potentially detect the desired neural responses (prior these positions). The chirp responses show an intensity specific growth function in the time domain prior the WPSS based indicator (marked by a red arrow) as well as a latency shift (top). A comparable behavior is shown by the intensity specific fullscale WPSS (middle). To improve comparability, areas of interest are highlighted by grey boxes. The intensity specific WPSS-map (i.e., 60 dB peSPL) demonstrates a noteworthy synchronization of oscillations in the pseudofrequency range of 150-300 Hz (bottom).

4.1 Results of Study 1

Figure 4.5 shows the grand average narrowband responses of the CI group using the chirp stimulus. The Figure structure is also being analogous to that of Figure 4.3, showcasing the intensity specific grand average narrowband responses, their respective fullscale WPSS, as well as a demonstrative intensity specific WPSS-map. The latter one demonstrates a phase synchronization, which spans over the majority of investigated pseudofrequencies, but a comparatively broader time period from approximately 10-33 ms. Although the averaged fullscale phase synchronizations are not quite as distinct as shown by the NH group, their global WPSS maximum was determined to be approximately 26 ms, where the largest value of about 0.6 is caused by the strongest stimulus intensity. This temporal occurrence is furthermore visible in the shown map. Utilizing this deflection in regularity as temporal indicator of the desired responses, as demonstrated in the NH group, it settles in minima deflections of the averaged responses. The prior maxima get therefore detected, indicated by the red arrow. These maxima occur approximately 22-24 ms after releasing the stimulus from the loudspeaker and amount to averaged amplitudes up to approximately $0.8 \mu\text{V}$. In general, the grand average responses look even more rounded and oscillatory as those shown by the NH group, consequently offering not quite as distinguishable morphology patterns. Besides, the detected maxima increase in amplitude and decrease in latency according to increasing stimulus intensities, however, except the one according to the softest, which is larger in amplitude than the next stronger stimulation. However, the fullscale WPSSs depict a order of deflections similar to order of stimulus strengths. In other words, all responses except the softest offer distinguishable morphology patterns across the intensity specific grand averaged responses, whereas the deflections in the WPSSs mirror the obtained order, respectively.

The grand average results of the CI group according to different stimulus intensities when using the click are shown in Figure 4.6, where the Figure structure is again being analogous to that of Figure 4.3. Here, the WPSS-map demonstrates a patch of regularity across all investigated pseudofrequencies spanning the time period of approximately 10-20 ms, however, not quite as distinct as shown by the NH group, but more defined as when using the chirp in CIs. The individual, intensity specific fullscale WPSS maxima also settle within this time period, where the global maximum results in approximately 17 ms. Here, the fullscale maximum

4.1 Results of Study 1

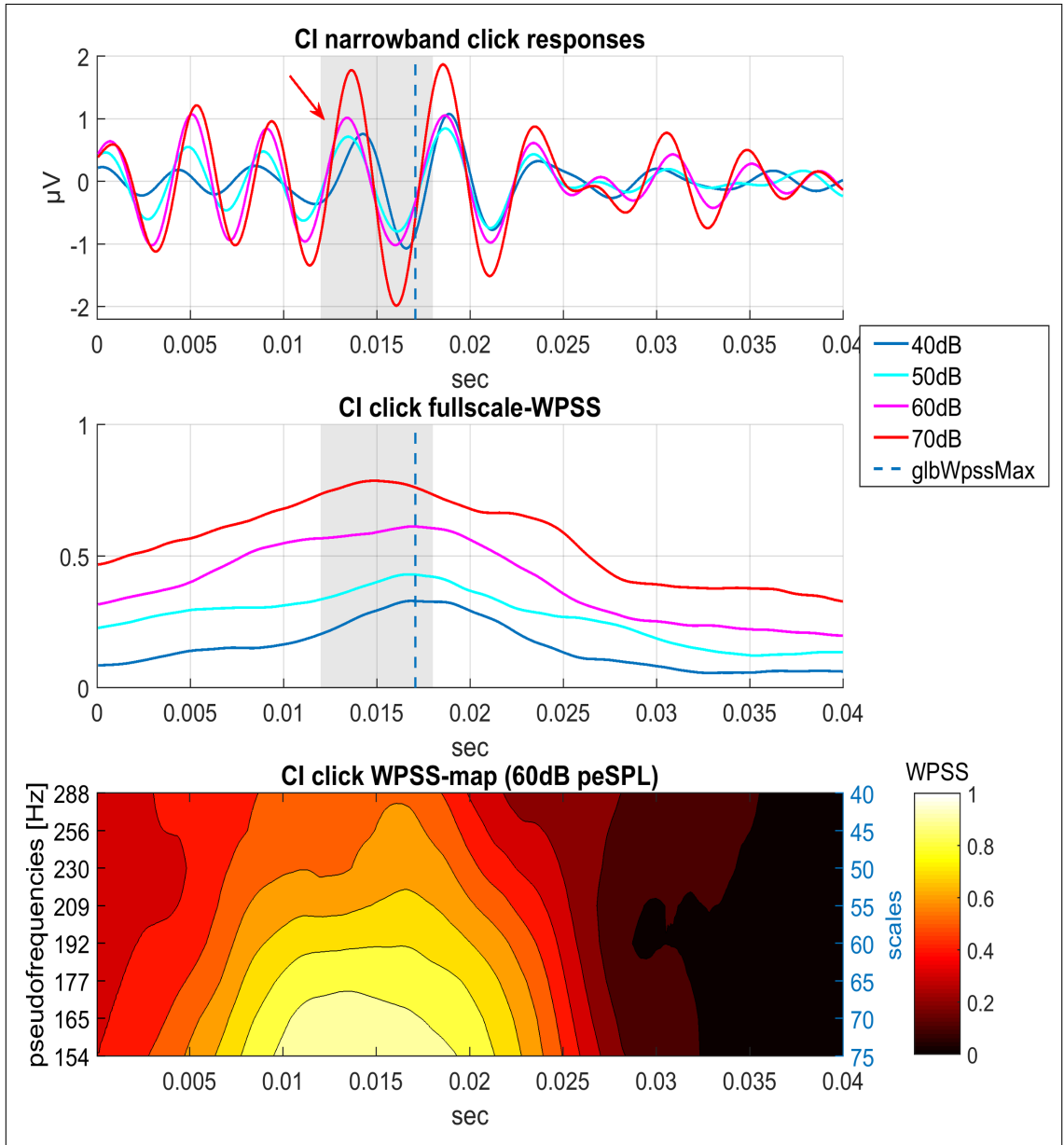


Figure 4.6: Grand average click free-field narrowband responses of the CI group, where the general Figure structure is being analogous to Figure 4.3. The temporal position of the global WPSS maximum is again denoted by the vertical dotted line at approximately 17ms. This point in time is subsequently used as temporal indicator to potentially detect the desired neural responses (prior these positions). The click responses show an intensity specific growth function in the time domain prior the WPSS based indicator (marked by a red arrow) as well as a latency shift (top). A comparable behavior is shown by the intensity specific fullscale WPSS (middle). To improve comparability, areas of interest are highlighted by grey boxes. The intensity specific WPSS-map (i.e., 60 dB peSPL) demonstrates a noteworthy synchronization of oscillations in the pseudofrequency range of 150-300 Hz (bottom).

4.1 Results of Study 1

respective to the used stimulus intensity of 70 dB peSPL amounts to about 0.7. As demonstrated when are using the chirp, this point in time reflects minima of oscillations in the respective, intensity specific grand average waveforms when using all intensities. The leading maxima are therefore again detected, denoted by the red arrow. These deflections settle in a time frame of approximately 12.5-14.5 ms besides demonstrating amplitudes in the range of about 0.8-1.9 μV . As shown when using the chirp stimulation, the amplitudes show a relative growing pattern with rising amplitudes and minor latency shifts according to increasing stimulus intensities, except the two softest stimulations. Here, both responses are similar in amplitudes, whereas the deflection according to the softest stimulation lags the other. These observations will be discussed in detail in Section 5. In general, the averaged response morphologies look rounded and demonstrate a high degree of superpositioned oscillations. However, the fullscale WPSSs demonstrates the strength of the stimulations in its order of magnitudes, respectively.

4.1.4 Confrontation and Statistics

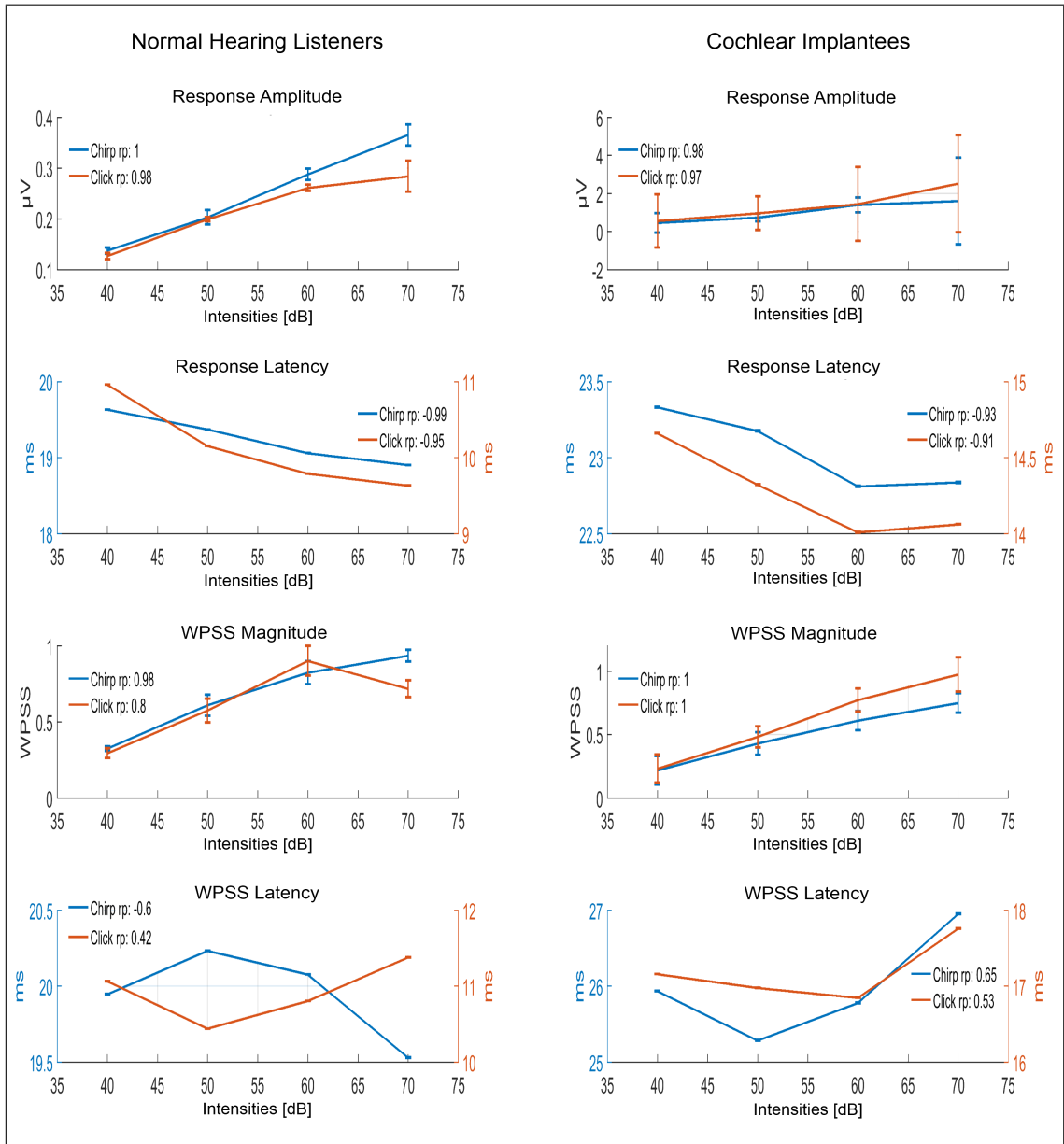


Figure 4.7: Overview of the free-field narrowband response features for the NH group (left column) as well as the CI group (right column) representing the detected median values and their variances as error bars for the chirp (blue) and the click (red). Grand average response amplitudes and variances are shown in the top row, grand average response latencies and variances are shown in the second row, grand average WPSS magnitudes and variances are illustrated in the third row, and grand average WPSS latencies and variances are depicted in the bottom row. Additionally, all subplots share the calculated Pearson linear coefficients r_p within the legend box.

4.1 Results of Study 1

We continued with the procedure of interpreting the manually determined maxima in the intensity specific average potentials prior the respective temporal position of their global WPSS maximum in amplitude as well as their respective fullscale WPSS magnitudes for both used stimuli and groups. The corresponding latencies were also investigated. A confrontation of the detected median values and their variances for the detected narrowband response maxima (upper row), their respective latencies (second row), the corresponding WPSS magnitudes (third row), as well as their latencies (bottom row) is shown in Figure 4.7. Both groups demonstrate an increase in the detected amplitudes and magnitudes alongside increasing stimuli intensities, although variances shown by CI users appear to be larger than those of the NH group, which is partially expected due to individuals' CI fitting and performance. Furthermore, both groups show a decrease in amplitude latencies, but not in the WPSS, which do not offer distinct patterns. Additionally, for all investigated features of the responses, we calculated the Pearson linear correlation coefficient r_p (values displayed in each corresponding legend box in Figure 4.7) using the respective median values to quantify possible linear trends, where an increase along the intensity specific response amplitudes and their respective WPSS magnitudes as well as a decrease in their respective latencies is expected. Positive correlations for the amplitudes and magnitudes as well as negative correlations for the their latencies are shown by both groups and stimuli, however, distinct correlations for the fullscale WPSS latencies were not found in any situation.

Furthermore, we present the results of our statistical analysis in Table 7.1 (attached within the Appendix). Based on the described detections, we first determined Friedman's non-parametric statistical ranking test, based on Krause and Metzler [1983], to investigate significant ($p \leq 0.05$) differences in treatment across multiple test attempts (in our case different intensities for each used stimulus), which allows for further statistical analysis among the tested intensities for both stimuli when positive (first column in Table 7.1). To improve readability, we marked the test results $^*(p \leq 0.05)$, $^{**}(0.05 < p \leq 0.1)$, and $^{***}(0.1 < p)$. In the NH groups' conventionally filtered responses (i.e., commonly used ABR frequency window) using both stimuli, we found significant differences in all tested features, whereas in their narrowband filtered responses, we found significant differences in all tested features, except in their WPSS latencies. The CI group shares

4.1 Results of Study 1

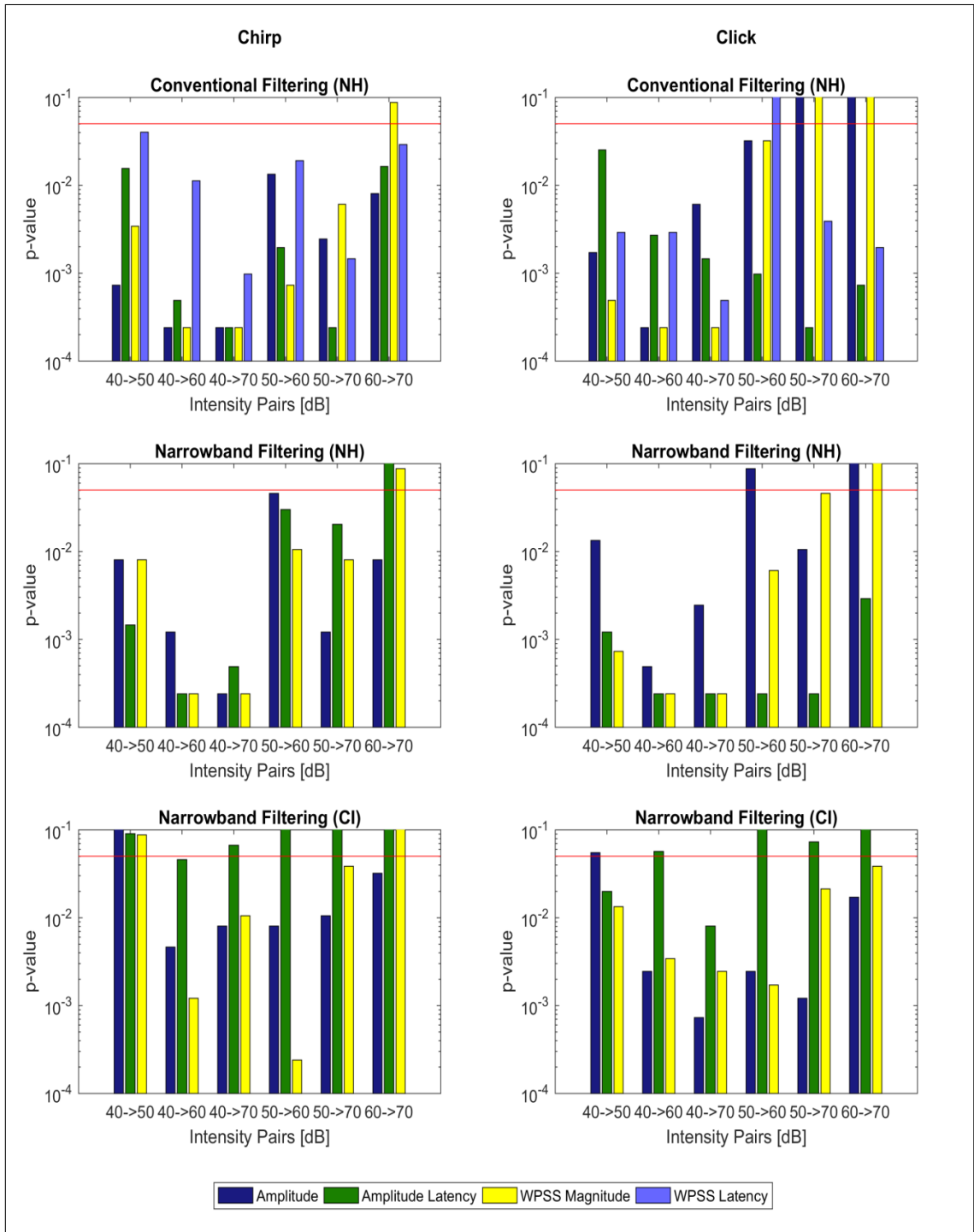


Figure 4.8: Resulting significance values using the Wilcoxon rank-sum paired difference test for the chirp (left column) and the click (right column) when examining conventional filtering in the NH group (top), narrowband filtering in the NH group (middle), and narrowband filtering in the CI group (bottom). The detected response amplitudes, their latencies, their fullscale WPSS magnitudes, as well as their latencies were tested for the intensity pairs of 40->50, 40->60, 40->70, 50->60, 50->70, 60->70 dB pe SPL. The confirmatory p-value of 0.05 is denoted by the red horizontal lines, respectively. When narrowband filtering no detected latency pairs showed significance in treatment (not shown).

these exceptions besides within their chirp evoked amplitudes, whereas all other tested features show significant differences in treatment when using both stimuli. We additionally calculated the one-tailed Wilcoxon rank-sum paired difference test, based on Krause and Metzler [1983], between all used intensities for all detected variables (columns 2-6 in Table 7.1). Note that all results for the chirp (left column) and the click (right column) are visualized in Figure 4.8, where the determined significance according to the different filter settings are shown in the following order: conventional filtering in the NH group (top), narrowband filtering in the NH group (middle), and narrowband filtering in the CI group (bottom). In the conventionally filtered NH group responses, only single tested pairs show no significant difference, e.g., chirp evoked magnitudes between the intensity pair of 60->70 dB peSPL, click evoked amplitudes as well as their magnitudes between the pairs of 50->70 dB peSPL and 60->70 dB peSPL, and click evoked fullscale latencies between the pair of 50->60 dB peSPL, where the arrow (->) denotes the direction of testing. When testing the narrowband filtered NH group responses, we also found significant differences in the tested pairs of amplitudes, latencies, and magnitudes for both stimuli. However, amplitude and magnitude differences between 60->70 dB peSPL show no significant differences alongside all tested fullscale latencies, except the amplitude pair evoked by the chirp. When investigating the narrowband filtered CI groups' responses, we found significant differences in the tested amplitude pairs except between 40->50 dB peSPL for both stimuli. These findings are partially shared by the fullscale magnitudes, whereas a few exceptions are found when using the chirp stimulation. However, nearly all tested latencies show no significant difference in treatment.

4.2 Results of Study 2

4.2.1 Responses With and Without Delay Compensation

The grand average ERPs of the NH control-group (top) and the CI patient-group (bottom) for all stimulation cases are depicted in Figure 4.9, where solid lines represent SUM_{MONO} responses and dashed lines represent binaural responses. Blue lines depict ERPs to the normal listening condition, i.e., SUM_{MONO} (ITD 0 ms) and BIN (ITD 0 ms) for the control-group as well as SUM_{MONO} (ITD 2.5 ms) and BIN (ITD 2.5 ms) for the patient-group. Therefore, red lines depict ERPs to the manipulated listening conditions, i.e., $SUM_{MONO-Asynch}$ (ITD 2.5 ms) and BIN_{Asynch} (ITD 2.5 ms) for the control-group as well as $SUM_{MONO-Comp}$ (ITD 0 ms) and BIN_{Comp} (ITD 0 ms) for the patient-group. A detailed description of the applied listening conditions is given in Section 3.3.2 and Section 3.3.6. Please note that this introduced line- and color-scheme holds for the rest of this study.

When comparing both groups' ERPs, all responses depict comparable response morphologies with the presence of common wave characteristics. The control-group demonstrates a W_V at $\approx 7-9$ ms, a potential P0 at ≈ 15 ms, a Na at $\approx 20-22$ ms, a Pa at ≈ 30 ms, and a Nb at $\approx 40-45$ ms in all listening conditions, which are labeled within the Figure. Although the visualized P0 looks degraded in the averaged responses, especially the W_V in combination with the Na-Pa-complex supports the identification of the responses and labeling wave characteristics. For comparison please see Figure 2.7, where similar latencies are shown. The patient-group, on the other hand, demonstrates a W_V at ≈ 5 ms, a potential P0 at $\approx 11-14$ ms, a Na at ≈ 17 ms, a Pa at ≈ 25 ms, and a potential, but degraded Nb ≥ 35 ms in all listening conditions, which are again labeled within the Figure. In direct comparison to the ERPs of the NH listeners the found W_V s and P0s look degraded, however, the Na-Pa-complex is also well-defined, therefore supporting the response identification and the labeling of their waves. Interestingly, the waves found in the patient-group appear approximately 2-5 ms prior those of the control-group, thus their responses look compressed in time, which resembles common latency findings in CIs (see Figure 2.9). Otherwise, the found ranges of amplitudes are quite comparable, except those of the W_V s and the P0s in the patient-group. More precisely, the NH listeners show well-defined W_V s, whereas

4.2 Results of Study 2

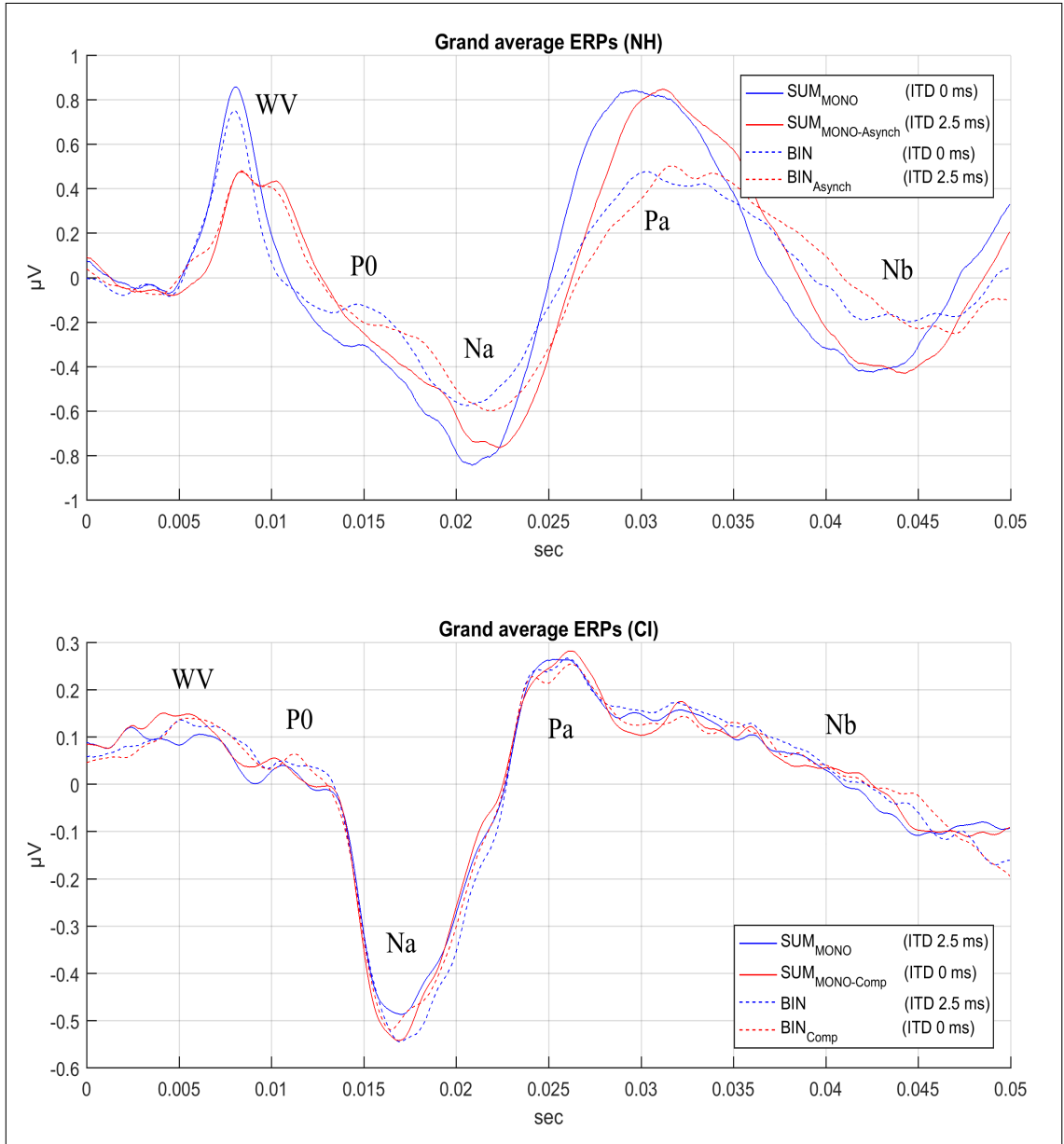


Figure 4.9: Grand average ERPs of the control-group (top) and the patient-group (bottom), both demonstrating a comparable morphology with the presence of the characteristic waves W_V , P_0 , Na , Pa , and Nb . In general, solid lines represent SUM_{MONO} responses and dashed lines represent binaural responses. Blue lines depict ERPs of the normal listening condition, i.e., SUM_{MONO} (ITD 0 ms) and BIN (ITD 0 ms) for the NH listeners as well as SUM_{MONO} (ITD 2.5 ms) and BIN (ITD 2.5 ms) for the CI users. Therefore, red lines depict acerp of the manipulated listening condition, i.e., $SUM_{MONO-Asynch}$ (ITD 2.5 ms) and BIN_{Asynch} (ITD 2.5 ms) for the control-group as well as $SUM_{MONO-Comp}$ (ITD 0 ms) and BIN_{Comp} (ITD 0 ms) for the patient-group. When comparing the responses of both groups in the manipulated listening condition, a clear decrease in the W_V amplitudes is observable for the NH listeners while an increase is noticeable for the CI implantees.

4.2 Results of Study 2

the patient-group shows degraded versions, which are more rounded and smaller in amplitude. These look-alikes and behaviors get also confirmed by findings in single participants' average ERPs of the control-group (NH#10, top) and of the patient-group (CI#6, bottom), which are depicted in Figure 4.10. The Figure structure as well as the line- and color-scheme are analogous to Figure 4.9. Besides minor dissimilarities, expected response morphologies and their waves W_V , P0, Na, Pa, and Nb are recognizable in both participants, since sharing a similar time signature compared to the grand average latencies. Noteworthy is the well-defined P0 shown by the bimodal CI user, which distinguishes in presence from findings in all other examined individuals' responses. Such findings further substantiate the obtained response identification.

However, when comparing the brainstem-level responses of the different listening conditions within the groups, respectively, relative changes in their morphologies, latencies and amplitudes are noticeable. In the normal listening condition, both, the grand average responses of the NH control-group as well as those of their highlighted participant, show a larger superpositioned deflection of the W_{VS} (SUM_{MONO}) than during their respective binaural stimulation (BIN), where the latter one is slightly advanced in temporal occurrence. Contrarily, in the asynchronous listening condition, the grand average responses depict at least an equally large deflection during binaural stimulation (BIN_{ASYNCH}) compared to the their respective sum of monaural stimulation responses ($SUM_{MONO-ASYNCH}$), whereas the emphasized individual participant shows a even larger deflection during binaural presentation. In general, resulting amplitudes according to the normal listening condition are larger (relative ratio of $\approx 50\%$), therefore offering more distinct manifestations of the desired W_{VS} , respectively.

In the patient-group, on the other hand, a quite reversed behavior is recognizable. In the normal listening condition, the grand average responses as well as those of their emphasized individual participant show larger amplitude deflections when stimulating binaurally (BIN) than as shown by the summation of the respective monaurally evoked responses (SUM_{MONO}). Therefore, during the compensated listening condition, the resulting summations (SUM_{COMP}) are larger in deflection compared to those of the binaural stimulation (BIN_{COMP}) in both visualized sets of responses. In general, found amplitudes during the compensated listening condition are larger (relative ratio of $\approx 50\%$).

4.2 Results of Study 2

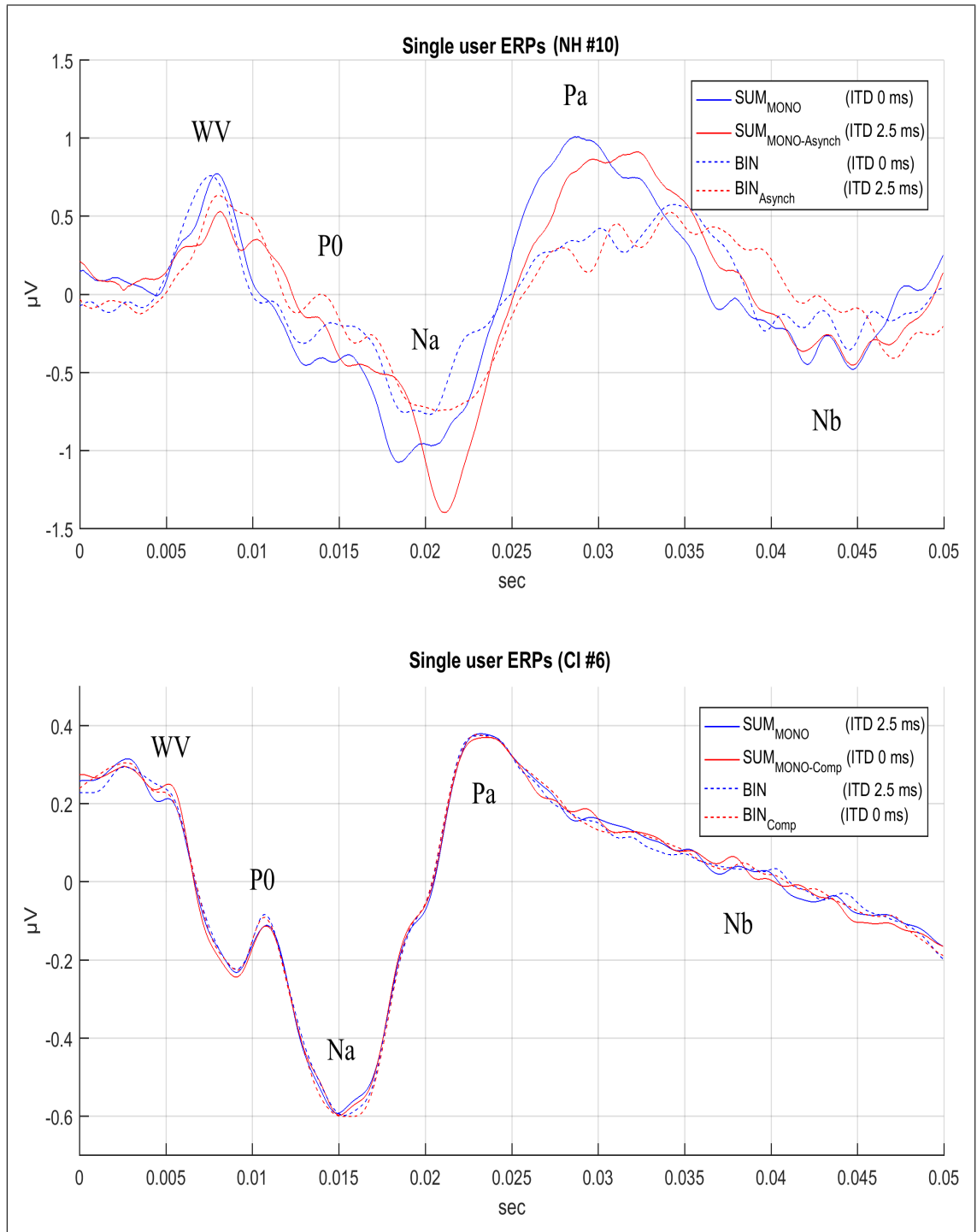


Figure 4.10: Single users average ERPs of the control-group (NH#10, top) and the patient-group (CI#6, bottom), both resembling the grand average morphologies shown in Figure 4.9 with the presence of the characteristic waves W_V , P_0 , Na , Pa , and Nb . The Figure structure and color scheme are analogous to that of Figure 4.9. Both participants demonstrate the expected behavior when comparing among the different listening conditions. Noticeable is a more distinct P_0 in the bimodal CI user.

4.2.2 Binaural Interaction Components

The resulting BICs for the normal listening condition (BIC (ITD 0 ms) for the control-group and BIC (ITD 2.5 ms) for the patient-group, both depicted by blue lines) and the manipulated listening conditions (BIC_{Asynch} (ITD 2.5 ms) for the control-group and BIC_{Comp} (ITD 0 ms) for the patient-group, both denoted by red lines) are depicted in Figure 4.11, where the visualizing structure and color scheme are analogous to that of Figure 4.9.

Resulting overall amplitude deflections of the control-group are larger in comparison, whereas both groups demonstrate distinct response phenomena even exceeding brainstem-level. Although, primarily investigating binaural interaction at brainstem-level, i.e., during the time period of the W_V , we additionally examined the determined BICs along the total response duration visually, in a comparable manner demonstrated by McPherson and Starr [1993]. Note that such binaural computations are originally defined for brainstem responses. Besides, low frequency oscillations within the BICs of the patient-group and the not defined moments in time for interaction analysis are additionally challenging such investigations. Thus, analyzing BICs beyond brainstem-level will be treated phenomenological. However, NH listeners show a larger residual positive amplitude in the temporal period of the W_V , a broader, but less negative deflection at the Na, a broader positive and leading deflection at the Pa, and a less negative deflection at the Nb during the normal listening condition. Compared with that, they show a diminished residual amplitude in the temporal period of the W_V , a greater negative deflection at the Na, a positive, but lagging deflection at the Pa, and a larger negative amplitude at the Nb during the asynchronous listening condition.

As indicated by the grand average responses (see Figure 4.9), the relative relationship of the patient-groups' resulting BICs among the different listening situations is partially reversed along the full response duration. During the normal listening condition, CI users show a smaller positive deflection in the period of the W_V , a greater positive amplitude at the Na, and an ongoing diminished amplitude during the Pa as well as the Nb. In comparison to that, they show a greater positive deflection during the period of the W_V , a positive, but smaller deflection during the Na, and larger positive, but oscillatory deflections covering the Pa as well as the Nb.

4.2 Results of Study 2

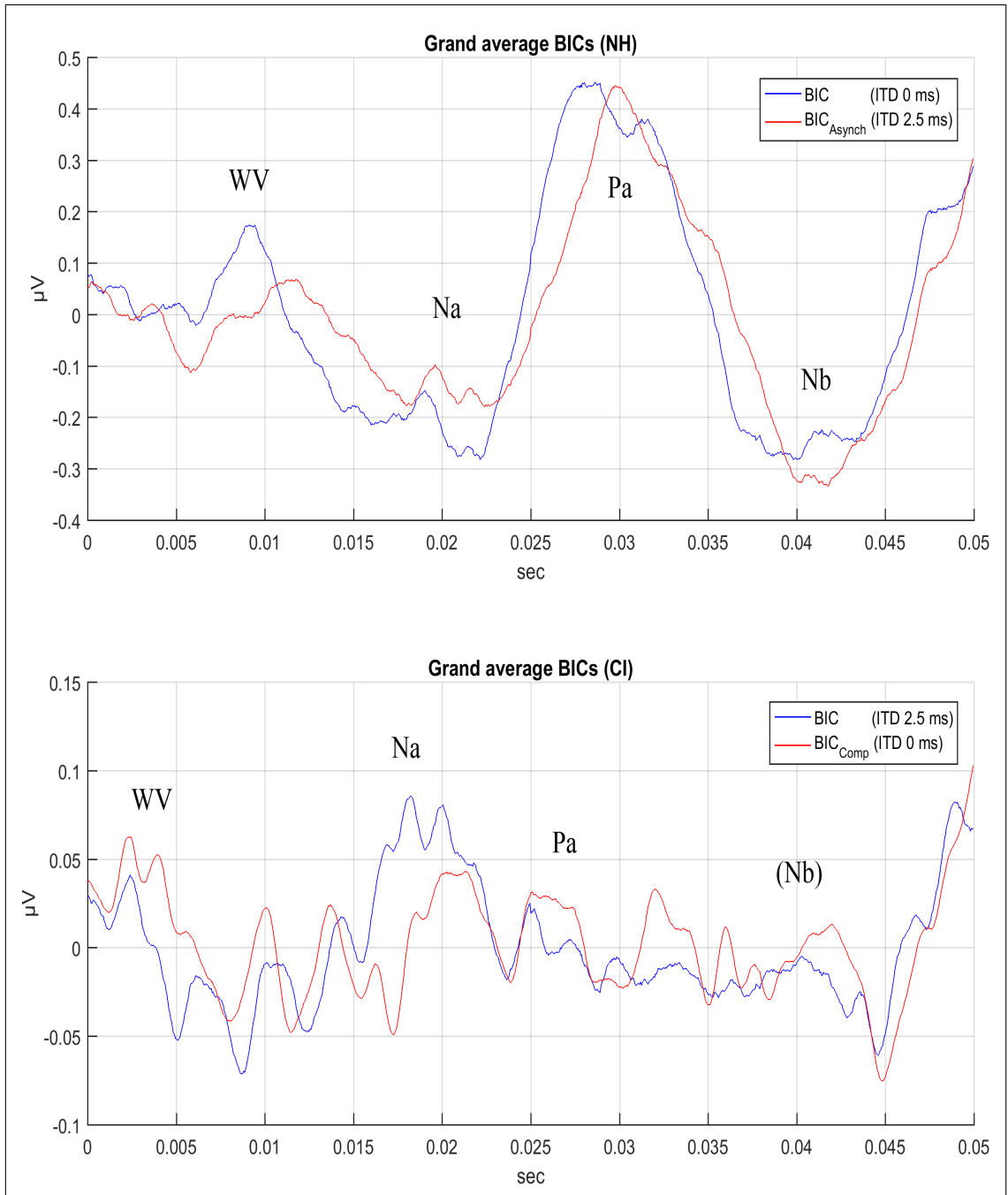


Figure 4.11: Grand average BIC results of the control-group (top) and the patient-group (bottom), where blue lines represent those of the normal listening condition, i.e., BIC (ITD 0 ms) for the NH listeners and BIC (ITD 2.5 ms) for the CI users, while red lines represent those of the manipulated listening condition, i.e., BIC_{Asynch} (ITD 2.5 ms) for the control-group and BIC_{Comp} (ITD 0 ms) for the patient-group. In the manipulated listening condition, NH listeners show a smaller amplitude in the temporal area of the W_V (≈ 7 -8 ms) and a larger amplitude in the temporal area of the Na (≈ 20 ms). In comparison, the implantees show a larger amplitude in the temporal area of the W_V (≈ 4 -5 ms), a smaller amplitude in the temporal area of the Na (≈ 18 -20 ms), and a larger amplitude in the temporal area of the Pa-Nb-complex (≥ 25 ms).

4.2.3 Confrontation and Statistics

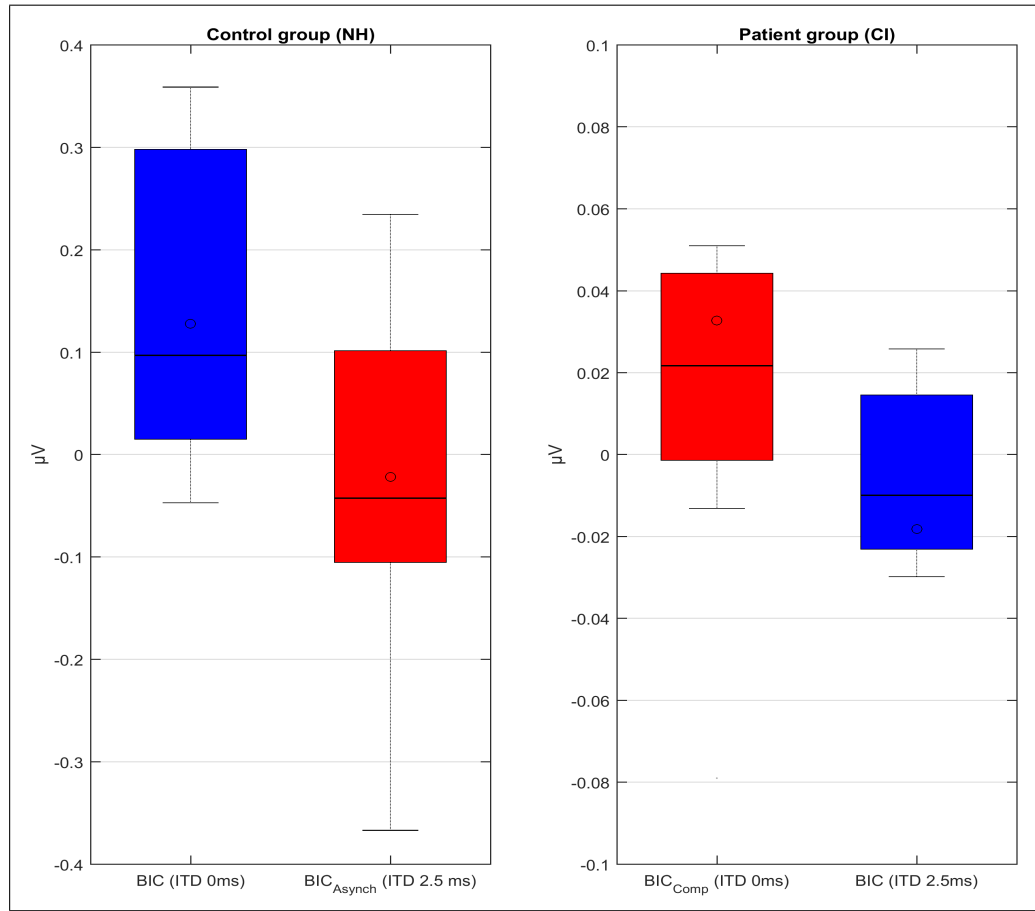


Figure 4.12: Overview of the W_V BIC amplitudes of the control-group (left) and the patient-group (right), where blue boxes represent the resulting amplitudes in the normal listening condition (BIC (ITD 0 ms) for the control-group and BIC (ITD 2.5 ms) for the patient-group) and red boxes represent those of the manipulated listening condition (BIC_{Asynch} (ITD 2.5 ms) for the control-group and BIC_{Comp} (ITD 0 ms) for the patient-group). While the NH listeners shows a significant decrease in the manipulated listening condition (9 out of 10 participants; p-value: 0.032), the implantees demonstrates a significant increase (9 out of 10 participants; p-value: 0.0445).

When analyzing the resulting BICs for all listening conditions focusing the temporal area of the W_V, 9 out of 10 control-group participants show a distinct decrease in amplitude in the asynchronous listening condition (BIC_{Asynch}) compared to the normal listening situation (BIC). As indicated, the patient-group demonstrates the opposite behavior, where 9 out of 10 participants show an increase in amplitude in the compensated listening condition (BIC_{Comp}) compared to the normal listening condition (BIC). Figure 4.12 showcases the results for the control-group (left) and

4.2 Results of Study 2

the patient-group (right), where amplitudes found in the normal listening condition are indicated in blue and those found in the manipulated listening conditions are indicated in red. A clear trend can be seen, where examined amplitudes partially overlap in value among the different listening situations, but mean and median values clearly indicate possible separation. When applying a one-tailed Wilcoxon rank-sum paired difference test, as similar used within Study 1 (see Section 4.1.4), the resulting p-value for the control-group values to 0.032 while for the patient-group it is 0.0445, thus both group-behaviors are statistically significant different according to their listening condition.

5 Discussion

5.1 Discussion of Study 1

5.1.1 Free-Field Apparatus

The definition of ERPs designates the general class of potentials that display stable time relationships to a definable reference event, which does not limit the event to certain presentation styles, e.g., headphones in AEPs [Corona-Strauss, 2009] or electric activations of the AN in EABRs [Bahmer et al., 2010], but insists on its unavoidable condition of time dependency and causal chain [Vaughan, 1969], e.g., detection of the prominent W_V deflection in the ABR which is assembled by averaging time-locked and deterministic regularity across single trials [Hall, 2007]. Note that the introduced method of free-field evoked auditory response analysis does not violate this unambiguous rule as long as measurement conditions kept constant and identified responses can be time related to their distinct origin. When taking the time point when the stimulus gets released from the loudspeaker, the constant traveling distance, and the sound velocity into account, apparatus based relative delays get rendered. Accounting these when correlating time dependencies of collected responses, a regular faithful realization of evoking auditory ERPs using an audiometric free-field configuration is achieved. Pleasantly, as a result, merging the reference event to one unique determining stimulation presentation when evoking responses in NH listeners as well as in CI implantees, therefore generally allowing for the use of real world stimuli [Fobel and Dau, 2004] while keeping the whole electrode array active, for an investigation and comparison of response characteristics, and for an estimation of device based technical induced delays. In other words, it potentially grants response analysis and comparability while incorporating 'real world' listening situations potentially unaffected by

included hearing devices (HA or CI). Keep in mind, that includes all kinds of hearing configurations: NH, unilateral, bilateral, and bimodal. By contrast, such insight are limited when comparing classical ABRs and EABRs, since they face a higher degree of freedom in influencing factors, they eventually bypass parts of the auditory processing chain in CIs, and at least offer complex adaptations to encompass comparable stimulus presentations [Firszt et al., 2002; Chatterjee et al., 2006; Bahmer et al., 2010].

Besides, there are some points noteworthy to discuss. First, is the system specific traveling distance of the stimulus, which needs to stay constant during the whole procedure. Such necessary adjustments of the head should be easy to accomplish, while in this study head movement was continuously limited and additionally controlled by the audiologist. Minor head movements as well as the relative small differential distance covering both groups' membranes were neglected. However, when investigating inter-trial synchronicity across collected single responses of NH listeners, distinct patches of regular activity are shown, therefore rendering specific temporal post-stimulus periods for both used stimuli, even when employing conventional filter settings and scales (compare WPSS-maps of Figure 4.1 and Figure 4.2). As demonstrated by conventional ABR measurements [Hall, 2007], the found deterministic behavior will result in synchronized, distinct peaks in the averaged response waveform [Strauss et al., 2004, 2013] (depicted by black lines in the respective Figures). Interestingly, responses caused by both used stimuli visualize one uniquely highlighted wave (both indicated by red arrows), respectively. Without a doubt, such narrow, sharp, and separateable waves would not occur, if system manipulating jitters based on head movements were included, which would rather cause diminished and flattened shapes. Thus, the mentioned waves are easily identifiable at approximately 18-19ms when using the chirp and at approximately 10ms when using the click, therefore promisingly resembling our response latency estimations by Equation 3.2.1. Further note that the obvious latency lag between both response waves nearly matches the duration difference of the used stimuli. When analyzing relative behavioral changes of these waves related to different stimulus intensities, i.e., a free-field adaptation of the commonly used BERA investigation, significant distinguishability for both stimuli is shown across nearly all investigated features and intensity-pairs (see Figure 4.8 and Table 7.1). These findings in NH listeners consequently support our identification and

5.1 Discussion of Study 1

labeling of these waves as W_{vs} , although being caused by a stimuli released from a loudspeaker in a free-field environment. A pool of NH participants of 10 and more seems sufficient for benchmarking this approach, whereas the additional use of robust and separate tools, like the WPSS [Corona-Strauss, 2009], to identify and analyze such untouched responses demonstrates to be especially beneficial and practical.

Secondly, is the speculation of stimulus distortion due to its traveling confronted with system based circumstances, e.g., the traveling distance and room audiometric characteristics, eventually affecting precise stimulation constructs like the chirp [Fobel and Dau, 2004]. Please note that it was the aim of this study to investigate general feasibility of this free-field approach, where using two different stimuli served as additional evaluation in response identification based on specific and unequal event durations, rather than investigating specific stimulus properties. Therefore, potential stimuli distortions and the resulting versions and shapes were not further examined, since drawbacks negatively affecting basic response analysis were not assumed. However, if necessary in future experiments, we emphasize to record the resulting stimuli using a sufficient microphone at the position of the participants head, to compare the released and the recorded versions, and to eventually adjust stimulation conditions and stimuli.

A third point that needs to be discussed addresses the potential information value and benefit for the neuroscientific research in CIs when using such an approach. In the previous Sections we introduced the NH human auditory system, its complex architecture, and its highly coordinated functioning, therefore allowing for precise binaural encoding of interaural information differences [Jeffress, 1948; Campbell and King, 2004]. Although eminent hearing benefits due to the use of a CI are globally accepted [Zeng, 2004; Hall, 2007], exact neurophysiological effects and influences on the auditory processing chain are still being discussed [Guerit et al., 2014; Skinner et al., 2002; Rosen et al., 1999; Siciliano et al., 2010; Kan et al., 2013]. Especially when considering the necessity of fine and balanced time coding in binaural processing cues of NH listeners, alterations of this auditory processing chain while eventually including technical driven delays arguably suggests to cause a misalignment. However, exact alterations are still unknown, what can be eventually explained by limitations in comparability of today's measurement methods, since they do not incorporate equal determining

stimulation events. Fortunately, such temporal insights get rendered by the introduced free-field approach, since it involves all investigated auditory chains in their totality. This becomes obvious when comparing temporal occurrences of synchronized, event related activity among both groups' responses. Even when narrowband filtering, which's reasoning will be discussed in detail in the following Sections, the previously identified temporal periods of related response regularity still hold in NH listeners (compare WPSS-maps of Figure 4.1 and Figure 4.3 as well as Figure 4.2 and Figure 4.4), where the temporal spans are even more defined. Note that this temporal refinement can potentially be explained due to tightened filter boundaries and scales, therefore limiting dispersive influences caused by frequencies which hold less information content, i.e., higher frequencies as successfully demonstrated by Corona-Strauss [2009]. Although not quite as distinct in temporal concentration, found respective global, fullscale WPSS maxima strongly indicate divergent and lagging post-stimulus time points in CI implantees, where the maximum phase synchronization occurs at approximately 26 ms when using the chirp and at approximately 17 ms when using the click (compare Figure 4.3 and Figure 4.5 as well as Figure 4.4 and Figure 4.6). Note that the obvious latency lag between both response waves resembles the duration difference of the used stimuli, as comparably shown by the NH listeners. This seems to capture crucial response latency alterations even exceeding critical binaural values of several milliseconds at brainstem-level [Jewett, 1970; Stollman et al., 1996; McPherson and Starr, 1993; Hosford et al., 1979; Campbell and King, 2004; Zirn et al., 2015, 2019; Strauss et al., 2004], however, it states an unambiguous result of this work by its own, since such differences are arguably not covered in today's CI neuroscience.

5.1.2 Response Alterations

In the previous Section, we covered the general feasibility of free-field evoked ABRs in NH listeners, even when using conventional filter settings, therefore offering quite similar response morphologies compared to those of conventional ABRs [Hall, 2007]. Please note that similar responses of CI users, while using their entire frequency-to-electrode allocated array, are so far untouched and unseen, arguably leaving expectations regarding their morphologies simple and undetailed. However, it is most likely to encounter accumulated affects of broadband stimulation artifacts caused by individual electrodes [Sinkiewicz, 2015; Gordon, 2007; Shallop, 1993], consequently covering the duration of the stimulus, therefore overlapping desired waves in an also unknown, but event related, manner. This assumption obviously challenges analysis of the so far unseen responses altogether. Actually, when using conventional filter boundaries alongside artifact filtering with meaningful threshold hardly any single trials could be collected in any CI user. Only when totally excluding artifact filtering, effectively one single CI user showed an interpretable ABR pattern in single, isolated trials (not shown). In other words, analysis of such free-field evoked responses in CI users, while employing conventional filter settings, seems not reliable. However, since divergent response morphologies are expected in any case, this offers the argumentative mindset for narrowing filter settings to still encompass reasonable response information as demonstrated by Yeung et al. [2004], while partially excluding disturbing influences of the broadband CI stimulation artifact sequence. This mindset was previously introduced in Section 3.2.3. We consequently searched for the frequency window that holds for the most part the desired exogenously driven synchronized regularity, what causes the prominent W_V in the average NH ABR waveform. Using the WPSS as a supporting indicator, we found the peak frequency within the range of 150-300 Hz (bottom rows in Figure 4.1 and Figure 4.2), where a noteworthy synchronized regularity takes place. Note that a similar narrowband ABR frequency window was successfully investigated by Corona-Strauss [2009]. However, when narrowband filtering ERPs those get distorted by the so called ringing artifact [Luu and Tucker, 2001; Yeung et al., 2004], as can be seen in Figures 4.3-4.6. Please note that the presence of such oscillations does not violate the determining rule of causality, since it is known that the magnitude of the caused distortion will depend on the size of the original event-related response wave in the average waveform [Yeung et al., 2004], what

automatically forces a synchronous event relation by its own. This behavior gets demonstrated across the responses of NH listeners when using both stimuli (compare black and blue lines in Figure 4.1 and Figure 4.2). Although oscillating, direct cross relations can be obtained reliably, therefore supporting the identification of neural correlates sharing substantial information content, e.g., the prominent W_V . By contrast, a one-to-one adaptation of cross correlation is not manageable in CI implantees, based on the mentioned unknown response latencies and the absence of conventionally filtered responses, thus incorporating additional evaluation criteria, like their respective WPSS in combination with the BERA protocol, demonstrates especially useful, what will be further discussed in the following Section. Thus, one is limited in analyzing only the narrowband filtered versions, whereas the comparison of inter- and intra-groups' responses when using identical filter settings gets not further affected. As a result, we are able to adapt identification procedures successfully demonstrated in narrowband filtered responses of NH listeners to those of CI users, what suggests to gain comparable insights into so far unseen potentials.

5.1.3 Response Characteristics, Behavior, and Interpretation

For response identification in CI users we adapted our findings from the NH group, where the maximum phase synchronization appears in the local minimum after the W_V in the ABR (Figure 4.1 and Figure 4.2), what induces the method of interpreting the very first maximum prior the temporal fullscale WPSS maximum as the desired neural correlate of the W_V . Figure 4.3 and Figure 4.4 (NH) as well as Figure 4.5 and Figure 4.6 (CI) show the group specific grand average results for both used stimuli, respectively. Note the mentioned temporal dependencies between the global WPSS maxima (denoted by the vertical dotted lines) and the leading maxima in the average intensity specific potentials, where the NH listeners show temporal WPSS maxima at ≈ 20 ms when using the chirp and at ≈ 11 ms when using the click. In contrast, CI users show those maxima at ≈ 26 ms when using the chirp and at ≈ 17 ms when using the click. This shows a consistent temporal lag for both stimuli of ≈ 6 ms according to the obtained WPSS maxima and of ≈ 3 -4 ms according to the obtained W_V maxima between both groups. Consequently, this has implications for the current research field of ITDs and binaural interaction [Jewett, 1970; Stollman et al., 1996; McPherson and Starr, 1993; Hosford et al., 1979] since interaural lags exceeding 600-1,000 μ s will arguably prohibit meaningful integration of binaurally presented information at the brainstem-level. We further adapted the BERA protocol when using both stimuli to additionally investigate relative changes across the intensity specific responses [Hall, 2007]. This step is necessary because offering additional evidence if the correct peak (the desired response) is found. When investigating the neural behavior according to increasing stimulus intensities [Hall, 2007] the NH listeners distinctly show the expected amplitude growth as well as the expected latency shifting in both used stimuli (Figure 4.3 and Figure 4.4), besides this is partially visible in their corresponding WPSS. By contrast, this neural behavior is not as distinct as in the CI users' grand average responses, but holds when investigating their corresponding WPSS (Figure 4.5 and Figure 4.6). For a better comparison, the identified response features (amplitudes, WPSS magnitudes, and respective latencies) are summarized in Figure 4.7, showing the detected grand average median values as well as their respective variances for both groups, respectively. In general, an increase in amplitudes and magnitudes alongside a decrease in respective latencies is observable for both groups and stimuli with increasing

stimulus intensities. However, since the trend shown by median values of observed maxima demonstrates the hypothesized neural behavior, whereas when utilizing average values does not (compare average maxima of 40 and 50 dB pe SPL in Figure 4.5 and Figure 4.6), this eventually affirms potential outliers. Thus, this needs to be investigated in successive studies with larger group sizes.

Another observation that needs to be discussed is the around ten times increased response amplitude shown by CI users, what can potentially be explained by former results of EABR measurements [Bahmer et al., 2010; Miller et al., 2008; Thai-Van et al., 2007], where W_V amplitudes are in fact in the range of those of conventional ABRs. The major difference is that we especially aimed for a use of the whole electrode array in our experiment (instead of using single isolated electrodes like in conventional EABR measurements) by using broadband stimuli (chirp and click) potentially leading to a summation of EABRs in the range of the number of active implant electrodes (>10). Although the implant electrodes do not fire simultaneously, the temporal lag between two successively firing electrodes can be considered negligible, supporting the idea of a summation of EABRs leading to increased amplitudes in CI users when leaving their complete electrode array active during free-field stimulation. Note that these findings are not detectable in conventional EABR measurements. Necessarily, the validity of this hypothesis needs further investigations, however, we emphasize that there exist no alternatives to employing the whole electrode array and associated preprocessing chain (microphone, sound processor and filter bank) in obtaining evoked responses closely representing the users' daily-life listening situations. Using statistical analysis (Friedman and Wilcoxon tests), we found significant paired differences between the used intensities in nearly all conventionally filtered features of the NH group (see Figure 4.8 and Table 7.1). We also found significant differences in nearly all detected, narrowband filtered amplitudes in both stimuli and groups, indicating that differences of approximately 10 dB pe SPL are for the most part distinguishable using the neural correlate. However, intensity steps of 20 dB pe SPL exhibit significant increases across all compared intensity pairs in both groups. Comparable results are observable for the WPSS magnitude in both stimuli and groups, where 10 dB steps do not exhibit significant increases in the neural correlate, while 20 dB steps do. By contrast, this behavior changes when investigating the latencies of narrowband filtered responses. We could not observe

significant differences in any WPSS latency in both stimuli and groups. While we found significant differences in narrowband filtered NH listeners' response latencies in almost every condition, results were not significant for the CI users, although Figure 4.8 (second row/column) indicates a similar behavior. These findings get additionally supported by the calculated Pearson linear correlation coefficients (r_p), which demonstrate the expected trends across tested features but the WPSS latencies. However, there are two possible explanations regarding this diversity. On the one hand this might be affected by the narrowband filtering itself, excluding higher frequencies, what potentially reduces temporal resolution. These assumptions are based on the statistical findings, where WPSS latencies are distinguishable when using the conventional frequency window but not when using the narrowband frequency window in the NH group, where the difference in treatment is narrowband filtering. On the other hand temporal resolution of scale-average WPSS (fullscale WPSS) is bounded by the time-frequency uncertainty of the lowest incorporated scale, thus potential significant changes in the peak locations may be masked by temporal smearing.

To summarize, the interpretation of conventionally filtered CI users' free-field responses alongside meaningful artifact filtering when leaving the complete electrode array active is practically infeasible. Although signal quality and differentiability get altered when those responses being narrowband filtered, visual (Figures 4.3-4.6) alongside statistical (Table 7.1) analysis of those responses do in fact grant unique accessibility for interpretation of CI users' true-to-life responses at brainstem-level.

5.2 Discussion of Study 2

5.2.1 Sequencing and Deconvolution

McPherson and Starr [1993] were one of the first who demonstrated advanced insights into binaural interaction across the auditory pathway, therefore exceeding isolated response analysis of single stages, thus unified BICs covering all temporal classes of the AEP were achieved, i.e., ABR, AMLR, and ALR. On the one hand, based on the temporal and spatial occurrence of the responses of interest, variant waves with differential amplitudes are detectable, therefore requiring specific amounts of trials when conventionally averaging to gain the deterministic waveform with reasonable SNR. Thus, when analyzing ABRs more trials are needed than when investigating ALRs [Hall, 2007]. On the other hand, slower stimulus rates are required for longer latency responses [Tharpe and Seewald, 2016], thus based on the specific and uneven durations of the categorized responses, also differential and specific inter stimulus intervals are required when using classical and non-overlapping stimulation procedures. Noteworthy, when translating our approach of collecting 1,000 responses synchronously covering ABRs as well as AMLRs respective to four different listening situations (see Section 3.3.6) into classic isochronous stimulation procedures, stimulation rates as slow as approximately 1-2 Hz are recommended to use in NH listeners [Tharpe and Seewald, 2016]. Without a doubt, resulting measurement lengths would be tedious and unreasonable, which even more increase when considering that commonly multiple thousand trials are collected to gain sufficient SNRs in ABRs [Hall, 2007]. Effectively, we obtained a mean stimulation rate of 30.25 Hz while using stimulation sequences of 10 interleaved repetitions, where the resulting responses were disentangled using the CL(A)D method to elicit one representative response [Holt and Özdamar, 2014, 2016], therefore effectively reducing the total measurement duration (in our case approximately 25 minutes). Although higher stimulation rates in isochronous AMLR measurements were successfully reported in NH adult listeners [Tharpe and Seewald, 2016], resulting SNRs decreased based on jittering amplitudes even across commonly collected amounts of responses [Tucker et al., 2002]. In contrast to that, based on the optimization method proposed by Kohl et al. [2019a], SNRs of our introduced deconvolution approach demonstrate superior gain factors c_{dec} and g_{dec} over the mentioned conventional averaging, respectively (see Figure 3.3). Consequently,

this suggest to be practically useful, especially when considering analysis of so far unseen responses synchronously covering the brainstem and upper brainstem-level stages in CI users in an adequate amount of time.

Importantly, AEPs in CI implantees are affected by the prominent stimulation artifact [Sinkiewicz, 2015; Gordon, 2007; Shallop, 1993], therefore challenging their analysis (see Section 2.5.2). Based on the work of Schebsdat et al. [2018] and the reasoning in Study 1 (see Section 3.2.3), we adapted special narrowband filtering in both tested groups of this Study to still encompass sufficient response information content besides partial exclusion of influencing distortion caused by the artifact. However, measurement conditions, protocols, and the span of the selected frequency window strongly divagate across the Studies, thus consequent differences in response identification and labeling of found characteristics need special clarification. Since we applied a novel stimulation procedure while employing an even more compressed frequency window to treat artifact sequences caused by whole array stimulations in Study 1 (see Section 3.2), we strictly limited expectations regarding response analysis, thus we focused on correlations rather than classical AEPs in CI users. Consequently, we avoided labeling of resulting waves, e.g., the prominent W_V in the narrowband filtered average response, which is necessary to identify when investigating binaural interaction. In contrast to that, the identification of response characteristics assembled comparably practicable in this Study, where a more conventional stimulation technique was used while incorporating less electrodes of the array in CI users, thus a softer distortion caused by stimulation artifacts was expected. As a result, this allowed for the adjustment of more reasonable filter boundaries in preprocessing [Corona-Strauss, 2009], therefore supporting classical response analysis and comparability [Hall, 2007], in which the incorporation of the SNR optimization method by Kohl et al. [2019a] obviously demonstrated additional beneficance. Further supportive were synchronous measurements of upper brainstem-level stages, where found Na-Pa-complexes particularly facilitated spatial and temporal classifications. Thus, in total, a sufficient response identification was achieved in both groups and therefore the labeling of their response characteristics, e.g., the desired W_{Vs} .

5.2.2 Response Characteristics and Interpretation

In the normal listening condition, the control-groups grand average responses of SUM_{MONO} and BIN show a distinct ERP morphology including all prominent waves: W_V, P0, Na, Pa, and Nb, although the P0 appears degraded (Figure 4.9, top). Notable is the well defined and obvious W_V ($\approx 7-9$ ms), which is mandatory for the subsequent BIC analysis. All waves occur reasonable in time and amplitude, comparable to [McPherson and Starr, 1993]. The acquired morphology is robust across all participants within the control-group (e.g., NH#10 in Figure 4.10, top), supporting the general feasibility of the introduced narrowband sequential deconvolution approach to access ERPs exceeding the classical timeframe of ABRs up to parts of the successive middle latency responses in NH listeners - besides offering a faster acquisition time [Delgado and Özdamar, 2004; Kohl et al., 2019a].

As expected, when comparing the responses of the normal listening condition against each other, the SUM_{MONO} peak appears larger and slightly later than the BIN peak (see Figure 4.9 and Figure 4.10, both top), which will result in a positive residual peak in the BIC (see blue line in Figure 4.11, top) - objectively indicating binaural interaction [Stollman et al., 1996]. Similiar and comparable morphologies are shown by the patient-group in the normal listening condition, where all prominent waves occur in the grand average SUM_{MONO} and BIN responses (see Figure 4.9, bottom). Note the well defined and obvious Na-Pa-complex which, based on its prominence, supports identification of the desired ERP. In direct comparison to the control-group, overall amplitudes are smaller, more rounded, and the waves occur earlier in time ($\approx 2-5$ ms). Hence, the morphologies look compressed in time, which is a common finding in CI ERPs [McLaughlin et al., 2013; Gilley et al., 2006; Abbas and Brown, 1991]. Additionally, narrowband filtering contributes to this phenomenon [Schebsdat et al., 2018]. Consequently, the focused W_V also occurs earlier at ≈ 5 ms. These findings are also reflected by single-subject ERPs within the patient-group (e.g., CI#6 in Figure 4.10, bottom), which demonstrates the feasibility of the introduced ERP acquisition technique in CI users. When comparing the responses of the normal listening condition against each other, the SUM_{MONO} peak appears smaller and slightly later than the BIN peak. Therefore, no positive residual peak results in the BIC and hence no binaural interaction gets detected (see blue line in Figure 4.11, bottom).

5.2 Discussion of Study 2

Generally, both groups show distinct morphology patterns in the normal listening condition, including parts of the successive middle latency responses depicting all prominent features, although certain waves appear diminished. The P0 is degraded in both groups' grand average ERPs as well as the Nb in the patient-group. One possible reason for this behavior could be the introduced acquisition technique. Note that due to this approach being novel, its potential influence on the resulting ERP morphology remains to be further investigated. Another reason could be the narrowband filtering, since it is well known that single ERP features are dominantly associated with certain frequency ranges [Hall, 2007].

5.2.3 Delay Compensations and Binaural Interaction

When establishing the estimated delay (2.535 ms, described in Section 3.3.2) during stimulation, the basic morphology of the responses of both groups remain unchanged for the most part. The unambiguous difference between stimulation conditions emerge in the sizes of the amplitude deflections of the single waves, where the W_V is the most prominent. When introducing the delay in the control-group, a bilateral asynchronous stimulation is achieved. As expected, in the grand average responses, this results in a contraction of the W_V amplitudes in the $SUM_{MONO-Asynch}$ and BIN_{Asynch} responses, thus those peaks balance in amplitude and in latency (see red lines in Figure 4.9, top). The expected behavior is even more obvious in the responses of single participants, where the $SUM_{MONO-Asynch}$ peaks are even smaller than the BIN_{Asynch} peaks (see red lines in Figure 4.10, top). Consequently, no positive deflection in the resulting BIC_{Asynch} occurs, therefore, no binaural interaction gets detected (see red line in Figure 4.11, top). By contrast, as expected, the patient-group demonstrates the opposite behavior when establishing the delay to compensate the hearing device based latency lag. In the grand average $SUM_{MONO-Comp}$ and BIN_{Comp} responses as well as in those of single participants, the resulting W_V s gain in amplitude (see red lines in Figure 4.9 and Figure 4.10, both bottom). The peak of the $SUM_{MONO-Comp}$ response is then larger than the peak of the BIN_{Comp} response, hence a positive deflection occurs in the BIC_{Comp} and therefore, binaural interaction gets detected (see red line in Figure 4.11, bottom).

In total, 9 out of 10 participants of the control-group demonstrate a significant (p-value: 0.032) degradation of the residual peak in the resulting BIC_{Asynch} when establishing an asynchronous stimulation - if a peak was present at all (see Figure 4.12, left). Conversely, 9 out of 10 participants of the patient-group demonstrate a significant (p-value: 0.0445) enhancement of the residual peak in the resulting BIC_{Comp} when compensating the technical delay (see Figure 4.12, right). These findings support the estimated size of the found latency, where the HA leads the CI, which was compensated in this study. Furthermore, it emphasizes the necessity of balancing the interaural delay to improve binaural interaction in asymmetric hearing treatments.

Interestingly, the described behavior of the resulting BICs based on the different listening conditions cannot only be seen at the temporal area of the corresponding W_{VS} , but also during other features of the acquired ERPs, e.g., Na, Pa, and Nb (see Figure 4.11). When stimulating synchronously, the resulting BIC (BIC for the control-group and BIC_{COMP} for the patient-group) at the temporal area of Na is smaller and at the temporal area of Pa and Nb it is overall larger in the resulting amplitude, compared to the asynchronous stimulation, respectively. Note that these findings partially confirm McPherson and Starr [1993], additionally emphasizing the idea of analyzing BIC results beyond brainstem-level to enhance diagnostic insights.

In total, these findings support the estimated durations of the obtained technical induced latencies, where in our case the HA leads the CI, which was compensated in this study. By contrast, Zirn et al. [2019] reported the very same behaviour, but in the opposite direction with the CI leading the HA. The obvious substantial variation in intrinsic delays between hearing devices of different manufacturers necessitates detailed measurements of the device-specific values. Furthermore, both findings strongly emphasize the potential benefits of balancing the interaural delay to improve binaural processing by significant increases in the associated psychoacoustics [Zirn et al., 2019] and neural correlates of successful binaural interaction [Schebsdat et al., 2018, 2019].

6 Conclusion

In this work, we first introduced a novel method to measure and analyze narrow-band filtered neural correlates of free-field auditory evoked brainstem responses in CI implantees that does not bypass CI preprocessing, making an investigation of response morphologies and latencies to real-world stimuli and furthermore a comparison to those of NH listeners feasible. This approach is unique and shows its benefits in comparison to EABR measurements, which face a higher degree of influencing factors, bypass CI preprocessing altogether, and mostly concentrate on single isolated implant electrodes, which does not reflect the CI implantees' true-to-life listening situation. It promises an objective support in CI fitting procedures and future studies aiming at optimal binaural interaction and fusion, where ITDs based on precise temporal encoding are fundamental. Note that the importance of such a precise temporal tuning is strongly emphasized by results of our second Study, which demonstrates the feasibility of a novel deconvolution-based ERP acquisition technique in acquiring responses exceeding the timeframe of brainstem-level responses, consequently allowing for an ERP analysis in NH listeners and even in bimodal CI implantees, in the latter case hardly being influenced by the prominent CI artifact due to adaptations of the stimulation sequence for narrowband SNR improvements. Therefore, it offers an adequate BIC analysis to, not only, investigate the influence on this component when carefully compensating interaural delays (i.e., intrinsic device based latency differences). Thus, utilizing this method and introducing an estimated latency compensation, significant improvements in the resulting BIC were found in both NH listeners and bimodal implantees. In total, the demonstrated results and also the estimated latency difference should be investigated in larger group sizes to further consolidate the results, but rather confirm the demand for binaural solutions than treating HLos in an isolated and monaural manner.

However, we have to point out some limitations. The experiments must be considered pilot studies, as the number of participated CI users was limited, consequently leading to bigger variances due to inter- and intra- groups' variability. Increasing the number of participants in progressive studies will strengthen the reliability of measurements, minimize the error in response identifications and wave detections, and eventually allow for statistical analysis of subgroups, e.g., manufacturer specific response morphologies in Study 1. Additional patient data will further elaborate structural frequency boundaries and scales for narrowband filtering, thus potentially the most convenient compromise and separation of the desired exogenously driven synchronized regularity and the unwanted superimposed stimulation artifact can get achieved. Please note that based on incorporated filter settings and results of Study 1 we already relaxed the investigated frequency window successfully in Study 2. Another potentially beneficial remark would be the incorporation of the individual sensation levels rather than objective intensities (i.e., dB peSPL), eventually leading to smaller variances, since it would better reflect the individuals' auditory perception. Especially when considering investigations of relative, behavioral changes, e.g., due to BERA measurements, an established subjective based loudness perception suggests to be rather practical.

Besides, we would like to point out some potentially conducive refinements regarding future measurements proceeding the introduced works. On the one hand, while the testing of two different stimuli with divergent durations demonstrated profitable in Study 1, we would rather recommend using three deviant intensities when testing stimuli, e.g., the sensation levels '*just audible*', '*comfortable loud*', and their framed center. This would still offer sufficient response references in addition with a reduction in measurement length, which potentially can be reinvested to increase the amount of repetitions, thus further increasing their SNRs. On the other hand, since Study 2 successfully demonstrated the benefits when precisely adjusting interaural latencies, a detailed evaluation of the estimated device based delay would be of greater interest. Therefore, the additional testing of a cluster of deviant delays spanning the predicted latency is recommended, which would potentially allow for a trend analysis of derived BIC amplitudes and the detection of a maximum, i.e., the best delay compensation. Finally, of course, we suggest the combination of the free-field apparatus (Study 1) and the deconvolution-based ERP acquisition technique with SNR optimization (Study 2), which strongly

implies to gain novel and unique insights into so far unseen AEPs in CI users based on the reasoning given throughout this work.

7 Appendix (Study 1)

Table 7.1: Significance Table illustrating the statistical analysis with Friedman's ranking tests (pFried) and the one-tailed Wilcoxon paired difference tests (pIntensity#1 -> Intensity#2), where *($P \leq 0.05$), **($0.05 < P \leq 0.1$), and ***($0.1 < P$).

Tested features	pFried	p40 -> 50	p40 -> 60	p40 -> 70	p50 -> 60	p50 -> 70	p60 -> 70
NH group conventional frequency window (150-1,500 Hz):							
Chirp amplitude	0.00002*	0.00073*	0.00024*	0.00024*	0.01343*	0.00244*	0.00806*
Chirp latency	0*	0.01563*	0.00049*	0.00024*	0.00195*	0.00024*	0.01636*
Chirp WPSS magnitude	0.00001*	0.00342*	0.00024*	0.00024*	0.00073*	0.0061*	0.08813**
Chirp WPSS latency	0.00063*	0.04028*	0.01123*	0.00098*	0.01904*	0.00146*	0.0293*
Click amplitude	0.00173*	0.00171*	0.00024*	0.0061*	0.03198*	0.1167***	0.48486***
Click latency	0.00004*	0.02539*	0.00269*	0.00146*	0.00098*	0.00024*	0.00073*
Click WPSS magnitude	0.00011*	0.00049*	0.00024*	0.00024*	0.03198*	0.10181***	0.1167***
Click WPSS latency	0.0007*	0.00293*	0.00293*	0.00049*	0.26538***	0.00391*	0.00195*
NH group narrowband frequency window (150-300 Hz):							
Chirp amplitude	0.00002*	0.00806*	0.00122*	0.00024*	0.04614*	0.00122*	0.00806*
Chirp latency	0.00004*	0.00146*	0.00024*	0.00049*	0.03027*	0.02051*	0.10938***
Chirp WPSS magnitude	0.00002*	0.00806*	0.00024*	0.00024*	0.0105*	0.00806*	0.08813**
Chirp WPSS latency	0.09789**	0.06177**	0.05713**	0.37378***	0.29102***	0.08813**	0.10547***
Click amplitude	0.00033*	0.01343*	0.00049*	0.00244*	0.08813**	0.0105*	0.1167***
Click latency	0*	0.00122*	0.00024*	0.00024*	0.00024*	0.00024*	0.00293*
Click WPSS magnitude	0.00007*	0.00073*	0.00024*	0.00024*	0.0061*	0.04614*	0.33862***
Click WPSS latency	0.2301***	0.38232***	0.16602***	0.22876***	0.49121***	0.13306***	0.146***
CI group narrowband frequency window (150-300 Hz):							
Chirp amplitude	0.01346*	0.1167***	0.00464*	0.00806*	0.00806*	0.0105*	0.03198*
Chirp latency	0.45198***	0.09033**	0.04614*	0.06738**	0.24023***	0.2832***	0.4248***
Chirp WPSS magnitude	0.00085*	0.08813**	0.00122*	0.0105*	0.00024*	0.03857*	0.25928***
Chirp WPSS latency	0.43678***	0.37427***	0.3042***	0.15552***	0.13428***	0.21191***	0.22607***
Click amplitude	0.00007*	0.05493**	0.00244*	0.00073*	0.00244*	0.00122*	0.01709*
Click latency	0.02964*	0.02002*	0.05688**	0.00806*	0.17188***	0.07275**	0.32715***
Click WPSS magnitude	0.00026*	0.01343*	0.00342*	0.00244*	0.00171*	0.02124*	0.03857*
Click WPSS latency	0.23084***	0.40283***	0.49341***	0.19531***	0.13306***	0.13721***	0.14624***

Bibliography

- Abbas, P. J. and Brown, C. J. (1991). Electrically Evoked Auditory Brainstem Response: Growth of Response With Current Level. *Hearing Research*, 51:123–138.
- Abrams, D. A. (2008). Temporal Features of Speech in the Auditory System: Normal and Dyslexic Children and Animal Model. *ProQuest*.
- Agmon-Snir, H., Carr, C. E., and Rinzel, J. (1998). The Role of Dendrites in Auditory Coincidence Detection. *Nature*, 393:268–272.
- Ainslie, P. J. and Boston, J. R. (1980). Comparison of Brain Stem Auditory Evoked Potentials for Monaural and Binaural Stimuli. *Electroencephalography and Clinical Neurophysiology*, 49:291–302.
- Atcherson, S. R., Damji, Z., and Upson, S. (2011). Applying a Subtraction Technique to Minimize Cochlear Implant Artifact With Soundfield and Direct Audio Input Stimulations. *Cochlear Implants International*, 12(4):234–237.
- Atcherson, S. R. and Stoody, T. M., editors (2012). *Auditory Electrophysiology: A Clinical Guide*. Thieme Medical Publishers, Inc., New York.
- Augustine, J. R. (2014). *Human Neuroanatomy*. John Wiley & Sons, Incorporated.
- Baars, B. J. and Gage, N. M. (2010). *Cognition, Brain, and Consciousness: Introduction to Cognitive Neuroscience*. Introduction to Cognitive Neuroscience Series. Elsevier Science.
- Bahmer, A., Polak, M., and Baumann, U. (2010). Recording of Electrically Evoked Auditory Brainstem Responses After Electrical Stimulation With Biphasic, Triphasic and Precision Triphasic Pulses. *Hearing Research*, 259:75–85.
- Bardy, F., Dillon, H., and Van Dun, B. (2014). Least-Squares Deconvolution of Evoked Potentials and Sequence Optimization for Multiple Stimuli Under Low-Jitter Conditions. *Clinical Neurophysiology*, 125(4):727–737.
- Bear, M. F., Connors, B. W., and Paradiso, M. A. (2007). *Neuroscience: Exploring the Brain*. Lippincott Williams & Wilkins.
- Bernarding, C. (2015). *Cognitive Neurodynamics of Listening Effort*. PhD thesis, Universität des Saarlandes, Saarbrücken, Germany.

Bibliography

- Bernarding, C., Corona-Strauss, F. I., Latzel, M., and Strauss, D. J. (2010). Auditory Streaming and Listening Effort: An Event Related Potential Study. In *Engineering in Medicine and Biology Society (EMBC)*. Annual International Conference of the IEEE.
- Bernarding, C., Strauss, D. J., Hannemann, R., Latzel, M., Seidler, H., Jobst, U., Bellaghech, A., Landwehr, M., and Corona-Strauss, F. I. (2011). The Effects of Age and Hearing Impairment on the Extraction of Listening Effort Correlates. In *Engineering in Medicine and Biology Society (EMBC)*. Annual International Conference of the IEEE.
- Beutner, D., Delb, W., Frenzel, H., Hoppe, U., Huttenbrink, K. B., Mlynski, R., Limberger, A., Schonweiler, R., Schwab, B., Todt, I., Walger, M., Wesarg, T., Zahnert, T., and Zeh, R. (2018). Guideline "Implantable hearing aids"-short version: German S2k guideline of the Working Group of German-Speaking Audiologists, Neurotologists and Otologists (ADANO), of the German Society of Oto-Rhino-Laryngology, Head and Neck Surgery (DGHNO) in collaboration with the German Society of Audiology (DGA), the German Society of Phoniatrics and Pediatric Audiology (DGPP), and patient representatives. *HNO*, 66(Suppl 2):71–76.
- Biacabe, B., Chevallier, J. M., Avan, P., and Bonflis, P. (2001). Functional Anatomy of Auditory Brainstem Nuclei: Application to the Anatomical Basis of Brainstem Auditory Evoked Potentials. *Auris, Nasus, Larynx*, 28:85–94.
- Birbaumer, N., Braitenberg, V., Schmidt, R., Schaible, H., Brinkmeier, H., Dudel, J., Eysel, U., Handwerker, H., Hatt, H., et al. (2006). *Neuro- und Sinnesphysiologie*. Springer-Lehrbuch. Springer Berlin Heidelberg.
- Bohnert, A., Nyffeler, M., and Keilmann, A. (2010). Advantages of a Nonlinear Frequency Compression Algorithm in Noise. *European Archives of Oto-Rhino-Laryngology*, 267:1045–1053.
- Bohórquez, J. and Özdamar, Ö. (2008). Generation of the 40-Hz Auditory Steady-State Response (ASSR) Explained Using Convolution. *Clinical Neurophysiology*, 119:2598–2607.
- Brantberg, K., Fransson, P.-A., Hansson, H., and Rosenhall, U. (1999). Measures of the Binaural Interaction Component in Human Auditory Brainstem Response Using Objective Detection Criteria. *Scandinavian University Press*, 28:15–26.
- Buchner, H. and Armbruster, S. (2005). *Evozierte Potenziale, neurovegetative Diagnostik, Okulographie: Methodik und klinische Anwendungen ; 59 Tabellen*. RRN - Referenz-Reihe Neurologie. Thieme.
- Buell, T. N., Trahiotis, C., and Bernstein, L. (1991). Lateralization of Low-Frequency Tones: Relative Potency of Gating and Ongoing Inter Aural Delays. *Journal of the Acoustical Society of America*, 90:3077–3085.

Bibliography

- Bures, Z. (2012). The Stochastic Properties of Input Spike Trains Control Neuronal Arithmetic. *Biological Cybernetics*, 106(2):111–122.
- Burkard, R. F., Eggermont, J. J., and Don, M., editors (2007). *Auditory Evoked Potentials - Basic Principles and Clinical Applications*. Lippincott Williams & Wilkins, Baltimore, Philadelphia.
- Buser, P. and Imbert, M. (1992). *Audition*. A Bradford Book. MIT Press.
- Campbell, R. A. A. and King, A. J. (2004). Auditory Neuroscience: A Time for Coincidence? *Current Biology*, 14:886–888.
- Carlyon, R. P., Macherey, O., Frijns, J. H., Axon, P. R., Kalkman, R. K., Boyle, P., Baguley, D. M., Briggs, J., Deeks, J. M., Briaire, J. J., Barreau, X., and Dorman, R. (2010). Pitch Comparisons Between Electrical Stimulation of a Cochlear Implant and Acoustic Stimuli Presented to a Normal-Hearing Contralateral Ear. *Journal of the Association for Research in Otolaryngology*, 11(4):625–640.
- Carmona, R., Hwang, W.-L., and Torrsani, B. (1998). *Practical Time-Frequency Analysis: Gabor and Wavelet Transforms with an Implementation S*. Academic Press.
- Celesia, G. G. and Hickok, G. (2015). *The Human Auditory System: Fundamental Organization and Clinical Disorders*. Handbook of Clinical Neurology. Elsevier Science.
- Chatterjee, M., Galvin, J. J., Fu, Q. J., and Shannon, R. V. (2006). Effects of Stimulation Mode, Level and Location on Forward-Masked Excitation Patterns in Cochlear Implant Patients. *Journal of the Association for Research in Otolaryngology*, 7(1):15–25.
- Ching, T. Y., van Wanrooy, E., and Dillon, H. (2007). Binaural-Bimodal Fitting or Bilateral Implantation for Managing Severe to Profound Deafness: A Review. *Trends in Amplification*, 11(3):161–192.
- Clark, G. (2006). *Cochlear Implants: Fundamentals and Applications*. Modern Acoustics and Signal Processing. Springer New York.
- Clark, G. M., Tong, Y. C., and Dowell, R. C. (1984). Comparison of Two Cochlear Implant Speech-Processing Strategies. *Annals of Otology, Rhinology, and Laryngology*, 93:127–131.
- Corona-Strauss, F. I. (2009). *On the Fast Detection of Auditory Brainstem Responses: A Novelty Detection Paradigm*. PhD thesis, Universität des Saarlandes, Saarbrücken, Germany.
- Corona-Strauss, F. I., Delb, W., Bloching, M., and Strauss, D. J. (2007). Ultra-Fast Quantification of Hearing Loss by Neural Synchronization Stabilities of Auditory Evoked Brainstem Activity. In *Conf IEEE Eng Med Biol Soc, Minneapolis, Minnesota, USA*.

Bibliography

- Corona-Strauss, F. I., Delb, W., Schick, B., and Strauss, D. J. (2009). Phase Stability Analysis of Chirp Evoked Auditory Brainstem Responses by Gabor Frame Operators. *IEEE Transactions on Neural Systems and Rehabilitation Engineering*, 17(6):530–536.
- Corona-Strauss, F. I., Delb, W., Schick, B., and Strauss, D. J. (2010). A Kernel-Based Novelty Detection Scheme for the Ultra-Fast Detection of Chirp Evoked Auditory Brainstem Responses. In *Engineering in Medicine and Biology Society (EMBC)*. Annual International Conference of the IEEE.
- Corona-Strauss, F. I., Schick, B., Delb, W., and Strauss, D. J. (2012). Notched-Noise Embedded Frequency Specific Chirps for Objective Audiometry Using Auditory Brainstem Responses. *Audiology Research*, 2(1):30–38.
- Dallas, P. (1992). The Active Cochlea. *Journal of Neuroscience*, 12(12):4575–4585.
- Dau, T. (2003). The Importance of Cochlear Processing for the Formation of Auditory Brainstem and Frequency Following Responses. *Journal of the Acoustical Society of America*, 113:936–950.
- Dau, T., Wegner, O., Mellert, V., and Kollmeier, B. (2000). Auditory Brainstem Responses With Optimized Chirp Signals Compensating Basilar-Membrane Dispersion. *Journal of the Acoustical Society of America*, 107(3):1530–1540.
- David, O., Kiebel, S. J., Harrison, L. M., Mattout, J., Kilner, J. M., and Friston, K. J. (2006). Dynamic Causal Modeling of Evoked Responses in EEG and MEG. *NeuroImage*, 30:1255–1272.
- Delgado, R. E. and Özdamar, Ö. (2004). Deconvolution of Evoked Responses Obtained at High Stimulus Rates. *Journal of the Acoustical Society of America*, 115(3):1242–1251.
- Dillon, H. (2012). *Hearing Aids*. Thieme.
- Dobie, R. A. and Norton, S. J. (1980). Binaural Interaction in Human Auditory Evoked Potentials. *Electroencephalography and Clinical Neurophysiology*, 49:303–313.
- Donaldson, G. S., Kreft, H. A., and Litvak, L. (2005). Place-pitch discrimination of single- versus dual-electrode stimuli by cochlear implant users (L). *J. Acoust. Soc. Am.*, 118(2):623–626.
- Donaldson, G. S., Viemeister, N. F., and Nelson, D. A. (1997). Psychometric Functions and Temporal Integration in Electric Hearing. *Journal of the Acoustical Society of America*, 101:3706–3721.
- Elzouki, A. Y., Harfi, H. A., Nazer, H. M., Stapleton, F. B., Oh, W., and Whitley, R. J., editors (2012). *Textbook of Clinical Pediatrics*. Springer Berlin Heidelberg.
- Eysenck, M. (2004). *Psychology: An International Perspective*. Psychology Press.

Bibliography

- Firszt, J. B., Chambers, R. D., Kraus, N., and Reeder, R. (2002). Neurophysiology of Cochlear Implant Users I: Effects of Stimulus Current Level and Electrode Site on the Electrical ABR, MLR, and N1-P2 Response. *Ear and Hearing*, 23:502–515.
- Fobel, O. and Dau, T. (2004). Searching for the Optimal Stimulus Eliciting Auditory Brainstem Responses in Humans. *Journal of the Acoustical Society of America*, 116(4):2213–2222.
- Francart, T., Lenssen, A., and Wouters, J. (2011). Sensitivity of Bimodal Listeners to Interaural Time Differences With Modulated Single- and Multiple-Channel Stimuli. *Audiology and Neurotology*, 16(2):82–92.
- Friesen, L. M. and Picton, T. W. (2010). A Method for Removing Cochlear Implant Artifact. *Hearing Research*, 259(1-2):95–106.
- Friesen, L. M., shannon, R. V., and 3rd Slatterly, W. H. (1999). The Effect of Frequency Allocation on Phoneme Recognition With the Nucleus 22 Cochlear Implant. *American Journal of Otology*, 20:729–734.
- Frijs, J. H., de Snoo, S. L., and ten Kate, J. H. (1996). Spatial Selectivity in a Rotationally Symmetric Model of the Eleectrical Stimulated Cochlea. *Hearing Research*, 95:33–48.
- Fu, Q. J. and Shannon, R. V. (1998). Effects of Amplitude Nonlinearity on Phoneme Recognition by Cochlear-Implant Users and Normal-Hearing Listeners. *Journal of the Acoustical Society of America*, 104:2570–2577.
- Fu, Q. J., Shannon, R. V., and 3rd. Galvin, J. J. (2002). Perceptual Learning Following Changes in the Frequency-to-Electrode Assignment With the Nucleus-22 Cochlear Implant. *Journal of the Acoustical Society of America*, 112:1664–1674.
- Gelfand, S. A. (2009). *Essentials of Audiology*. Thieme, New York, USA, 3 edition.
- Gilley, P. M., Sharma, A., Dorman, M., Finley, C. C., Panch, A. S., and Martin, K. (2006). Minimization of Cochlear Implant Stimulus Artifact in Cortical Auditory Evoked Potentials. *Clinical Neurophysiology*, 117(8):1772–1782.
- Giraud, A. L., Price, C. J., and Graham, J. M. (2001). Cross-Modal Plasticity Underpins Language Recovery After Cochlear Implantation. *Neuron*, 30:657–663.
- Glackin, B., Wall, J. A., McGinnity, T. M., Maguire, L. P., and McDaid, L. J. (2010). A Cochlea Neural Network Model of the Medial Superior Olive Using Spike Timing Dependent Plasticity for Sound Localization. *Frontiers in Computational Neuroscience*, 4(18):1–16.
- Glendenning, K. K., Brunso-Bechtold, J. K., Thompson, G. C., and Masterton, R. B. (1981). Ascending Auditory Afferents to the Nuclei of the Lateral Lemniscus. *Journal of Comparative Neurology*, 197:673–703.

Bibliography

- Gomaa, N. A., Rubinstein, J. T., and Lowder, M. W. (2003). Residual Speech Perception and Cochlear Implant Performance in Postlingually Deafened Adults. *Ear and Hearing*, 24:539–544.
- Gordon, K. A. (2007). Auditory Development Promoted by Unilateral and Bilateral Cochlear Implant Use. In *A Sound Foundation Through Early Amplification*.
- Gordon, K. A., Papsin, B. C., and Harrison, R. V. (2003). Activity-Dependent Developmental Plasticity of the Auditory Brain Stem in Children Who Use Cochlear Implants. *Ear and Hearing*, 24:485–500.
- Gordon, K. A., Papsin, B. C., and Harrison, R. V. (2006). An Evoked Potential Study of the Developmental Time Course of the Auditory Nerve and Brainstem in Children Using Cochlear Implants. *Audiology and Neurotology*, 11:7–23.
- Gordon, K. A., Papsin, B. C., and Harrison, R. V. (2007). Auditory Brainstem Activity and Development Evoked by Apical Versus Basal Cochlear Implant Electrode Stimulation in Children. *Clinical Neurophysiology*, 118:1671–1684.
- Grothe, B., Pecka, M., and Alpine, D. M. (2010). Mechanisms of Sound Localization in Mammals. *Physiological Reviews*, 90:983–1012.
- Guerit, F., Santurette, S., Chalupper, J., and Dau, T. (2014). Investigating Interaural Frequency-Place Mismatches via Bimodal Vowel Integration. *Trends in Hearing*, 18.
- Haab, L. (2015). *Numerical Modeling and Experimental Validation of Involuntary Attentional Capture and Long-Term Habituation by the Example of Tinnitus Aurium*. PhD thesis, Universität des Saarlandes, Saarbrücken, Germany.
- Hall, J. W. (2007). *New Handbook for Auditory Evoked Responses*. Pearson Education, Boston, MA.
- Hartmann, W. M. (2004). *Signal, Sound, and Sensation*. American Institute of Physics.
- Hashimoto, I., Ishiyama, Y., Yoshimoto, T., and Nemoto, S. (1981). Brain-Stem Auditory Evoked Potentials Recorded Directly from Human Brain-Stem and Thalamus. *Brain*, 104:841–859.
- He, S., Brown, C. J., and Abbas, P. J. (2010). Effects of Stimulation Level and Electrode Pairing on the Binaural Interaction Component of the Electrically Evoked Auditory Brain Stem Response. *Ear and Hearing*, 31(4):457–470.
- He, S., Brown, C. J., and Abbas, P. J. (2012). Preliminary Results of the Relationship Between the Binaural Interaction Component of the Electrically Evoked Auditory Brainstem Response and Interaural Pitch Comparisons in Bilateral Cochlear Implant Recipients. *Ear and Hearing*, 33(1):57–68.
- Hering, E., Martin, R., and Stohrer, M. (2012). *Physik fuer Ingenieure*. Springer-Verlag Berlin Heidelberg New York.

Bibliography

- Holt, F. D. and Özdamar, Ö. (2014). Simultaneous Acquisition of High-Rate Early, Middle, and Late Auditory Evoked Potentials. In *36th Annual International Conference of the IEEE Engineering in Medicine and Biology Society (EMBC)*, pages 1481–1484.
- Holt, F. D. and Özdamar, Ö. (2016). Effects of Rate (0.3-40/s) on Simultaneously Recorded Auditory Brainstem, Middle and Late Responses Using Deconvolution. *Clinical Neurophysiology*, 127(2):1589–1602.
- Horch, K. W. and Dhillon, G. S. (2004). *Neuroprosthetics Theory and Practice*. Series on Bioengineering and Biomedical Engineering. World Scientific.
- Hosford, H. L., Fullerton, B. C., and Levine, R. A. (1979). Binaural Interaction in Human and Cat Brain Stem Evoked Responses. *Journal of the Acoustical Society of America*, 65:86.
- Hu, H., Kollmeier, B., and Dietz, M. (2015). Reduction of Stimulation Coherent Artifacts in Electrically Evoked Auditory Brainstem Responses. *Biomedical Signal Processing and Control*, 21:74–81.
- Huss, M. and Moore, B. C. J. (2005). Dead Regions and Pitch Perception. *Journal of the Acoustical Society of America*, 117:3841–3852.
- International Electronic Commission (2014). Electroacoustics - Audiometric equipment - Part 1: Equipment for pure-tone and speech audiometry. IEC 1:2017.
- International Organization for Standardization (2014). Acoustics - Normal Equal-Loudness-Level Contours. ISO 226:2003.
- James, C., Blamey, P., Shallop, J. K., Incerti, P. V., and Nicholas, A. M. (2001). Contralateral Masking in Cochlear Implant Users With Residual Hearing in the Non-Implanted Ear. *Audiology and Neurotology*, 6(2):87–97.
- Javel, E. and Sheperd, R. K. (2000). Electrical Stimulation of the Auditory Nerve III. Response Initiation Sites and Temporal Fine Structure. *Hearing Research*, 140:45–76.
- Jeffress, L. A. (1948). A Place Theory of Sound Localization. *Journal of Comparative and Physiological Psychology*, 41:35–39.
- Jewett, D. L. (1970). Volume-Conducted Potentials in Response to Auditory Stimuli as Detected by Averaging in the Cat. *Electroencephalography and Clinical Neurophysiology*, 28:609–618.
- Jones, R. C., Stevens, S. S., and Lurie, M. H. (1940). Three Mechanisms of Hearing by Electrical Stimulation. *Journal of the Acoustical Society of America*, 12:281–290.
- Joris, P. and Yin, T. C. T. (2007). A Matter of Time: Internal Delays in Binaural Processing. *Trends in Neurosciences*, 30:70–78.

Bibliography

- Joris, P. X., Smith, P. H., and Yin, T. C. T. (1998). Coincidence Detection in the Auditory System. *Neuron*, 6:1235–1238.
- Kan, A., Stoelb, C., Litovsky, R. Y., and Goupell, M. J. (2013). Effect of Mismatched Place-of-Stimulation on Binaural Fusion and Lateralization in Bilateral Cochlear-Implant Users. *Journal of the Acoustical Society of America*, 134(4):2923–2936.
- Kandel, E. R., Schwartz, J. H., Jessell, T. M., Siegelbaum, S. A., and Hudspeth, A. J. (2000). *Principles of Neural Science*. McGraw-Hill Education Ltd.
- Karpoff, S. and Labus, D. M. (2007). *Portable Diagnostic Tests*. Lippincott Williams & Wilkins.
- Kiefer, J., Hohl, S., Sturzebecher, E., Pfennigdorff, T., and Gstöttner, W. (2001). Comparison of Speech Recognition with Different Speech Coding Strategies (SPEAK, CIS, and ACE) and Their Relationship to Telemetric Measures of Compound Action Potentials in the Nucleus CI 24M Cochlear Implant System. *Audiology*, 40:32–42.
- Klauke, I., Kohl, M. C., Hannemann, R., Kornagel, U., Strauss, D. J., and Corona-Strauss, F. I. (2015). Impact of Monaural Frequency Compression on Binaural Fusion at the Brainstem Level. In *37th Annual International Conference of the IEEE Engineering in Medicine and Biology Society (EMBC)*, pages 1646–1649.
- Koch, D. B., Osberger, M. J., Segal, P., and Kessler, D. (2004). HiResolution and Conventional Sound Processing in the HiResolution Bionic Ear: Using Appropriate Outcome Measures to Assess Speech Recognition Ability. *Audiology and Neurotology*, 9:214–230.
- Kohl, M. C., Schebsdat, E., Schneider, E. N., Niehl, A., Strauss, D. J., Özdamar, Ö., and Bohórquez, J. (2019a). Fast Acquisition of Full-Range Auditory Event-Related Potentials Using an Interleaved Deconvolution Approach. *Journal of the Acoustical Society of America*, 145:540–550.
- Kohl, M. C., Schebsdat, E., Schneider, E. N., and Strauss, D. J. (2019b). Denoising of Single-Trial Event-Related Potentials by Shrinkage and Phase Regularization of Analytic Wavelet Filterbank Coefficients. In *Neural Engineering (NER), 9th International IEEE/EMBS Conference on*.
- Kral, A. (2013). Auditory Critical Periods: A Review from System’s Perspective. *Neuroscience*, 247:117–133.
- Kral, A., Hartmann, R., and Tillein, J. (2002). Hearing After Congenital Deafness: Central Auditory Plasticity and Sensory Deprivation. *Cerebral Cortex*, 12:797–807.
- Krause, B. and Metzler, P. (1983). *Angewandte Statistik. Lehr- und Arbeitsbuch für Psychologen, Mediziner, Biologen und Pädagogen*. VEB Deutscher Verlag der Wissenschaften, Berlin.

Bibliography

- Lin, P., Lu, T., and Zeng, F. G. (2013). Central Masking With Bilateral Cochlear Implants. *Journal of the Acoustical Society of America*, 133(2):962–969.
- Litvak, L., Delgutte, B., and Eddington, D. (2001). Auditory Nerve Fiber Response to Electric Stimulation: Modulated and Unmodulated Pulse Trains. *Journal of the Acoustical Society of America*, 110:368–379.
- Loizon, P. C. (1998). Mimicking the Human Ear. *IEEE Signal Processing Magazine*, 15:101–130.
- Long, C. J., Eddington, D. K., and Colburn, H. S. (2003). Implants Sensitivity as a Function of Interaural Electrode Position With a Bilateral Cochlear-Implant User. *Journal of the Acoustical Society of America*, 114:1565–1574.
- Luu, P. and Tucker, D. M. (2001). Regulating Action: Alternating Activation of Midline Frontal and Motor Cortical Networks. *Clinical Neurophysiology*, 112(7):1295–1306.
- Madell, J. and Flexer, C. (2013). *Pediatric Audiology: Diagnosis, Technology, and Management*. Thieme.
- Martin, B. A. (2007). Can the Acoustic Change Complex be Recorded in an Individual With a Cochlear Implant? Separating Neural Responses from Cochlear Implant Artifact. *Journal of the American Academy of Audiology*, 18(2):126–140.
- Maurer, K., Lang, N., and Eckert, J., editors (2005). *Praxis der evozierten Potentiale*. Steinkopf Verlag, Darmstadt, Germany.
- McLaughlin, M., Lopez Valdes, A., Reilly, R. B., and Zeng, F. G. (2013). Cochlear Implant Artifact Attenuation in Late Auditory Evoked pPotentials: A Single Channel Approach. *Hearing Research*, 302:84–95.
- McLaughlin, M., Verschooten, E., and Joris, P. X. (2010). Oscillatory Dipoles as a Source of Phase Shifts in Field Potentials in the Mammalian Auditory Brainstem. *Journal of Neuroscience*, 30(40):13472–13487.
- McPherson, D. L. and Starr, A. (1993). Binaural Interaction in Auditory Evoked Potentials: Brainstem, Middle- and Long-Latency Components. *Hearing Research*, 66(1):91–98.
- Meddis, R., Lopez-Poveda, E., Fay, R., and Popper, A. (2010). *Computational Models of the Auditory System*. Springer Handbook of Auditory Research. Springer US.
- Melcher, J. R. and Kiang, N. Y. S. (1996). Generators of the Brainstem Auditory Evoked Potential in Cat. III: Identified Cell Populations. *Hearing Research*, 93:52–71.
- Mühler, R. and Ziese, M. (2010). Technischer Leitfaden Cochlea Implant. *Universitäts-HNO-Klinik Magdeburg*.

Bibliography

- Miller, C. A., Brown, C. J., Abbas, P. J., and Chi, S.-L. (2008). The Clinical Application of Potentials Evoked from the Peripheral Auditory System. *Hearing Research*, 242:184–197.
- Moller, A. (2006). *Hearing: Anatomy, Physiology, and Disorders of the Auditory System*. Hearing Series. Elsevier Science.
- Moller, A. R. and Jannetta, P. J. (1983). Interpretation of Brainstem Auditory Evoked Potentials: Results from Intracranial Recordings in Humans. *Scandinavian Audiology*, 12:125–133.
- Moore, D., Fuchs, P., Plack, C., Rees, A., and Palmer, A. (2010). *Oxford Handbook of Auditory Science: Hearing*. Oxford Handbook of Auditory Science. OUP Oxford.
- Moore, D. R. (2006). Auditory Processing Disorder (APD): Definition, Diagnosis, Neural Basis, and Intervention. *Audiological Medicine*, 4:4–11.
- Moore, J. K. (1987). The Human Auditory Brain Stem: A Comparative View. *Hearing Research*, 29:1–32.
- Mussiek, F. E. and Chermak, G. D., editors (2007). *Handbook of Central Auditory Processing Disorder: Auditory Neuroscience and Diagnoses*. Plural Publishing.
- Neely, S. T., Norton, S. J., Gorga, M. P., and Jesteadt, W. (1988). Latency of Auditory Brain-Stem Responses and Otoacoustic Emissions Using Tone-burst Stimuli. *Journal of the Acoustical Society of America*, 83(2):652–656.
- Newman, J. (2010). *Physics of the Life Sciences*. Springer New York.
- Norrix, L. W., Trepanier, S., Atlas, M., and Kim, D. (2012). The Auditory Brainstem Response: Latencies Obtained in Children While under General Anesthesia. *Journal of the American Academy of Audiology*, 23(1):57–63.
- Özdamar, Ö., Bohórquez, J., and Ray, S. S. (2007). Pb(P1) Resonance at 40 Hz: Effects of High Stimulus Rate on Auditory Middle Latency Responses (MLRs) Explored using Deconvolution. *Clinical Neurophysiology*, 118:1261–1273.
- Peng, X., Yuan, H., Chen, W., Wang, T., and Ding, L. (2017). New Metric for Optimizing Continuous Loop Averaging Deconvolution (CLAD) Sequences Under the 1/f Noise Model. *PLOS ONE*, 12(4):1–24.
- Pisoni, D. B. and Cleary, M. (2003). Measures of Working Memory Span and Verbal Rehearsal Speed in Deaf Children After Cochlear Implantation. *Ear and Hearing*, 24:106S–120S.
- Purves, D., Augustine, G. J., Fitzpatrick, D., Hall, W. C., LaMantia, A., McNamara, J. O., and Williams, S. M. (2004). *The Auditory System*. Neuroscience, Sinauer Associates, Inc.

Bibliography

- Riedel, H. and Kollmeier, B. (2002). Comparison of Binaural Auditory Brainstem Responses and the Binaural Difference Potential Evoked by Chirps and Clicks. *Hearing Research*, 169:85–96.
- Roeser, R., Valente, M., and Hosford-Dunn, H. (2011). *Audiology: Diagnosis*. Thieme.
- Rosen, S., Faulkner, A., and Wilkinson, L. (1999). Adaptation by Normal Listeners to Upward Spectral Shifts of Speech: Implications for Cochlear Implants. *Journal of the Acoustical Society of America*, 106:3629–3636.
- Schebsdat, E., Corona-Strauss, F. I., Hessel, H., Seidler, H., Bellaghech, A., Rusczyk, L., Müller, O., and Strauss, D. J. (2015). Binaural Interaction in Unilateral Cochlear Implant Users: Neural Correlates in Free-Field Single Trial Responses. In *Conf Proc IEEE Eng Med Biol Soc*.
- Schebsdat, E., Hessel, H., Seidler, H., and Strauss, D. J. (2016). Detection of Binaural Interaction in Free-Field Evoked Auditory Brainstem Responses by Time-Scale Representations. In *38th Annual International Conference of the IEEE Engineering in Medicine and Biology Society (EMBC)*, pages 3732–3735.
- Schebsdat, E., Kohl, M. C., Corona-Strauss, F. I., Seidler, H., and Strauss, D. J. (2018). Free-Field Evoked Auditory Brainstem Responses in Cochlear Implant Users. *Audiology Research*, 8(2):44–53.
- Schebsdat, E., Kohl, M. C., Geissler, G., Bohórquez, J., Strauss, D. J., and Chalupper, J. (2019). Quantification of Binaural Interaction Facilitated By Interaural Latency Compensation in Bimodal Cochlear Implantees. *IEEE Transactions on Neural Systems and Rehabilitation Engineering*. (submitted).
- Schebsdat, E., Strauss, D. J., and Wolfe, J. (2017). Objective Evaluation of the Subjectively Perceived Loudness of Cochlear-Implant Users. In *Neural Engineering (NER), 8th International IEEE/EMBS Conference on*.
- Schmidt, R., Thews, G., and Lang, F. (2013). *Physiologie des Menschen*. Springer-Lehrbuch. Springer Berlin Heidelberg.
- Serman, M., Hannemann, R., and Kornagel, U. (2012). White Paper: micon Frequency Compression. *Siemens*.
- Shallop, J. K. (1993). Objective Electrophysiological Measures from Cochlear Implant Patients. *Ear and Hearing*, 14:58–63.
- Shannon, R. V. (1992). Temporal Modulation Transfer Functions in Patients With Cochlear Implants. *Journal of the Acoustical Society of America*, 91:2156–2164.
- Shannon, R. V., Zeng, F. G., and Kamath, V. (1995). Speech Recognition With Primarily Temporal Cues. *Science*, 270:303–304.

Bibliography

- Sharma, A., Dorman, M. F., and Spahr, A. J. (2002). Asensitive Period for the Development of the Central Auditory System in Children With Cochlear Implants: Implications for Age of Implantation. *Ear and Hearing*, 23:532–539.
- Shuman, H. (2008). *The Electrically Evoked Binaural Interaction Component of the Auditory Brainstem Response: Effect of Electrode Pairing and Comparison With Psychophysical Measure of Pitch Matching*. PhD thesis, The University of Iowa, USA.
- Siciliano, C. M., Faulkner, A., Rosen, S., and Mair, K. (2010). Resistance to Learning Binaurally Mismatched Frequency-to-Place Maps: Implications for Bilateral Stimulation With Cochlear Implants. *Journal of the Acoustical Society of America*, 127(3):1645–1660.
- Simpson, A. (2009). Frequency-Lowering Devices for Managing High-Frequency Hearing Loss: A Review. *Trends in Amplification*, 13(2):87–106.
- Simpson, A., Hersbach, A. A., and McDermott, H. J. (2005). Improvements in Speech Perception with an Experimental Nonlinear Frequency Compression Hearing Device. *International Journal of Audiology*, 44:281–292.
- Sinkiewicz, D., Friesen, L., and Ghoraani, B. (2017). A novel method for extraction of neural response from single channel cochlear implant auditory evoked potentials. *Medical Engineering Physics*, 40:47–55.
- Sinkiewicz, D. Q. (2015). *A Novel Method for Extraction of Neural Response from Cochlear Implant Auditory Evoked Potentials*. Thesis, Rorchester Institute of Technology, Kate Gleason College of Engineering, USA.
- Skinner, M. W., Ketten, D. R., Holden, L. K., Harding, G. W., Smith, P. G., Gates, G. A., Neely, J. G., Kletzker, G. R., Brunson, B., and Blocker, B. (2002). CT-Derived Estimation of Cochlear Morphology and Electrode Array Position in Relation to Word Recognition in Nucleus-22 Recipients. *Journal of the Association for Research in Otolaryngology*, 3(3):332–350.
- Stevens, S. (1937). On Hearing by Electrical Stimulation. *Journal of the Acoustical Society of America*, 8:191–195.
- Stevens, S. and Jones, R. (1939). The Mechanism of Hearing by Electical Stimulation. *Journal of the Acoustical Society of America*, 10:261–269.
- Stollman, M. H., Snik, A. F., Hombergen, G. C., Nieuwenhuys, R., and ten Koppel, P. (1996). Detection of the Binaural Interaction Component in the Auditory Brainstem Response. *British Journal of Audiology*, 30(3):227–232.
- Strauss, D. J., Corona-Strauss, F. I., Trenado, C., Bernarding, C., Reith, W., Latzel, M., and Froehlich, M. (2010). Electrophysiological Correlates of Listening Effort: Neurodynamical Modeling and Measurement. *Cognitive Neurodynamics*, 4:119–131.

Bibliography

- Strauss, D. J., Delb, W., and Plinkert, P. K. (2004). Analysis and Detection of Binaural Interaction in Auditory Evoked Brainstem Responses by Time-Scale Representations. *Computers in Biology and Medicine*, 34:461–477.
- Strauss, D. J., Teubner, T., Steidl, G., and Corona-Strauss, F. I. (2013). Exploiting the Self-Similarity in ERP Images by Nonlocal Means for Single-Trial Denoising. *Neural Systems and Rehabilitation Engineering*, 21(4):576–583.
- Svirsky, M. A., Robbins, A. M., and Kirk, K. I. (2000). Language Development in Profoundly Deaf Children With Cochlear Implants. *Psychological Science*, 11:153–158.
- Thai-Van, H., Cozma, S., Boutitie, F., Disant, F., Truy, E., and Collet, L. (2007). The Pattern of Auditory Brainstem Response Wave V Maturation in Cochlear-Implanted Children. *Clinical Neurophysiology*, 118:676–689.
- Tharpe, A. M. and Seewald, R. (2016). *Comprehensive Handbook of Pediatric Audiology*. Plural Publishing.
- The Ear Foundation (2019). www.earfoundation.org.uk, (last accessed 15.03.2019).
- Tucker, D. A., Dietrich, S., Harris, S., and Pelletier, S. (2002). Effects of Stimulus Rate and Gender on the Auditory Middle Latency Response. *Journal of the American Academy of Audiology*, 13(3):146–153.
- van den Honert, C. and Stypulkowski, P. H. (1986). Characterization of the Electrically Evoked Auditory Brainstem Response (ABR) in Cats and Humans. *Hearing Research*, 21:109–126.
- van Dijk, J. E., van Olphen, A. F., and Langereis, M. C. (1999). Predictors of Cochlear Implant Performance. *Audiology*, 38:109–116.
- Vaughan, H. G. J. (1969). The Relationship of Brain Activity to Scalp Recordings of Event-Related Potentials. In Donchin, E. and Lindsley, D. B., editors, *Average Evoked Potentials: Methods, Results and Evaluations*. U.S. Government Printing Office, Washington, D.C., USA.
- Wang, T., Özdamar, Ö., Bohórquez, J., Shen, Q., and Cheour, M. (2006). Wiener Filter Deconvolution of Overlapping Evoked Potentials. *Journal of Neuroscience Method*, 158:260–270.
- Wess, J. M., Brungart, D. S., and Bernstein, J. G. W. (2017). The Effect of Interaural Mismatches on Contralateral Unmasking With Single-Sided Vocoders. *Ear and Hearing*, 38(3):374–386.
- Wilson, B. S. and Dorman, M. F. (2008). Cochlear Implants: Current Designs and Future Possibilities. *Journal of Rehabilitation, Research & Development*, 45:695–730.

Bibliography

- Wilson, B. S., Finley, C. C., Lawson, D. T., Wolford, R. D., Eddington, D. K., and Rabinowitz, W. M. (1991). Better Speech Recognition With Cochlear Implants. *Nature*, 352:236–238.
- Woldorff, M. G. (1993). Distortion of ERP Averages due to Overlap from Temporally Adjacent ERPs: Analysis and Correction. *Psychophysiology*, 30:98–119.
- Wong, D. D. and Gordon, K. A. (2009). Beamformer Suppression of Cochlear Implant Artifacts in an Electroencephalography Dataset. *IEEE Transactions on Biomedical Engineering*, 56(12):2851–2857.
- Yeung, N., Bogacz, R., Holroyd, C. B., and Cohen, J. D. (2004). Detection of Synchronized Oscillations in the Electroencephalogram: An Evaluation of Methods. *Psychophysiology*, 41(6):822–832.
- York, D. H. (1990). *Bioinstrumentation and Biosensors*, chapter Noninvasive Measurement of Intracranial Pressure. MARCEL DEKKER, New York.
- Zeng, F.-G. (2004). *Trends in Cochlear Implants*. PhD thesis, Departments of Anatomy and Neurobiology, Biomedical Engineering, Cognitive Sciences, and Otolaryngology-Head and Neck Surgery, University of California, Irvine, California.
- Zeng, F. G., Grant, G., and Niparko, J. (2002). Speech Dynamic Range and Its Effect on Cochlear Implant Performance. *Journal of the Acoustical Society of America*, 111:377–386.
- Zeng, F. G. and Shannon, R. V. (1999). Psychophysical Laws Revealed by Electric Hearing. *Neuroreport*, 10:1931–1935.
- Zirn, S., Angermeier, J., Arndt, S., Aschendorff, A., and Wesarg, T. (2019). Reducing the Device Delay Mismatch Can Improve Sound Localization in Bimodal Cochlear Implant or Hearing-Aid Users. *Trends in Hearing*, 23:1–13.
- Zirn, S., Arndt, S., Aschendorff, A., and Wesarg, T. (2015). Interaural Stimulation Timing in Single Sided Deaf Cochlear Implant Users. *Hearing Research*, 328:148–156.

List of Publications

Journal Papers (MEDLINE listed)

M. C. Kohl, **E. Schebsdat**, E. N. Schneider, A. Niehl, D. J. Strauss, Ö. Özdamar, and J. Bohórquez (2019). "Fast Acquisition of Full-Range Auditory Event-Related Potentials Using an Interleaved Deconvolution Approach," *J. Acoust. Soc. Am.* **145**, 540-550.

E. Schebsdat, M. C. Kohl, G. Geissler, J. Bohórquez, D. J. Strauss, and J. Chalupper (2019). "Quantification of Binaural Interaction Facilitated By Interaural Latency Compensation in Bimodal Cochlear Implantees," *IEEE Trans. Neur. Sys. Rehabil. Eng.* (submitted).

E. Schebsdat, M. C. Kohl, F. I. Corona-Strauss, H. Seidler, and D. J. Strauss (2018). "Free-Field Evoked Auditory Brainstem Responses in Cochlear Implant Users," *Audiol. Res.* **8**(2), 44-53.

Conference Proceedings

M. C. Kohl, **E. Schebsdat**, E. Schneider, and D. J. Strauss (2019). "Denoising of Single-Trial Event-Related Potentials by Shrinkage and Phase Regularization of Analytic Wavelet Filterbank Coefficients," in *9th Int. IEEE Eng. Med. Biol. Soc. Conf. Neur. Eng.*.

E. Schebsdat, J. Wolfe, and D. J. Strauss (2017). "Objective Evaluation of the Subjectively Perceived Loudness of Cochlear-Implant Users," in *8th Int. IEEE Eng. Med. Biol. Soc. Conf. Neur. Eng.*.

E. Schebsdat, H. Hessel, H. Seidler, and D. J. Strauss (**2016**). "Detection of Binaural Interaction in Free-Field Evoked Auditory Brainstem Responses by Time-Scale Representations," in *38th Annual Int. Conf. IEEE Eng. Med. Biol. Soc.*, 3732-3735.

E. Schebsdat, F. I. Corona-Strauss, H. Hessel, H. Seidler, A. Bellaghech, L. Rusczyk, O. Müller, and D. J. Strauss (**2015**). "Binaural Interaction in Unilateral Cochlear Implant Users: Neural Correlates in Free-Field Single Trial Responses," in *37th Annual Int. Conf. IEEE Eng. Med. Biol. Soc.*, 3732-3735.

Acknowledgements

A scientific work is never the product of a single person, therefore, now it's time to thank all the people who have helped me to create the results of my dissertation. My special thanks go to my supervisor,

Prof. Dr. Dr. Daniel J. Strauss, who made the production of this interdisciplinary work possible for me in the first place. In particular, I would like to thank him for entrusting me this fascinating topic and for the warm welcome to his working group *Systems Neuroscience & Technology Unit*. As a student I got to know Prof. Strauss as an excellent teacher, who first introduced me to biosignal processing and the objective analysis of biological systems. I would particularly like to thank for the freedom he gave me throughout my doctorate. His competent advice and help contributed significantly to the success of this work.

I would also like to thank **Dr. Harald Seidler** and his renowned clinic team for the warm welcome, their specialist support and the freedom they gave me in accomplishing the necessary studies. Furthermore, I would like to thank all patients who supported me in my studies and from whom I was able to learn so much. The presented work would not have been possible without you.

Special thanks to **Dr. Horst Hessel**, **Dr. Josef Chalupper** and **Gunnar Geissler** for the opportunity to work on such interesting scientific topics, their provided technical support, and the joint development of new ideas and promising approaches. Besides, I would like to thank **Dr. Jérôme Servais** for sharing so many thoughts and ideas with me and for inviting me to his operating theater. Thank you for so many experiences, your guidance and your trust. I truly hope that this is just the beginning of a long and successful journey together.

Furthermore, I would like to thank **Dr. Farah I. Corona-Strauss, Dr. Lars Haab, Dr. Corinna Bernarding and Dr. Novaf Özgün** for their technical discussions, their great cooperation and their unrestricted and patient willingness to share with me their well-founded neurophysiological knowledge. You form the foundation of the working group, which has supported me and many colleagues so solidly. I have the greatest respect for you all for that.

Manuel C. Kohl, you were my light in darkest hours. Even when everything seemed to be against me, you reminded me to proudly hold my head up. When resistance became too strong, you helped me keep my course. Without any doubt, you were my best and strongest ally in so many fights. Thank you for believing in me and never letting me down. Thank you for all discussions, joint developements, successfull work, beneficial coffee breaks, creative π -rotational troubleshootings, and many joint orders from the universe. I really consider myself lucky to have had such a fantastic colleague. Without you I would certainly not have made it.

I couldn't imagine any better colleagues than I found them in this working group. Thanks for all the helpful conversations, technical discussions and all the motivation I got from you, be it in the lab or off the job. Special thanks to **Patrick J. Schäfer, Elena N. Schneider, Annika Niehl, Marie-Claire Herbig, Andreas Schröer, Philipp Flotho, Tobias Grün, Benedikt Buchheit, Caroline Lehser, Zeinab Morteza pouraghdam, Mayur Bhamborae** and all employees who are not named here. Without your knowledge, without your ideas and without your criticism my research project would be never got this far. It would not have been the same without you. Patrick J. Schäfer, from the first semester to the doctorate, we share the longest way. You are my oldest companion and will not be forgotten. I'll wait for you behind the finish line and when you get there, we'll catch all the stars over the skyline of Saarbrücken.

Thank you my friends, who always supported me with motivating and professional conversations. Heartfelt thanks to **Khaled Blah, Kathrin Rubly, Markus Marquardt, Simon Marquardt, Nina Osten, Stephanie Krier, Leon Busch, Lea Brust, Hannah Müller, Christina Rossek, Selina Lambert, Sharon Niemann** (an extra thank you for proofreading), **Karsten**

Fritzen, David Schütz, Matthias Hild, Henrik Lensch, Oliver Brieger, David Sonntag, Nora Vargas and to so many others for giving me such a wonderful home. Thank you for always supporting me, not only in this adventure. I cannot imagine a world without you.

Finally, I would like to thank **my family** who, in every way, have laid the foundation for my path. Thank you for your unreserved support and confidence. A thank you also to my brothers **Rainer and Angelo**, whom always helped me not losing my way and faith. Thank you very much.

Curriculum Vitae

Aus datenschutzrechtlichen Gründen wird der Lebenslauf in der elektronischen Fassung der Dissertation nicht veröffentlicht.

